

Elsevier Editorial System(tm) for Journal of Hydrology
Manuscript Draft

Manuscript Number: HYDROL11293R1

Title: INTEGRATING TOPOGRAPHY, HYDROLOGY AND ROCK STRUCTURE IN WEATHERING RATE
MODELS OF SPRING WATERSHEDS

Article Type: Research Paper

Keywords: spring watersheds; hydrology; travel time; surface area; weathering rates; modeling;
equilibria; Vouga river basin; THROW model

Corresponding Author: Dr. Fernando A.L. Pacheco,

Corresponding Author's Institution: Trás-os-Montes e Alto Douro Univ.

First Author: Fernando A.L. Pacheco

Order of Authors: Fernando A.L. Pacheco; Cornelis H Van der Weijden

Fernando A.L. Pacheco
Department of Geology and Centre for Chemistry
Trás-os-Montes and Alto Douro University
5000 Vila Real
Portugal

Professor Prof Baveye
Editor
Journal of Hydrology

November 22, 2011

HYDROL-S-11-00530: Editor decision - revise (minor revision)

Dear Prof Baveye,

We are very pleased with your decision regarding our manuscript. We addressed the very minor corrections pointed out by reviewer #2, as can be consulted in the DOC file *Revision_Notes*. The revised version of the manuscript is given in the DOC file *Revision_Changes_Marked* (an annotated manuscript showing the very minor changes relative to the original manuscript, affecting just a few lines of that ms. The final version of the manuscript is given in the DOC file *Manuscript_Final*. Tables are provided as a separate DOC file. Figures are provided as TIFF format images, with resolution 600 or 1200 DPI.

We hope you are satisfied with the revised version, and that the paper can be published soon.

Kind regards,

Fernando A.L. Pacheco

Revision Notes

Reviewer #1

No corrections to be made.

Reviewer #2

1) The abstract contains some formulas. I think it is better to delete them from the abstract.

The formulas were deleted.

2) p.7, 155: Please check the calculation of percolation time of soil water to reach the bedrock. Based on the given K , it should be at least 3.75 days, i.e. >3.75 days.

The sentence was corrected: where the text was " $< 3,75$ days" is now "at least 3,75 days".

3) p.8, 188-190: The sequence of sentences beginning with "Altogether." do not make sense. How does a model operating with a minimum amount of information affects the type of methods used in the model?

The sentence was deleted (in fact, it was not an essential sentence).

4) Perhaps a better phrase can be used instead of the term "aquifer formation constant". It sounds like the hydraulic conductivity and porosity have something to do with the formation of the aquifer.

Throughout the text (in 7 places), the term "*formation constants*", although used regularly in hydrologic texts to describe aquifer hydraulic parameters such as K and n_e , was replaced by "*hydraulic parameters*".

5) p.19, 461-64: Here the authors mention that no spring flow discharge was information was available. However, it is not clear what was done to compensate for this. The authors should make it clear to the reader by rephrasing the sentence and using better wording, what was done exactly. Perhaps this issue can be clarified in the previous methods section of the manuscript.

The way how we compensated for the lacking of spring flow discharges is explained in the section "*Aquifer Formation Hydraulic Parameters and Travel Times of Spring Watersheds*". However, in the section ("*Aquifer Formation Hydraulic Parameters and Travel Times of Stream Watersheds*") we now added the following sentence to make this more clear: "*The hydraulic conductivities (K) and effective porosities (n_e) resulting from this characterization were then used as proxies of the K and n_e values of the spring watersheds, as explained in the next section, which also describes how groundwater travel times were downscaled from the larger (stream) the smaller (spring) scales.*"

6) Table 2: What are the reference numbers?

The papers corresponding to the reference numbers are given in the legend of Table 2.

RESEARCH HIGHLIGHTS

- develop a weathering model that incorporates rock structure in the rate equation
- conceive a weathering model especially designed for fracture artesian springs
- Create a model that integrates topography, hydrology, rock structure and weathering

18 ABSTRACT

19 Weathering rate models designed for watersheds combine chemical data of discharging waters with
20 morphologic and hydrologic parameters of the catchments. At the spring watershed scale,
21 evaluation of morphologic parameters is subjective due to difficulties in conceiving the catchment
22 geometry. Besides, when springs emerge from crystalline massifs, rock structure must be accounted
23 in formulas describing the area of minerals exposed to the percolating fluids, for a realistic
24 evaluation of the rates. These particular features are not included in the available approaches and
25 for that reason a new model was developed, coined THROW model. This is a lumped approach that
26 integrates (T)opography, (H)ydrology, (RO)ck structure and (W)eathering in a single algorithm.
27 The study area comprises several stream watersheds and spring sites of the Vouga River basin
28 (northern Portugal), shaped on granites. Firstly, the THROW model couples a terrain modeling
29 analysis with hydrologic models based on discharge rates, to determine hydraulic conductivities
30 (K), effective porosities (n_e) and annual recharges (V_r) at the stream watershed scale. Subsequently,
31 these parameters are used in a water balance model to estimate concomitant groundwater travel
32 times (t). The mean K [$(4.7 \pm 3.2) \times 10^{-7} \text{ m} \cdot \text{s}^{-1}$] and n_e [$(2.0 \pm 1.3) \times 10^{-2}$] values are adopted as proxies
33 for the spring watersheds and a firm regression equation is defined between time and stream
34 watershed area (A). Secondly, two more runs of terrain modeling analysis are executed to
35 extrapolate morphologic parameters for the spring watersheds. The first run hinges on scaling
36 properties of the drainage networks, known as Horton laws, and is used to scale watershed areas
37 across stream orders (i). The scaling function is described by another regression equation. The
38 second run evaluates the order of a spring watershed, defined as equivalent order (i_{eq}) and equated
39 to the mean order of the surrounding stream watersheds. Having calculated the i_{eq} , spring watershed
40 areas and travel times were downscaled using the regression equations ($A < 10 \text{ km}^2$ and $t = 1.4\text{--}2.8$
41 yr). Standing on the physical and hydrologic parameters of the spring watersheds, the THROW
42 model finally calculates plagioclase weathering rates in the vicinity of the spring sites. The SiB
43 model (Pacheco and Van der Weijden, 1996) was used before to estimate the contribution of
44 plagioclase dissolution to the chemical composition of these springs (Van der Weijden and
45 Pacheco, 2006). The chemical data were now coupled with K , n_e and t in a rate equation to estimate
46 chemical weathering rates of plagioclase in the basin. In the THROW model, the rate equation
47 describes the exposed surface area as a function of fracture spacings, openings and porosities
48 (Pacheco and Alençoo, 2006). The calculated rates ($W_{pl} = (2.5 \pm 1.2) \times 10^{-14} \text{ mol} \cdot \text{m}^{-2} \cdot \text{s}^{-1}$) are
49 consistent with previous reports and with results of experimental kinetic models. The SiB results
50 predict formation of halloysite and gibbsite along the flow path, which were indeed close to
51 equilibrium with the dissolved Al and Si activities.

52

53 INTRODUCTION

54 The assessment of chemical weathering rates of silicate minerals has been the topic of numerous
55 studies, as this process is important in global geochemical cycles, particularly in relation to fluxes
56 of carbon dioxide (CO₂) and global warming (Berner et al., 1983; Drever and Clow, 1995; Dupré et
57 al., 2003; Hartmann et al., 2009; among others). These studies have been carried out at various
58 scales, including the micro to hand specimen scales (the laboratory approach) or the soil profile to
59 watershed scales (the field approach). At the watershed scale, the majority of studies were focused
60 on rivers (Oliva et al., 2003; Tardy et al., 2004; Velbel, 1985; White, 2002; White et al., 2001; and
61 references therein) while a limited number were based on spring water data (Pacheco and Van der
62 Weijden, 2002; Pacheco and Alençoo, 2006). Studies at the spring watershed scale are important
63 because they bridge weathering results from the hand specimen or soil profile to the river basin
64 scales. Numerical models have been developed and applied to calculate weathering rates. At the
65 watershed scale, operation of these models requires prior assessment of very diverse data, such as
66 morphologic parameters of the catchments, aquifer hydraulic parameters and recharge, groundwater
67 travel times, fluid compositions, etc., incoming from very different disciplines, including
68 geomorphology, hydrology or geochemistry, reason why the most recent models are based on the
69 so-called lumped approach whereby the results of several model components are integrated. For
70 example, Godd ris et al. (2006) combined a module of chemical weathering in soil horizons and
71 underlying bedrock (the WITCH model of Godd ris et al., 2006, 2009; Roelandt et al., 2010) with a
72 module of water and carbon cycles in forested ecosystems (the ASPECTS model of Rasse et al.,
73 2001) to simulate, on a seasonal basis, the concentrations of silica and major base cations within the
74 soil horizons and the stream of a granitic small experimental watershed. Violette et al. (2010)
75 designed two symmetrical box modules to perform a coupled hydrological and geochemical
76 modeling: (i) a hydrological module specifically developed for the experimental watershed; (ii) the
77 WITCH module. The hydrologic modules commonly incorporated into lumped approaches are

78 usually designed to work with stream watersheds, and the concomitant geochemical modules relate
79 the fluid compositions to weathering reactions in the saprolite horizon and quantify the area of
80 minerals involved in weathering reactions (the exposed surface area) as a function of the saprolite
81 materials texture (e.g. Violette et al., 2010). Despite their broad applicability, available lumped
82 approaches are inoperative when the study is focused on springs emerging from crystalline rocks,
83 because they cannot accommodate some singularities of fracture artesian spring watersheds relative
84 to geometry and exposed surface area. For that reason, a new approach is required to deal with such
85 cases.

86 A lumped approach suited to deal with fracture artesian springs must incorporate a topographic
87 module that can assess watershed morphologic parameters (area, volume, length of water channels),
88 yet recognizing that spring sites can hardly be connected to a water channel. This type of springs
89 emerges at the intersection between the Earth's surface and conductive fractures. Usually, this
90 corresponds to points in the vicinity of water channels but rarely to points in a specific channel. In
91 these cases, delineation of watershed boundaries becomes a subjective task that limits any
92 subsequent morphologic characterization. An appropriate topographic module has to calculate the
93 morphologic parameters avoiding the step of watershed delineation, however such a specific
94 method is not part of any current lumped approach. Additionally, the lumped approach must also
95 bears that fracture artesian springs represent water packets that predominantly follow the easiest
96 routes of the crystalline rocks, such as fissures, fractures or joints, interacting with minerals exposed
97 at their walls. The area of fluid–mineral interaction is not equal to the area of the catchment, but is
98 restricted by inhomogeneous fluid migration through the fracture networks (Drever and Clow,
99 1995; Velbel, 1989, 1993). Moreover, minerals in the fractures are generally embedded in the rock
100 matrix and are only partly exposed to the fluid. Along the pathway from recharge area to spring site,
101 a water packet has been in contact with mineral surfaces that have different weathering histories.
102 For this reason, the exposed surface area will be an average of newly exposed minerals and of

103 minerals already affected by weathering. Furthermore, the spring water samples represent combined
104 water packets, each having traveled different pathways with various contact times and exposure to
105 different surface areas (Oliva et al., 2003). As a consequence, the calculated weathering rate will
106 represent an average. For the reasons described above, the geochemical module of the lumped
107 approach should define the exposed surface area as a function of rock structure, whenever the
108 studied watersheds are shaped on crystalline rocks and the analyzed water samples are represented
109 by groundwater. Nevertheless, this is not observed in the available models. Invariably, this area is
110 calculated from the crystal dimensions of the minerals (geometric surface area) or by gas adsorption
111 (BET method) that accounts for the so-called surface roughness (Brantley et al., 1999; Brantley and
112 Mellott, 2000; Lüttge 2005; Zhang and Lüttge, 2009), although it has already been recognized that
113 the results might not be representative of the area exposed to groundwater in a watershed (Brantley
114 and Mellott, 2000; Drever and Clow, 1995; Hellmann and Tisserand, 2006; White and Peterson,
115 1990a,b).

116 The present study sought to calculate weathering rates of plagioclase at the spring watershed scale
117 in granitic environment. Given the above mentioned singularities of fracture artesian spring
118 watersheds, the main purpose of this paper was to develop a lumped approach integrating, (a) a
119 topographic module that can estimate the morphologic parameters of the spring watersheds; (b) a
120 geochemical module that defines the exposed surface area as a function of rock structure. The
121 lumped approach will be coined as the (T)opography, (H)ydrology, (RO)ck structure and
122 (W)eathering model, or simply THROW model. The module developed for assessing the spring
123 watershed morphologic parameters is based on the concepts of stream order (Strahler, 1957) and
124 statistical self-similarity of drainage networks (Horton, 1945; Schuller et al., 2001). In an attempt to
125 account for the particularities of fluid transport in fractured rocks as described above, the area of
126 fluid–mineral interaction will be approximated in the geochemical module by a formula hinging on
127 rock fracture spacings, openings and porosities (Snow, 1968; Pacheco and Alencão, 2006).

128

STUDY AREA

129 The hydrographic basin of the Vouga (Figure 1) is located in northern Portugal between the sea
130 level of the Atlantic coast and 1100 meters above sea level, near the source of the river on Lapa
131 Mountain. The basin occupies 3362 km² of a region characterized by mountains in the eastern part
132 and a coastal plain in the western part. Altitudes in major mountains (Lapa, Freita, Caramulo) range
133 from 800 and 1100 meters. The main water course is 141 km long and debouches into the Ria de
134 Aveiro, a sandbar-built coastal lagoon with a small inlet/outlet connecting the lagoon to the Atlantic
135 ocean. The climate in this region is moderate, with precipitation varying from 800–1800 mm·y⁻¹
136 and air temperatures ranging from approximately 8°C in winter to 21°C in summer. The Vouga
137 River and several tributaries have been monitored for stream flow in hydrometric stations of the
138 Portuguese National Network. The locations of the stations are shown in Figure 1 and some
139 relevant data on identification and record length is presented in Table 1.

140 The mountainous part of the Vouga River basin is characterized by Palaeozoic metasediments of
141 the so-called Schist and Greywacke Complex (Beiras Group) that were intruded by syn- to post-
142 tectonic Hercynian granites. The coastal plain has a cover of Permian to Holocene sediments
143 consisting of quartzites, phyllites, conglomerates, sandstones, limestones, sands, etc (Figure 2). The
144 syn-tectonic granitoids consist mostly of medium- to coarse-grained granites to granodiorites,
145 whereas the post-tectonic granitoids consist mostly of coarsely porphyritic biotite granites
146 (Schermerhorn, 1956; Soen, 1958; Godinho, 1980; Medina, 1996). The average mineralogical
147 composition (in wt.%) of these rocks is: quartz (34.1), K-feldspar (14.4), plagioclase (albite-
148 oligoclase, but largely oligoclase; 31.0), biotite (3.7), and muscovite (16.8).

149 The mountainous part of the Vouga basin has a monotonous cover by cambisols. In the plain, soil
150 types are dominated by fluvisols, regosols, podzols and solonchaks. In the region, the profile of a
151 typical cambisol is characterized by a A horizon (0–30 cm depth) rich in organic matter, a B
152 horizon (30–55) rich in clay minerals and a C horizon (55–80) composed of weathered rock

153 (Martins, 1985). Average hydraulic conductivities of this soil type is $K = 2.47 \times 10^{-6} \text{ m} \cdot \text{s}^{-1}$ (Caetano
154 and Pacheco, 2008). When 1D flow is assumed, percolation time of soil water to the bedrock (h/K ,
155 where $h = 80 \text{ cm}$, the average thickness of cambisols) is at least 3.75 days. Small-size farm lands
156 and forests in total occupy 4/5 of the basin, the remaining 1/5 being represented by bare rock, urban
157 areas and water bodies. Although farming is more concentrated in the plain and forestry in the
158 mountains, the proportion of land used for agriculture in the highlands is significant and the
159 associated use of manure and fertilizers responsible for an important anthropogenic imprint to the
160 chemistry of shallow groundwaters. Some small urban areas have no sewage system and so
161 domestic effluents are discharged directly into the soils (Van der Weijden and Pacheco, 2006).

162

163

SPRING WATER SAMPLING AND ANALYTICAL TECHNIQUES

164 Perennial springs within the Vouga basin were sampled in the granitic areas during the summer
165 campaigns (June–July) of 1982–1985. In total, the number of sampled springs is 87. The location of
166 the spring sites is given in Figure 2. Sampling was made during the draught season to ensure that
167 spring waters would represent exclusively ground water. The pH was measured at the sampling site,
168 and alkalinity was analyzed in the field laboratory within 24 hours of sample collection using Gran
169 plots for end-point determination. Two samples of 100-mL each, one acidified with nitric acid to
170 pH 2, were stored and analyzed at the home laboratory. Sodium, potassium, magnesium, calcium,
171 aluminum, and silicon were analyzed by ICP-OES in the acidified sample, whereas chloride,
172 sulfate, and nitrate were determined by ion chromatography in the unacidified sample. The accuracy
173 of the results for the individual components was better than $\pm 5\%$. Samples for which the charge
174 balance was off by $> 10\%$ were discarded. The analytical results are reported in Appendix 1.

175

176

177

178

THE THROW MODEL

179 The THROW model is introduced in this paper as a lumped approach for the assessment of
180 weathering rates at the fracture artesian spring watershed scale. It is composed of three modules: the
181 topographic module, the hydrologic module and the weathering module. A run of the THROW
182 model begins with the topographic module, proceeds with the hydrologic module and ends up with
183 the weathering module, as illustrated in the flowchart of Figure 3. Each module is organized within
184 the dashed envelopes of the figure: the rectangles represent data essential for model operation; the
185 rounded rectangles represent model processes. Because the THROW model runs in a sequential
186 mode, the output of a given process is usually the input for the next process, until weathering rates
187 are finally calculated. The shaded rectangles, however, represent base information, obtained from
188 topographic, analytical or field measurements. The description of the topographic, hydrologic and
189 weathering modules is presented in the next sections.

190

191 **The Topographic Module**

192 The topographic module of the THROW model aims on estimating morphologic parameters (e.g.
193 area) of spring watersheds. There is a fundamental difficulty in dealing with these watersheds
194 because springs typically emerge in the vicinity of several water channels but not necessarily in any
195 channel. As a consequence, the outlining of spring watersheds is a biased task that hampers any
196 subsequent morphologic characterization. For that reason, morphologic parameters of spring
197 watersheds in the THROW model are estimated by an extrapolation technique based on scaling
198 properties of the drainage networks.

199

200 *The Horton Laws of Drainage Network Composition*

201 The continuous shaping of the Earth's surface by meteoric water results in the development of
202 drainage networks that can be conceived at various scales: river, stream, spring. Scaling properties

203 of drainage networks were early investigated and empirical scaling laws have been proposed by
204 Horton (1945), Strahler (1952) and Schumm (1956), becoming known as the Horton laws.
205 Subsequent research has shown that individual streams and the networks which they comprise are
206 fractals (La Barbera and Rosso, 1987, 1989; Roth et al, 1996; Tarboton, 1996; Schuller et al., 2001;
207 De Bartolo et al., 2006; among others), and the Horton laws provided the background for the
208 development of different measures of the fractal dimension. These empirical rating laws are based
209 upon hierarchical classification of the tributary system starting from streams lacking upstream
210 tributaries and giving increasing order numbers towards the outlet. For example, according to the
211 classification of Strahler (1957), water channels with no tributaries are described as 1st-order
212 channels and are fed by 1st-order watersheds, and the confluence of two i^{th} -order channels generates
213 a $(i+1)^{\text{th}}$ -order channel. Basically, the scaling laws state that the ratio of a morphologic parameter
214 (area or slope of the watershed, number or length of streams within the watershed) measured at
215 order i and order $i+1$ is constant. According to Rosso et al. (1991), the Horton laws of network
216 composition are geometric-scaling relationships because they hold regardless of the order or
217 resolution at which the network is viewed and because they yield self-similarity of the catchment–
218 stream system, or at least self-affinity in cases where the scaling factors in the longitudinal and
219 transverse directions are not equal (Nikora and Sapozhnikov, 1993) or self-organization in cases
220 where complex drainage networks are to be described as multi-fractal systems (De Bartolo et al.,
221 2000, 2004, 2006; Gaudio et al., 2006). Because these laws typically hold for a wide range of scales
222 in nature, they can be employed to extrapolate watershed morphologic parameters across scales. A
223 generalised equation for the relationship between morphologic parameter A and order i can be
224 written as:

$$225 \quad A = f(i) \tag{1}$$

226 where f is a scaling function. Because springs usually emerge in the vicinity but away from the
227 water channels their watersheds cannot be associated to a particular Strahler order. In general,

228 neighbouring channels differ from each other in their order and therefore watersheds of springs
 229 must be classified according to the concept of equivalent order (i_{eq}), which is defined here as an
 230 average of the orders of the surrounding streams. Unlike stream orders, which are integers,
 231 equivalent spring orders will be real numbers. When a spring site is situated in a region where, for
 232 example, $i_{eq} = 1.5$, this means that the catchment area of the spring is larger than the average area of
 233 1st-order watersheds and smaller than the average area of 2nd-order watersheds. For spring
 234 watersheds, morphologic parameters are determined by Equation 1, where i is replaced by i_{eq} .

235

236 *Carrying Out the Topographic Module on a GIS Platform*

237 The topographic module of the THROW model is executed on a Geographic Information System
 238 (GIS) comprising the ArcGIS (ESRI, 2007) and ArcHydro (ESRI, 2009) computer packages, and
 239 operates in two sequential runs (Figure 3). In the first run, ArcHydro executes a terrain modeling
 240 analysis based on the Digital Elevation Model of the study area (e.g. Figure 1) whereby the
 241 drainage network and watersheds are drawn and classified according to their Strahler orders.
 242 Subsequently, the same package assesses morphologic parameters of each watershed, including
 243 area, volume and length of water channels, and calculates average values for each order. Based on
 244 these average values, relationships between the parameters and concomitant orders (Equation 1) are
 245 defined using least squares regression. In the second run, the *Density Function* of ArcGIS toolbox is
 246 used to calculate equivalent orders for the spring watersheds. Firstly, the map with the drainage
 247 network is overlapped by a grid of cells with dimensions 100×100 m and, within each cell, the
 248 lengths of streams are measured (L_i) and multiplied by the corresponding order (i). Secondly, the
 249 previous step is repeated for every order appearing in the cell and then the products $L_i \times i$ are
 250 summed and divided by the total length of streams within the cell (L), giving the i_{eq} :

$$251 \quad i_{eq} = \frac{\sum_{i=1}^n L_i \times i}{L} \quad (2)$$

252 The i_{eq} of a given spring watershed is determined from the map of equivalent orders computed using
253 Equation 2 by evaluating the i_{eq} at the location coordinates of the spring site. The corresponding
254 morphologic parameters will be assessed afterwards using the i_{eq} values in Equation 1.

255

256 **The Hydrologic Module**

257 This module aims on estimating hydrologic parameters of the fractured aquifer at the watershed
258 scale. It comprises a set of methods to calculate hydraulic conductivity and effective porosity,
259 evaluate annual recharge, and assess groundwater travel time. The module's flowchart is illustrated
260 in Figure 3. The data required for its operation encompass the outflows measured at the spring sites
261 and results from the topographic module.

262

263 *Spring Outflows and Aquifer Hydraulic Parameters*

264 The outflow or discharge of a fracture artesian spring some time after a precipitation event occurs
265 from upstream aquifers along the underground flow path to the spring. This type of flow is known
266 as base flow and the analysis of base flows recognized as recession flow analysis. When combined
267 with physically based flow equations, recession analysis can be used as a tool for aquifer
268 characterization, namely for assessment of hydraulic conductivity and effective porosity (Szilagyi
269 and Parlange, 1999; Szilagyi et al., 1998; Mendoza et al., 2003; Van de Giesen et al., 2005;
270 Malvicini et al., 2005; among others).

271 For the analysis of spring outflows, the THROW model adopted a technique developed by Brutsaert
272 and Nieber (1977) for stream flow recession analysis, called the Brutsaert method. Declining
273 groundwater reservoirs control both stream base flow recession and upland spring outflow
274 recession, so the method should be equally valid for both situations. The use of the Brutsaert
275 method is advantageous because it is independent of the ambiguity inherent in identifying when
276 base flow starts (Malvicini et al., 2005). Refinements and extensions on the method have been made

277 in Zecharias and Brutsaert (1985,1998), Brutsaert (1994), Brutsaert and Lopez (1998); Rupp and
 278 Selker (2005); among others. The Brutsaert method is founded on the Boussinesq equation
 279 (Boussinesq, 1903, 1904), which describes the drainage from an ideal unconfined rectangular
 280 aquifer bounded below by a horizontal impermeable layer and flowing laterally into a water
 281 channel. There are several theoretical solutions of the Boussinesq equation that have the general
 282 form of a power function (Rupp and Selker, 2006):

$$283 \quad \frac{dQ}{dt} = aQ^b \quad (3)$$

284 where Q ($\text{m}^3 \cdot \text{s}^{-1}$) is the recession flow, t is time, and a and b are constants. The coefficient a can be
 285 directly related to the groundwater reservoir's characteristics and b is an exponent whose value
 286 depends on the recession flow regime. There are two distinct flow regimes: the short-time and the
 287 long-time regime. Short-time flows generally have a higher Q than long-time flows. Brutsaert and
 288 Lopez (1998) showed the following solution for short-time flow:

$$289 \quad a = \frac{1.13}{Kn_e D^3 L^3}, b=3 \quad (4a)$$

290 where K is the hydraulic conductivity, n_e the effective porosity, D the aquifer thickness and L the
 291 length of upstream channels intercepting groundwater flow. The long-time flow is adequately
 292 described by the so-called linear solution of Boussinesq (1903).

$$293 \quad a = \frac{0.35\pi^2 KDL^2}{n_e A^2}, b=1 \quad (4b)$$

294 where A is the upland drainage area. Equations 4a and 4b can be combined to describe K and n_e as a
 295 function of a and the morphologic parameters of the watershed (A , D , L). On the other hand, D can
 296 be approached to the ratio V/A . In that case,

$$297 \quad K = 0.57 \sqrt{\frac{a_1}{a_3}} \left(\frac{A^3}{V^2 L^2} \right) \quad (5a)$$

$$298 \quad n_e = \frac{1.98}{V \sqrt{a_1 a_3}} \quad (5b)$$

299 where a_i represents the value of a when $b = i$ (1 or 3).

300 To estimate K and n_e using Equations 5a,b it is required a previous run of the topographic module,
 301 the results of which provide numbers for A , V and L . The values of a_1 and a_3 can be read in a scatter
 302 plot of $\ln(\Delta Q/\Delta t)$ versus $\ln(Q)$. According to the Brutsaert method, the lower envelope of the scatter
 303 points is represented by two straight lines, one with a slope $b = 1$, and the other with a slope $b = 3$,
 304 and the y-values where the lines intercept $\ln(Q) = 0$ (or $Q = 1$) are the parameters a_1 and a_3 .

305

306 *Spring Base Flows and Aquifer Recharge*

307 Recession flow analysis is also used as a tool for aquifer recharge estimation. In this case, recession
 308 segments are selected from the hydrographic record of the spring and their geometric properties
 309 (e.g. slope) combined with analytical models to provide measures of the aquifer recharge.

310 Underlying the methods of recession flow analysis is the storage-outflow model adopted to
 311 represent discharge from natural storage compartments during the recession phase. Many complex
 312 functions have been developed in this context, for example to explain the outflow from karstic
 313 aquifers (Padilla et al., 1994), channel banks (Cooper and Rorabaugh, 1963), surface depressions
 314 such as lakes or wetlands (Griffiths and Clausen, 1997), etc., but many other recession flow models
 315 assume a linear relationship between storage and outflow, described by the classic exponential
 316 decay function of Boussinesq (1877):

$$317 \quad Q = Q_i e^{-\alpha t} \quad (6)$$

318 where Q_i is the base flow at the beginning of a recession period and α is the recession constant. One
 319 of these methods has been developed by Meyboom (1961) and is now incorporated into the
 320 THROW model. Starting with Equation 6, Meyboom (1961) noted that a plot of discharge versus
 321 time on a semilogarithmic paper would yield a straight line, the slope of which defines the recession
 322 constant. In this case, the Equation 6 can be re-written as:

$$323 \quad Q = \frac{Q_i}{10^{t/t_1}} \quad (7)$$

324 where t_1 is the time corresponding to a log-cycle of discharge. Integrating Equation 7 from $t = 0$
 325 (beginning of the recession) and $t = \text{infinity}$ (complete depletion of the aquifer) gives:

$$326 \quad V_t = \frac{Q_i t_1}{2.3} \quad (8a)$$

327 where V_t is the total potential groundwater discharge. By analogy, the residual potential
 328 groundwater discharge (V_s) can be approached by:

$$329 \quad V_s = \frac{Q_f t_1}{2.3} \quad (8b)$$

330 where Q_f is the base flow at the end of the recession phase. Considering a sequence of two recession
 331 periods, aquifer recharge (V_r) between periods will be defined as the difference between V_t ,
 332 evaluated at the beginning of period 2, and V_s estimated at the end of period 1, i.e.:

$$333 \quad V_r = (Q_i - Q_f) \frac{t_1}{2.3} \quad (9)$$

334

335 *Groundwater Travel Times*

336 Groundwater transit (or travel) time is defined as the elapsed time when the water molecules exit
 337 the flow system (Bolin and Rodhe, 1973; Etcheverry and Perrochet, 2000; Rueda et al., 2006). A
 338 point of reference for mean transit times are often the hydraulic turnover times, since they define
 339 the turnover timescale based on the best understanding or assumption of the catchment subsurface
 340 volume and mobile storage if the unsaturated zone transit time is small compared to the total transit
 341 time of the system. The concept of hydraulic turnover time was adopted by the THROW model to
 342 estimate the travel time of groundwater within the spring watershed boundaries (t , s). According to
 343 McGuire and McDonnell (2006), if a simple water balance is considered, the hydraulic turnover
 344 time is defined as the ratio of the mobile catchment storage (equated to Vn_e , m^3) to the volumetric
 345 flow rate (equated to the aquifer recharge: V_r , $\text{m}^3 \cdot \text{s}^{-1}$):

$$346 \quad t = \frac{Vn_e}{V_r} \quad (10)$$

347 **Weathering Module**

348 This module combines the chemical composition of spring waters and of their host rocks in a mass
 349 balance algorithm to calculate the number of moles of primary minerals and of secondary products
 350 dissolved or precipitated along the flow path. In a subsequent stage, these mass transfers are
 351 combined with aquifer hydraulic parameters and groundwater travel time in a rate equation to
 352 obtain mineral weathering rates (Figure 3).

353

354 *Geochemical Mass Balance Calculations*

355 There are essentially two types of geochemical models for assessing mineral weathering rates at the
 356 watershed scale. The first approach estimates solid-state weathering rates based on the differences
 357 between elemental, isotopic and mineral compositions measured in present-day regoliths and in the
 358 assumed protolith. In this case, rates represent the entire time span of a weathering episode,
 359 commonly on the order of thousands to million years. The second approach calculates solute-flux
 360 rates that stand for contemporary weathering during groundwater percolation in the rocks, in which
 361 case time is a window to the weathering episode spanning few years or decades. The THROW
 362 model is based on the solute-flux approach and uses the SiB algorithm of Pacheco and Van der
 363 Weijden, (1996), extended by Pacheco et al. (1999) and Pacheco and Van der Weijden (2002), to
 364 perform the geochemical mass balance calculations. A brief description of the method is given in
 365 the next paragraphs.

366

367 The SiB algorithm comprehends a set of mole balance and charge balance equations of the form:

$$368 \text{ Mole balance equations } \sum_{j=1}^{q_1} \beta_{ij} [M_j] + [Y_i]_p = [Y_i], \text{ with } i = 1, q_2 \quad (11a)$$

$$369 \text{ Charge balance equation } \sum_{i=1}^{q_3} z_i [Y_i]_p = [Cl^-] + 2[SO_4^{2-}] + [NO_3^-] \quad (11b)$$

370 where q_1 , q_2 and q_3 are the number of primary minerals involved in the weathering process, the
 371 number of inorganic compounds that usually are released from weathering reactions ($q_2 = 6 = \text{Na}^+$,
 372 K^+ , Mg^{2+} , Ca^{2+} , HCO_3^- and H_4SiO_4^0), and the number of the latter compounds that usually are also
 373 derived from atmospheric plus anthropogenic sources – lumped as “pollution” ($q_3 = 4 =$ the four
 374 major cations); suffixes t and p mean total and derived from “pollution”, respectively. The expected
 375 sources of anthropogenic pollution are manures, commercial fertilizers and domestic and(or)
 376 industrial effluents; Y represents a dissolved compound; M represents a mineral; Cl^- , SO_4^{2-} and
 377 NO_3^- are the major dissolved anions assumed to represent exclusively atmospheric plus
 378 anthropogenic inputs; square brackets ([]) denote concentrations of a dissolved compound or a
 379 dissolved mineral; b_{ij} is the ratio of the stoichiometric coefficients of dissolved compound i and
 380 mineral j , as retrieved from the weathering reaction of mineral j ; $b_{ij}[\text{M}_j] = [\text{Y}_i]r_j$, where $[\text{Y}_i]r_j$ is the
 381 concentration of a dissolved compound i derived from reaction of M_j moles of mineral j ; z_l is the
 382 charge of cation l .

383 The number of equations in Set 11a,b is seven. The unknowns of the system are the [M] and the
 384 [Y]p variables, in total q_1+q_3 . The SiB algorithm uses the Singular Value Decomposition procedure
 385 as described in Press et al. (1991) to solve the set of equations because this procedure can handle
 386 efficiently (through least squares or minimizing procedures) the cases where the set is undetermined
 387 ($q_1+q_3 > 7$) or overdetermined ($q_1+q_3 < 7$). In systems with fluid flow, precipitation of secondary
 388 products along the flow path follows certain sequences (Helgeson et al., 1969; Steefel and Lasaga,
 389 1992; Steefel and Van Cappellen, 1990). The SiB algorithm describes these sequences as reactions
 390 of primary minerals to mixtures of secondary products (for example alteration of plagioclase to $c_1 \times$
 391 halloysite + $(1-c_1) \times$ gibbsite, with $0 \leq c_1 \leq 100\%$; alteration of biotite to $c_2 \times$ vermiculite + $(1-c_2)$
 392 \times halloysite, with $0 \leq c_2 \leq 100\%$). Only a few of these mixtures will explain the chemical
 393 composition of the spring waters. To be labelled as valid mixture, the selected values of c_1 and c_2
 394 must result in a solution of Set 11a,b satisfying $[\text{M}] \geq 0$ and $[\text{Y}]p \geq 0$. Among the valid mixtures,

395 the SiB algorithm selects a best-fit one by checking all against predefined external boundary
396 conditions.

397

398 *Rate Equation*

399 The weathering rate of a mineral M is commonly defined by the relationship:

$$400 \quad W_M = \frac{[M]}{t} \times \frac{V_r}{A_M} \quad (12)$$

401 where W_M ($\text{mol}\cdot\text{m}^{-2}\cdot\text{s}^{-1}$) is the rate and $[M]$ ($\text{mol}\cdot\text{m}^{-3}$) its concomitant dissolved concentration, t (s)
402 is the average travel time of water packets flowing through the spring watershed, V_r (m^3) is the
403 volume of water entering the spring watershed in a unit time, and A_M (m^2) is the surface area of M
404 in contact with that volume of aquifer water. To adequately describe the reactive surface area of a
405 fracture artesian spring watershed, weathering modules must incorporate rock structure in the
406 calculation of A_M . This is accomplished by the THROW model. In this model, A_M is calculated by a
407 formula developed by Pacheco and Alencão (2006) describing the area of fracture surfaces in
408 contact with aquifer water in unit time:

$$409 \quad A_M = 2\alpha_M V_r \times \sqrt{\frac{\rho_w g n_e}{12\mu_w K}} \quad (13)$$

410 where α_M is the proportion of mineral M in the rock, μ_w is the dynamic viscosity of water ($1.14 \times$
411 $10^3 \text{ kg}\cdot\text{s}^{-1}\cdot\text{m}^{-1}$ at $T = 15^\circ\text{C}$), and g is the acceleration of gravity ($9.81 \text{ m}\cdot\text{s}^{-2}$). Replacing this equation
412 in Equation 12 and rearranging gives:

$$413 \quad W_M = \frac{[M]}{2t\alpha_M} \sqrt{\frac{12\mu_w K}{\rho_w g n_e}} \quad (14)$$

414 Derivation of Equation 14 stands on four fundamental assumptions. The first assumption is that
415 water in a thin soil cover percolates mainly through the macropores (Hornberger et al., 1990;
416 Velbel, 1993; Drever, 1997; Rodhe and Killingtveit, 1997), resulting in relatively short transit times
417 to the fracture network lying beneath, where water–mineral interactions will take place. The second

418 assumption is that flow in fractured rock units is limited to preferential flow paths and is slow given
419 the typically low hydraulic conductivity, thus resulting in extended travel time. The third
420 assumption is that infiltrating water pushes the old water ahead according to piston flow (Appelo
421 and Postma, 2005), meaning that solute transport occurs predominantly by advection. Equation 14
422 does not account for the time required by solutes to travel from dead ends along microfractures to
423 gravity flow fractures by diffusion (Meunier et al., 2007). Weathering rates calculated by this
424 equation may thus be overestimated. The fourth assumption is that the area available for weathering
425 reactions is restricted to minerals facing fracture walls with the same composition as the rocks in
426 which they occur, although this assumption is not valid for fractures that have been lined with silica
427 or other secondary products. Under such circumstances, the spring water chemistry will be
428 dominated by water–mineral interactions along the dominant flow paths and, more importantly, by
429 contact with the fracture walls and not by interactions with the whole inventory of minerals and
430 soils and solid rocks in the aquifer.

431

432

RESULTS

433

434 **Results of the Topographic Module**

435 The topographic module of the THROW model (Figure 3) was applied to the Digital Elevation
436 Model of Vouga basin (Figure 1), in the sector where springs were sampled (the granite area; Figure
437 2). Firstly, ArcHydro (ESRI, 2007) was used to delineate watersheds within that area, taking into
438 account the order i of the associated stream. The results are illustrated in Figure 4a. The number of
439 1st-order watersheds is 1241, covering an average area $A = 0.44 \text{ km}^2 \cdot \text{watershed}^{-1}$, whereas the
440 whole granite area encompasses a 6th-order watershed with an area $A = 955.39 \text{ km}^2$. A plot of A
441 versus i (Figure 4b) shows a firm correlation between these variables, confirming that Horton laws
442 of network composition hold for the studied area. In keeping with this observation, the generalized

443 relationship between morphologic parameters and order (Equation 1) can, for the granite area of the
444 Vouga River basin, be replaced by the function fitting the scatter points in Figure 4b. Using a least
445 squares method, it was found that such function is represented by an exponential equation:

$$446 \quad A = 0.1e^{1.49 \times i} \quad (R^2 = 0.99) \quad (15)$$

447 Secondly, a map of equivalent orders (i_{eq}) was drawn for the granite area (Figure 5) and discrete
448 orders were determined for each spring by evaluating the i_{eq} at the location coordinates of the spring
449 site. The results are summarized in Appendix 1. Most sampled springs (94%) emerge where $i_{eq} =$
450 1–3. Equation 15 can be used to extrapolate the catchment area of the springs if i is replaced by i_{eq}
451 in this equation. These areas vary from 0.4 to 180.9 km², although most of them (the ones with $i_{eq} =$
452 1–3) are smaller than 10 km². These results, also summarized in Appendix 1, are consistent with
453 previous reports (Pacheco and Van der Weijden, 2002).

454

455 **Results of the Hydrologic Module**

456

457 *Aquifer Hydraulic Parameters and Travel Times of Stream Watersheds*

458 The hydrologic module of the THROW model (Figure 3) could not be applied to the studied springs
459 because the required spring outflows were lacking. To compensate for this, the hydrologic
460 characterization of the region was based on the application of the THROW model to seven stream
461 watersheds located upstream of the hydrometric stations represented in Figure 1. The hydraulic
462 conductivities (K) and effective porosities (n_e) resulting from this characterization were then used as
463 proxies of the K and n_e values of the spring watersheds, as explained in the next section, which also
464 describes how groundwater travel times were downscaled from the larger (stream) the smaller
465 (spring) scales.

466 The hydrologic characterization of the stream watersheds is summarized in Table 1. The initial stage
467 of topographic characterization (1st-run of the topographic module; Figure 3) indicated that

468 watershed areas (A) range from 22 to 649 km², watershed volumes (V) from 7 to 317 km³ and water
469 channel lengths (L) from 24 to 177 km. Subsequent application of the Brutsaert method gave
470 numbers for hydraulic conductivity (K) and effective porosity (n_e). The application of the method to
471 Station 1 (location given in Figure 1) is illustrated in Figure 6. In this figure, black dots represent 17
472 years of monthly average stream flows compiled from the hydrographic record of the station
473 (period 1936/37–1953/54), available at the Portuguese National Water Institute (www.inag.pt). The
474 dashed lines are the lower envelopes to the scatter points. According to the Brutsaert method, the
475 intercept- y of these lines are parameters a_1 and a_3 of Equations 5a,b. For Station 1, $\log(a_1) = -19.5$
476 and $\log(a_3) = -22.5$. Combining these values with morphologic parameters of the watershed (A , V ,
477 L ; Table 1) in Equations 5a,b gives $K = 2.4 \times 10^{-7} \text{ m}\cdot\text{s}^{-1}$ and $n_e = 3.7 \times 10^{-2}$. The average K and n_e ,
478 when considering the values obtained for the seven watersheds, are $(4.7 \pm 3.2) \times 10^{-7} \text{ m}\cdot\text{s}^{-1}$ and
479 $(2.0 \pm 1.3) \times 10^{-2}$, respectively. These values are consistent with fractured rock hydraulic
480 conductivities and effective porosities (Domenico and Schwartz, 1990). Application of the
481 hydrograph method of Meyboom (1961) provided estimates for the aquifer recharge (V_r). The
482 application of the method to Station 1 is illustrated in Figure 7. As in Figure 6, the black dots are
483 discharge rate measurements representative of a given month. The straight lines are fits to base
484 flows of the recession periods. They are parallel because their slope is a function of the aquifer
485 hydraulic parameters (K and n_e), which do not change over the time scales represented in the graph
486 (two years). Based on the geometry of the dashed lines and on its relation with the base flow
487 measurements, values were determined for Q_f (180 L·s⁻¹), Q_i (21000 L·s⁻¹) and t_1 (100 days), which
488 have been used in Equation 9 to calculate V_r ($78 \times 10^6 \text{ m}^3$). This value is valid solely for the
489 hydrologic years 1939/40 and 1940/41, represented in Figure 7. For the entire record length of
490 Station 1 (17 hydrologic years), the average aquifer recharge is $57 \times 10^6 \text{ m}^3$, and when the seven
491 stations are taken altogether, $V_r = (53 \pm 39) \times 10^6 \text{ m}^3$ (Table 1). Finally, using the values of V , n_e and

492 V_r in Equation 10, average travel times of groundwater in the seven stream watersheds were
 493 calculated, varying from 7 to 107 years (Table 1).

494
 495 *Aquifer Hydraulic Parameters and Travel Times of Spring Watersheds*

496 The hydrologic parameters of spring watersheds were extrapolated from the values assessed at
 497 larger scales (previous section). Figure 8 plots travel time, hydraulic conductivity and effective
 498 porosity as a function of watershed area, using the values calculated for the seven stream
 499 watersheds (Table 1). The relationship between the hydrologic parameters and area is unequivocal,
 500 being expressive for t as:

$$501 \quad t = 0.16A + 1.37 \quad (R^2 = 0.98) \quad (16)$$

502 The bigger K and n_e values of larger basins reflect of the accentuated heterogeneity of these basins
 503 relative to the smaller ones (Domenico and Schwartz, 1990). The bigger travel times are inherently
 504 associated to longer flow paths. According to Equation 14, a simultaneous increase in K and n_e has
 505 a limited impact on the estimates of weathering rates (W), because W is a function of $(\sqrt{K/n_e})$. For
 506 the seven watersheds, the minimum value of $\sqrt{K/n_e}$ is $2.5 \times 10^{-3} \text{ m}^{1/2} \cdot \text{s}^{-1/2}$, whereas the maximum is
 507 $8.2 \times 10^{-3} \text{ m}^{1/2} \cdot \text{s}^{-1/2}$, so, regardless the values adopted for the aquifer hydraulic parameters the impact
 508 on weathering rates would not exceed a factor of 3.2. Contrarily to K and n_e , changes in t have a
 509 tremendous impact on those estimates, because W is a function of $1/t$. Based on this assessment, it
 510 was assumed that K and n_e were constant within the catchment areas of the springs and equal to the
 511 mean values estimated for the seven stream watersheds (Table 1): $K = 4.7 \times 10^{-7} \text{ m} \cdot \text{s}^{-1}$ and $n_e =$
 512 2.0×10^{-2} . On the other hand, Equation 16 was used to extrapolate (downscale) travel times for
 513 spring waters. These times varied from 1.4 to 30.3 years, but for springs with $A < 10 \text{ km}^2$, they
 514 ranged from 1.4 to 2.8 years. The entire record of spring water travel times is depicted in Appendix
 515 1.

516

517 **Results of the Weathering Module**

518 The hydrochemistry of springs in the Vouga basin and the chemical weathering of associated
519 granites and metasediments have been discussed in great detail by Van der Weijden and Pacheco
520 (2006). This study encompassed an application of the SiB algorithm to the spring water
521 compositions summarized in Appendix 1. The SiB mole balance calculator is one of the THROW
522 model components. For that reason, the results obtained in 2006 were adopted for the present study,
523 being summarized in Appendix 2. In brief, the analytical data indicated that chemical weathering of
524 plagioclase and biotite determined the inorganic chemical composition of the springs. For
525 plagioclase, it was calculated an average mass transfer of $[PI] = 148 \pm 56$ micromoles per liter of
526 water. In the geochemical calculations, it was assumed that plagioclase weathered into mixtures of
527 halloysite and, depending on whether rainfall was larger or smaller than $1000 \text{ mm}\cdot\text{y}^{-1}$, gibbsite or
528 smectite. It was also assumed that weathering of biotite produced mixtures of halloysite and
529 vermiculite. The results showed that weathering of plagioclase produced $[\text{smectite}] = 2 \pm 11 \text{ }\mu\text{M}$,
530 $[\text{halloysite}] = 68 \pm 42 \text{ }\mu\text{M}$ and $[\text{gibbsite}] = 14 \pm 21 \text{ }\mu\text{M}$, i.e. that halloysite is the dominant secondary
531 product precipitating along the flow paths.

532 For the calculation of plagioclase weathering rates (W_{PI}), it was assumed that the weight fraction of
533 this mineral in the granites was consistently $\alpha_{PL} = 0.31$. The remaining input data to the rate
534 equation (Equation 14) are the dissolved concentrations of plagioclase ($[PI]$) reported in Appendix
535 2, the spring water travel times of (t) listed in Appendix 1, and the aquifer hydraulic parameters (K
536 $= 4.7 \times 10^{-7} \text{ m}\cdot\text{s}^{-1}$ and $n_e = 2.0 \times 10^{-2}$). The calculated W_{PI} values are within the interval $(2.5 \pm 1.2) \times 10^{-14}$
537 $\text{mol}\cdot\text{m}^{-2}\cdot\text{s}^{-1}$ ($-\log(W) = 13.7 \pm 0.3$).

538

539

540

541

542

DISCUSSION

543

544 **Thermodynamic Validation of the SiB Results**

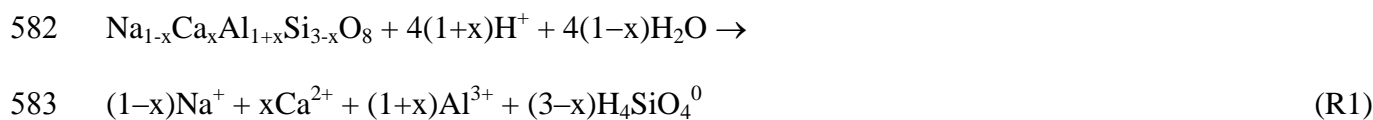
545 The concentrations of dissolved plagioclase ([Pl]) and the amounts of precipitated secondary
546 products ([gibbsite], [halloysite] and [smectite]) were determined by Van der Weijden and Pacheco
547 (2006) using mole balance calculations and are listed in Appendix 2. These results are supported by
548 equilibrium models. Paces (1978) reviewed the secondary phases that may control the
549 concentrations of Al and Si in natural waters. The order of increasing stability of aluminum
550 hydroxide phases is amorphous $\text{Al}(\text{OH})_3$, microcrystalline gibbsite, and gibbsite. The same order
551 for aluminosilicates is allophane, halloysite, and kaolinite. The calculated Q/K_{eq} ratios of these
552 secondary phases, where Q is the ion activity product (IAP) calculated from the activities of the
553 relevant dissolved species (Appendix 1) and K_{eq} is the solubility product, are reported in Appendix
554 2 (columns 8–13). Plots of the actual total Al concentrations in the spring waters against pH
555 (Appendix 1) can be compared with the equilibrium curves of these phases (Figures 9a,b). The
556 distribution of the measured values as well as the Q/K_{eq} values given in Appendix 2 show that
557 springs were in close equilibrium with microcrystalline gibbsite and halloysite/allophane.
558 Precipitation of metastable phases along the flow path of the fluids is consistent with the Ostwald
559 Step Rule. In general, Al hydroxide phases are expected to precipitate first, followed by
560 precipitation of aluminosilicates (Helgeson et al., 1969; Steefel and Lasaga, 1992). The studied
561 spring waters represented a mixture of water packets that followed different flow paths with
562 different velocities. Because the flow of groundwater across the granites is essentially through
563 fissures and fractures, it is impossible to determine exactly where the secondary products
564 precipitate. Simultaneous equilibrium with respect to gibbsite and halloysite, as calculated for 34
565 spring waters, could have occurred in a wider or narrower band along a characteristic flow path,
566 depending on the hydrodynamic dispersion (Steefel and Lasaga, 1992). Moreover, the ratio between

567 the kinetic dissolution and precipitation constants of the primary and secondary phases may have
 568 stretched the apparent stability fields of these phases, resulting in overlap instead of separation
 569 (Steeffel and Van Cappellen, 1990). The generally strong relation between the presence of ‘gibbsite’
 570 (SiB results) and degree of saturation with respect to microcrystalline gibbsite is shown in Figure
 571 10. The calculated amount of gibbsite precipitates ($[Gibbsite] > 0$) generally occurred within a
 572 rather narrow band of low saturation values. The samples with high Q/K_{eq} values relative to
 573 microcrystalline gibbsite were closer to equilibrium with amorphous $Al(OH)_3$ (Appendix 2).
 574 Analytical uncertainties in the determination of total dissolved Al, and consequently in the $\{Al^{3+}\}$
 575 values, were propagated in the accuracy and precision of the calculated Q values. For this reason,
 576 no rigid meaning is attributed to Q/K_{eq} values smaller than 1. The general correspondence between
 577 the results of the mass balance method (SiB) and the concomitant calculated equilibria makes a
 578 strong case for the precipitation of the metastable phases.

579

580 **Residual Undersaturation of Spring Waters with Respect to Plagioclase**

581 The congruent dissolution of plagioclase can be represented by the reaction:



584 with $K_{eq} = \{\text{Na}^+\}^{(1-x)} \{\text{Ca}^{2+}\}^x \{\text{Al}^{3+}\}^{(1+x)} \{\text{H}_4\text{SiO}_4^0\}^{(3-x)} / \{\text{H}^+\}^{4(1-x)}$

585 where x is the mole fraction of anorthite in plagioclase and $\{ \}$ represents activity.

586 The actual IAP (ion activity product) for reaction R1, calculated on the basis of the analytical data
 587 (Appendix 1), is generally smaller than K_{eq} . As explained in Appendix 2, the degree of
 588 undersaturation can be expressed as the Gibbs free energy of dissolution (ΔG_r). Most springs are
 589 undersaturated with respect to plagioclase (negative ΔG_r), the exceptions being springs 2070, 2071
 590 and 2072 (Appendix 2, last column). ΔG_r has been used as a key parameter in many kinetic
 591 dissolution models (Beig and Lüttge, 2006; Lasaga, 1998; Lüttge, 2006; Maher et al., 2009; and

592 numerous references therein). Its role in such models becomes more important as the solution
593 approaches equilibrium ($\Delta G_r \rightarrow 0$). Dissolution rates are highest and constant far from equilibrium
594 (i.e., the so-called dissolution plateau). During ongoing dissolution, undersaturation decreases and
595 approaches equilibrium in a linear fashion or in a sigmoidal manner characterized by a typical
596 critical ΔG_r^{crit} , beyond which the dissolution mechanism dramatically changes from a rapid to a
597 slow mode, proceeding linearly until equilibrium is realized (Burch et al, 1993; Hellman and
598 Tisserand, 2006). Other modes of dissolution rates as a function of ΔG_r have been observed and can
599 be explained by the presence and persistence of etch pits on the dissolving mineral surface (Oelkers
600 et al., 1994; Lüttge, 2006). Further discussion of the processes and mechanisms, and the underlying
601 theories and observations is beyond the scope of this paper. It is worth mentioning, however, that
602 the median and average values of ΔG_r ($-20 \text{ kJ}\cdot\text{mol}^{-1}$), as well as that of almost all individual values
603 calculated for the spring waters, were higher than the ΔG_r^{crit} of about $-28\pm 3 \text{ kJ}\cdot\text{mol}^{-1}$ for albite
604 (Burch et al., 1993; Arvidson and Lüttge, 2009), and were at least close to $\Delta G_r^{crit} \approx -18 \text{ kJ}\cdot\text{mol}^{-1}$
605 (Lasaga and Lüttge, 2004; Lüttge, 2006). This means that the rate of plagioclase dissolution had
606 already slowed once the ground water arrived at the spring site. It must be realized, however, that
607 the rates must have been much higher when the ground waters started their journey along the flow
608 channels. Considering that only the water composition at the terminals of the water flow were
609 known, the data do not allow for comparisons of the calculated weathering rates with kinetic
610 models of the dissolution rates of the plagioclases.

611

612 **Rates of Plagioclase Weathering**

613

614 *Comparison with Reported Weathering Rates*

615 Weathering rates calculated in the present study ($(2.5\pm 1.2)\times 10^{-14} \text{ mol}\cdot\text{m}^{-2}\cdot\text{s}^{-1}$) are very close to the
616 range of rates reported for Panola granite plagioclase: $(0.21-7)\times 10^{-14} \text{ mol}\cdot\text{m}^{-2}\cdot\text{s}^{-1}$ (White and

617 Brantley, 2003) measured in column-flow experiments after 6.2 years. Commonly reported
618 laboratory rates are, on average, around $4 \times 10^{-12} \text{ mol} \cdot \text{m}^{-2} \cdot \text{s}^{-1}$ (White and Brantley, 2003), and are
619 thus two to three orders of magnitude higher than the W_{PI} determined by this study. Laboratory
620 experiments, however, are usually conducted far from equilibrium conditions, with higher
621 fluid/rock ratios than field conditions, and under high temperatures and low pH, which accelerate
622 the dissolution reactions. Some experiments are conducted at ambient temperatures and at field-
623 similar pH, but researchers rarely attempt to restrict the fluid/rock ratios or use pre-weathered
624 samples.

625 The weathering rates reported in this study can also be compared with the field weathering rates
626 reported by other studies (Table 2). Considering the differences in weathering conditions (climate,
627 temperature, vegetation, soil thickness, age, etc.) and problems related to the determination of
628 exposed surface areas, the range of reported values is not surprising. Arvidson and Lüttge (2010)
629 argued that the complex chemical and thermal histories of the minerals along the reaction path have
630 importance for mineral reactivity in natural basins. This may thus be the cause of the apparent
631 variability in the reaction rates under natural weathering conditions. In addition, weathering rates
632 correlate better with the fluid residence times than with the age of the weathering materials (Maher,
633 2010). The W_{PI} values determined in our study depended on the calculated travel times of the fluids
634 and surface areas exposed to the fluids. Given these uncertainties, the weathering rates for
635 oligoclase obtained in our study compare well with the results obtained by other studies, as
636 summarized in Table 2.

637

638 *Influence of the Exposed Surface Area*

639 In the THROW model section (Hydrologic Module), a formula hinging on the volumetric fracture
640 density concept was presented and used to estimate the exposed surface area (Equation 13). This
641 method requires prior knowledge of the aquifer recharge (V_r), which is available for sub-basins of

642 the Vouga basin (Table 1). The exposed surface areas calculated by this method for these sub-
 643 basins were $A_{Pl} = 4.79 \times 10^{11} - 1.19 \times 10^{13} \text{ m}^2$ (median $3.83 \times 10^{12} \text{ m}^2$). If all plagioclase grains were in
 644 contact with the flowing groundwater, and not only the grains facing the fracture walls, then the
 645 exposed surface area would be given by:

$$646 \quad A_{Pl} = \gamma_{Pl} S_{Pl} \quad (17)$$

647 where γ_{Pl} (kg) is the mass of plagioclase grains in contact with aquifer water in unit time (one year)
 648 and S_{Pl} ($\text{m}^2 \cdot \text{kg}^{-1}$) is the geometric surface area of oligoclase, assumed to be $24.7 \pm 14.0 \text{ m}^2 \cdot \text{kg}^{-1}$
 649 (Blum, 1994). The value of γ_{Pl} can be deduced from the annual recharge (V_r , m^3), the effective
 650 porosity of the aquifer, the weight fraction of plagioclase (α_{Pl}) in the rock, and the specific weight
 651 of plagioclase (ρ_{Pl} , $\text{kg} \cdot \text{m}^{-3}$), as follows:

$$652 \quad \gamma_{Pl} = \frac{V_r}{n_e} \alpha_{Pl} \rho_{Pl} \quad (18)$$

653 Considering that the weight fraction of plagioclase in the Vouga granites is on average 0.31, and the
 654 specific weight of oligoclase is $2650 \text{ kg} \cdot \text{m}^{-3}$, the calculated area of oligoclase in the sub-basins,
 655 determined using Equation 17, is $A_{Pl} = 1.67 \times 10^{13} - 1.03 \times 10^{14} \text{ m}^2$ (median $5.04 \times 10^{13} \text{ m}^2$). The ratios
 656 between the exposed surface areas, estimated using Equation 13 and Equation 17, are
 657 $1.34 \times 10^{-2} - 3.75 \times 10^{-1}$ (median 8.63×10^{-2}). The results show that, due to the inhomogeneous fluid
 658 migration through the fracture networks, the area of fluid–mineral interactions is reduced to some
 659 9% of the total area available for reaction. Identical results were obtained by Pacheco and Alençõo
 660 (2006).

661

662

CONCLUSIONS

663

664

665

666 artesian springs. The distinctive points of the THROW model include an assessment of
667 morphologic parameters of spring watersheds based on scaling properties of the drainage networks,
668 known as the Horton laws (Horton, 1945), and an evaluation of the area of minerals exposed to the
669 percolating fluids using a formula based on fracture spacings, openings and porosities (Snow, 1968;
670 Pacheco and Alençoo, 2006). The methods used to estimate spring watershed areas and
671 groundwater travel times indicate that most fracture artesian springs in the Vouga basin granites are
672 fed by catchments with areas ranging from 0.4 to 8.9 km², and that the travel time of water emitted
673 from these springs is 1.4 to 2.8 years. The chemical composition of the springs, all sampled in the
674 early summer season, is the result of weathering of minerals exposed to percolating waters at
675 fracture surfaces, especially oligoclase; the proportion of solutes acquired by spring waters in
676 contact with saprolitic plagioclases along the weathering front is assumed to be insignificant. The
677 oligoclase weathering rates (W_{Pl}) were within the interval $(2.5 \pm 1.2) \times 10^{-14}$ mol·m⁻²·s⁻¹, which is very
678 close to the range of rates determined in granite environments under field conditions in other studies
679 (White and Brantley, 2003; among others). In general, the waters collected at the spring sites in the
680 Vouga granites were in equilibrium with microcrystalline gibbsite and(or) halloysite/allophane, and
681 undersaturated with respect to albite-oligoclase. The range of the calculated dissolution rates was, at
682 least in part, caused by the fact that the spring waters consist of packets of water that are exposed to
683 different pathways and travel times that have been in contact with fresh and weathered oligoclases.
684

685 **References**

686

687 Anderson, G.M. (1996). *Thermodynamics of Natural Systems*. John Wiley & Sons, Inc. New York
688 etc., 382 pp.

689

690 Appelo, C.A.J., Postma, D. (2005). *Geochemistry, Groundwater and Pollution*. A.A. Balkema,
691 Rotterdam, 649 pp.

692

693 Arvidson, R.S., Lüttge, A. (2010). Mineral dissolution kinetics as a function of distance from
694 equilibrium—New experimental results. *Chem. Geol.* 269:79–88.

695

696 Beig, M.S., Lüttge, A. (2006). Albite dissolution kinetics as a function of distance from
697 equilibrium: Implications for natural feldspar weathering. *Geochim. Cosmochim. Acta* 70: 1402–
698 1420.

699

700 Berner, R.A., Lasaga, A.C., Garrels, R.M. (1983). The carbonate-silicate geochemical cycle and its
701 effect on atmospheric carbon dioxide over the past 100 Million years. *Am. J. Sci.* 283: 641–683.

702

703 Blum, A.E. (1994). Feldspars in weathering. In Parson, I. (Ed.) *Feldspars and Their Reactions*.
704 Kluwer Academic Publishers, Dordrecht, The Netherlands. p. 595–630.

705

706 Bolin, B., Rodhe, H. (1973). A note on the concepts of age distribution and transit time in natural
707 reservoirs. *Tellus* 25(1): 58–62.

708

709 Boussinesq, J. (1877). Essai sur la théorie des eaux courantes. *Mem. Acad. Sci. Inst. Fr.* 23: 252–
710 260.

711

712 Boussinesq, J. (1903). Sur le débit, en temps de sécheresse, d'une source alimentée par une nappe
713 d'eaux d'infiltration. *C. R. Hebd. Seanc. Acad. Sci. Paris* 136: 1511–1517.

714

715 Boussinesq, J. (1904). Recherches théoriques sur l'écoulement des nappes d'eau infiltrées dans le
716 sol et sur débit de sources. *J. Math. Pures Appl.* 10: 5–78.

717

718 Brantley, S.L., Mellott, N.P. (2000). Surface area and porosity of primary silicate minerals. *Am.*
719 *Mineral.* 58: 1767–1783.

720

721 Brantley, S.L., White, A.F., Hodson, M.E. (1999). Surface area of primary silicate minerals.
722 Chapter 14 in B. Jamtveit & P. Meakin (Eds.). *Growth, dissolution and pattern formation in*
723 *geosystems*. Kluwer Academic Publishers. p. 291–326.

724

725 Brutsaert, W. (1994). The unit response of groundwater outflow from a hillslope. *Water Resour.*
726 *Res.* 34: 233–240.

727

728 Brutsaert, W., Lopez, J.P. (1998). Basin-scale geohydrologic drought flow features of riparian
729 aquifers of the southern Great Plains. *Water Resour. Res.* 30: 2759–2763.

730

731 Brutsaert, W., Nieber, J.L. (1977). Regionalized drought flow hydrographs from a mature glaciated
732 plateau. *Water Resour. Res.* 13: 637–643.

733

- 734 Burch, T.E., Nagy, K.L., Lasaga, A.C. (1993). Free energy dependence of albite dissolution kinetics
735 at 80°C and pH 8.8. *Chem. Geol.* 105: 137–162.
736
- 737 Caetano, C.A.R., Pacheco, F.A.L. (2008). Modelação de escoamentos fluviais na região de Trás-os-
738 Montes e Alto Douro utilizando o modelo SWAT. In: V Seminário Recursos Geológicos, Ambiente
739 e Ordenamento do Território, UTAD, Vila Real, 16–18 October 2008. Special Volume in CD-
740 ROM, p. 44–53.
741
- 742 Cooper, H.H. Jr., Rorabaugh, M.I. (1963). Groundwater movements and bank storage due to flood
743 stages in surface streams. *USGS Water Supply Paper 1536-J*: 343–366.
744
- 745 De Bartolo, S.G., Gabriele, S., Gaudio, R. (2000). Multifractal behaviour of river networks.
746 *Hydrology and Earth System Sciences* 4(1): 105–112.
747
- 748 De Bartolo, S.G., Gaudio, R., Gabriele, S. (2004). Multifractal analysis of river networks: a sand-
749 box approach. *Water Resour. Res.* 40: 1–10.
- 750 De Bartolo, S.G., Veltri, M., Primavera, L. (2006). Estimated generalized dimensions of river
751 networks. *J. Hydrol.* 322: 181–191.
752
- 753 Domenico, P.A., Schwartz, F.W. (1990). *Physical and Chemical Hydrogeology*. John Wiley & Sons
754 Inc., New York, 824pp.
755
- 756 Drever, J.I. (1997). Weathering processes. In: Saether, P.M., de Caritat, P. (Eds.). *Geochemical
757 processes, weathering and groundwater recharge in catchments*. A.A. Balkema, Rotterdam /
758 Brookfield. p. 3–19.
759
- 760 Drever, J.I., Clow, D.W. (1995). Weathering rates in catchments. In: A.F. White & S.L. Brantley
761 (Eds.). *Chemical Weathering Rates of Silicate Minerals*. Reviews in Mineralogy, Volume 31,
762 Mineralogical Society of America, Washington D.C., USA. p. 463–483.
763
- 764 Dupré, B., Dessert, C., Oliva, P., Goddérís, Y., Viers, J., François, L., Millot, R., Gaillardet, J.
765 (2003). Rivers, chemical weathering and Earth's climate. *C.R. Geosci.* 335: 1141–1160.
766
- 767 ESRI (2007). *ArcMap* (version 9.3). New York St., Redlands, USA, 131p.
768
- 769 ESRI (2009). *ArcHydro Tools – Tutorial* (version 1.3). New York St., Redlands, USA, 131p.
770
- 771 Etcheverry, D., Perrochet, P., (2000). Direct simulation of groundwater transit-time distributions
772 using the reservoir theory. *Hydrogeology Journal* 8(2): 200–208.
773
- 774 Faure, G. (1998). *Principles and Applications of Geochemistry* (2nd edition). Prentice Hall, Upper
775 Saddle River, NJ, USA, 600 pp.
776
- 777 Gaudio, R., De Bartolo, S.G., Primavera, L., Gabriele, S., Veltri, M. (2006). Lithologic control on
778 the multifractal spectrum of river networks. *J. Hydrol.* 327: 365–375.
779
- 780 Goddérís, Y., François, L.M., Probst, A., Schott, J., Moncoulon, D., Labat, D., Viville, D. (2006).
781 Modelling weathering processes at the catchment scale: the WITCH numerical model. *Geochim. et
782 Cosmochim. Acta* 70, 1128–1147.
783

- 784 Godd ris, Y., Roelandt, C., Schott, J., Pierret, M.C., Francois, L.M. (2009). Towards an integrated
785 model of weathering, climate, and biospheric processes. In: Oelkers, E.H., Schott, J. (Eds.),
786 *Thermodynamics and Kinetics of Water–Rock Interaction*. Mineralogical Soc Amer., Vol. 70, p.
787 411–434.
788
- 789 Godinho, M.M. (1980). O Plutonito do Caramulo. Mem rias e Not cias, publica es do Museu e
790 Laborat rio Mineral gico e Geol gico da Universidade de Coimbra, 89/90: 269 pp.
791
- 792 Griffiths, G.A., Clausen, B. (1997). Streamflow recession in basins with multiple water storages. *J.*
793 *Hydrol.* 190: 60–74.
794
- 795 Hartmann, J., Jansen, N., D rr, H.H., Kempe, S, K hler, P. (2009). Global CO₂-consumption by
796 chemical weathering: What is the contribution of highly active weathering regions? *Global Planet.*
797 *Change* 69: 185–194.
798
- 799 Helgeson, H.C., Garrels, R.M., Mackenzie, F.T. (1969). Evaluation of irreversible reactions in
800 geochemical processes involving minerals and aqueous solutions—II. Applications. *Geochim.*
801 *Cosmochim. Acta* 33: 455–481.
802
- 803 Hellmann, R., Tisserand, D. (2006). Dissolution kinetics as a function of the Gibbs free energy of
804 reaction: An experimental study based on albite feldspar. *Geochim. Cosmochim. Acta* 70: 364–383.
805
- 806 Hornberger, G.M., Beven, K.J., Germann, P.E. (1990). Interferences about solute transport in
807 macroporous forest soils from time series models. *Geoderma* 46: 249–262.
808
- 809 Horton, R. E. (1945). Erosional development of streams and their drainage basins: hydrophysical
810 approach to quantitative morphology. *Geol. Soc. Am. Bull.* 56: 275–370.
811
- 812 La Barbera, P., Rosso, R. (1987). Fractal geometry of river networks. *Trans. Am. Geophys. Union*
813 68: 1276.
814
- 815 La Barbera, P., Rosso, R. (1989). On the fractal dimension of stream networks. *Water Resour. Res.*
816 25: 735–741.
817
- 818 Langmuir, D. (1997). *Aqueous Environmental Geochemistry*. Prentice Hall, Upper saddle River,
819 New Jersey, USA, 600 pp.
820
- 821 Lasaga, A.C. (1998). *Kinetic Theory in the Earth Sciences. Princeton Series in Geochemistry*
822 (Holland, H.D., editor). Princeton University Press. Princeton, New Jersey, 811 pp.
823
- 824 Lasaga, A.C., L ttge, A. (2004). Mineralogical approaches to fundamental crystal dissolution
825 kinetics—Dissolution of an A₃B structure. *Eur. J. Mineral.* 16: 713–729.
826
- 827 L ttge, A. (2005). Etch pit coalescence, surface area, and overall mineral dissolution rates. *Am.*
828 *Mineral.* 90: 1767–1783.
829
- 830 L ttge, A. (2006). Crystal dissolution kinetics and Gibbs free energy. *J. Electronic Spectroscopy*
831 *and Related Phenomena* 150: 248–259.
832

- 833 Maher, K. (2010). The dependence of chemical weathering rates on fluid residence time. *Earth*
834 *Planet. Sci. Letters* 294: 101–110.
835
- 836 Maher, K., Steefel, C.I., White, A.F., Stonestrom, D.A. (2009). The role of reaction affinity and
837 secondary minerals in regulating chemical weathering rates at the Santa Cruz Soil
838 Chronosequence, California. *Geochim. Cosmochim. Acta* 73: 2804–2831.
839
- 840 Malvicini, C. F., Steenhuis, T. S., Walter, M. T., Parlange, J.-Y., Walter, M. F. (2005). Evaluation
841 of spring flow in the uplands of Matalom, Leyte, Philippines. *Adv. Water Resour.*, 28: 1083–1090.
842
- 843 Martins (1985). Caracterização sumária dos solos de Trás-os-Montes e Alto Douro e sua ocupação.
844 Technical Report, Instituto Universitário de Trás-os-Montes e Alto Douro, 30 pp.
845
- 846 Martins, A.A.A., Madeira, M.V., Refega, A.A.G. (1995). Influence of rainfall on properties of soils
847 developed on granite in Portugal. *Arid Soil Res. Rehabil.* 9, 353–366.
848
- 849 McGuire, K.J., McDonnell, J.J. (2006). A review and evaluation of catchment transit time
850 modelling. *J. Hydrol.* 330: 543–563.
851
- 852 Medina, J.M.P.G. (1996). Contribuição para o Conhecimento da Geologia do Grupo das Beiras
853 (CXG) na Região do Caramulo–Buçaco (Portugal Central). PhD thesis, University of Aveiro, 183
854 pp.
855
- 856 Mendoza, G.F., Steenhuis, T.S., Walter, M.T., Parlange, J.Y. (2003). Estimating basin-wide
857 hydraulic parameters of a semi-arid mountainous watershed by recession flow analysis. *J. Hydrol.*
858 *279: 57–69.*
859
- 860 Meunier, A., Sardini, P., Robinet, J.C., Prêt, D. (2007). The petrography of weathering processes:
861 facts and outlooks. *Clay Miner.* 42: 415–435.
862
- 863 Meyboom, P. (1961). Estimating groundwater recharge from stream hydrographs. *J. Geophys. Res.*
864 *66: 1203–1214.*
865
- 866 Nikora, V.I., Sapozhnikov, V.B. (1993). River network fractal geometry and its computer
867 simulation. *Water Resour. Res.* 29: 3565–3575.
868
- 869 Nordstrom, D.K., Plummer, L.N., Langmuir, D., Busenberg, E., May, H.M., Jones, B.F., Parkhurst,
870 D.L. (1990). Revised chemical equilibrium data for major water–mineral reactions and their
871 limitations. In: *Chemical Modeling of Aqueous Systems II*. (Eds. Melchior D.C. and Bassett, R.L.).
872 ACS Symposium Series 416. American Chemical Society, Washington, DC 1990, pp. 398–413.
873
- 874 Oelkers, E.H., Schott, J., Devidal, J-L. (1994). The effect of aluminium, pH, and chemical affinity
875 on the rates of aluminosilicate dissolution reactions. *Geochim. Cosmochim. Acta* 58: 2011–2024.
876
- 877 Oliva, P., Viers, J, Dupré, B. (2003). Chemical weathering in granitic environments. *Chem. Geol.*
878 *202: 225–256.*
879
- 880 Paces, T. (1978). Reversible control of aqueous aluminum and silicate during the irreversible
881 evolution of natural waters. *Geochim. Cosmochim. Acta* 42: 1487–1493.
882

- 883 Pacheco, F.A.L., Alencão, A.M.P. (2006). Role of fractures in weathering of solid rocks:
884 narrowing the gap between experimental and natural weathering rates. *J. Hydrol.* 316: 248–265.
885
- 886 Pacheco, F.A.L., Van der Weijden, C.H. (1996). Contributions of water–rock interactions to the
887 composition of groundwater in areas with sizeable anthropogenic input. A case study of the waters
888 of the Fundão area, central Portugal. *Water Resour. Res.* 32: 3553–3570.
889
- 890 Pacheco, F.A.L., Van der Weijden, C.H. (2002). Mineral weathering rates calculated from spring
891 water data. A case study in an area with intensive agriculture, the Morais massif, NE Portugal. *Appl.*
892 *Geochem.* 17: 583–603.
893
- 894 Pacheco, F.A.L., Sousa Oliveira, A., Van der Weijden, A.J., Van der Weijden, C.H. (1999).
895 Weathering, biomass production and groundwater chemistry in an area of dominant anthropogenic
896 influence, the Chaves–Vila Pouca de Aguiar region, north of Portugal. *Water Air Soil Poll.* 115:
897 481–512.
898
- 899 Padilla, A., Pulido-Bosh, A., Mangin, A. (1994). Relative importance of baseflow and quickflow
900 from hydrographs of karst spring. *Ground Water* 32: 267–277.
901
- 902 Press, W.H., Flannery, B.P., Teukolsky, S.A., Vetterling, W.T. (1991), *Numerical Recipes in Pascal*,
903 Cambridge University Press, Cambridge, Massachusetts.
904
- 905 Rasse, D.P., Francois, L.M., Aubinet, M., Kowalski, A.S., Vande Walle, I., Laitat, E., Ge´rard, J.C.
906 (2001). Modelling short-term CO₂ fluxes and long-term tree growth in temperate forests with
907 ASPECTS. *Ecol. Modell.* 141, 35–52.
908
- 909 Rodhe, A., Killingtveit, A. (1997). Catchment hydrology. In: Saether, O.M. & de Caritat, P. (Eds.).
910 *Geochemical Processes, Weathering and Groundwater Recharge in Catchments*. A.A. Balkema.
911 Rotterdam / Brookfield, pp. 77–107.
912
- 913 Roelandt, C., Godderis, Y., Bonnet, M.P., Sondag, F. (2010). Coupled modeling of biospheric and
914 chemical weathering processes at the continental scale. *Global Biogeochemical Cycles* 24, 18.
915
- 916 Rosso, R., Enechi, B. La Barbera, P. (1991). Fractal relation of mainstream length to catchment area
917 in river networks. *Water Resour. Res.* 27: 381–387.
918
- 919 Roth, G., La Barbera, P., Greco, M. (1996). On the description of the basin effective drainage
920 structure, *J. Hydrol.*, 187(1-2): 119–135.
921
- 922 Rueda, F., Moreno-Ostos, E., Armengol, J. (2006). The residence time of river water in reservoirs.
923 *Ecological Modelling* 191(2): 260–274.
924
- 925 Rupp, D. E., Selker, J. S. (2005). Drainage of a horizontal Boussinesq aquifer with a power law
926 hydraulic conductivity profile, *Water Resour. Res.*, 41: W11422, doi:10.1029/2005WR004241.
927
- 928 Rupp, D. E., Selker, J. S. (2006). Drainage of a horizontal Boussinesq aquifer with a power law
929 hydraulic conductivity profile, *Water Resour. Res.*, 42: W12421, doi:10.1029/2006WR005080.
930

- 931 Schermerhorn, L.J.G. (1956). Igneous, Metamorphic and Ore Geology of the Castro d'Aire-São
932 Pedro do Sul region (northern Portugal). Ph.D thesis, University of Amsterdam, 617 pp.
933
- 934 Schuller, D.J., Rao, A.R., Jeong, G.D. (2001). Fractal characteristics of dense stream networks. *J.*
935 *Hydrol.* 243: 1–16.
936
- 937 Schumm, S.A. (1956). Evolution of drainage systems and slopes in Badlands at Perth Amboy, New
938 Jersey. *Geol. Soc. Amer. Bull.* 67: 597–646.
939
- 940 Snow, D.T. (1968). Rock fracture spacings, openings, and porosities. *J. Soil Mechanics*, 94: 73–91.
941
- 942 Soen, O.I. (1958). The Geology, Petrology and Ore Deposits of the Viseu region, northern Portugal.
943 PhD thesis, University of Amsterdam, 179 pp.
944
- 945 Steefel, C.I., Lasaga, A.C. (1992). Putting transport into water-rock interaction models. *Geology*
946 20: 680–684.
947
- 948 Steefel, C.I., Van Cappellen, P. (1990). A new kinetic approach to modeling water-rock interaction:
949 The role of nucleation, precursors, and Oswald ripening. *Geochim. Cosmochim. Acta* 54: 2657–
950 2677.
951
- 952 Strahler, A.N. (1952). Hypsometric (area-altitude) analysis of erosional topography. *Geological*
953 *Society American Bulletin* 63: 1117–1142.
954
- 955 Strahler, A. N. (1957). Quantitative analysis of watershed geomorphology. *Transactions of the*
956 *American Geophysical Union* 8(6): 913–920.
957
- 958 Szilagyi, J., Parlange, M.B. (1999). A geomorphology-based semi-distributed watershed model.
959 *Adv. Water Resour.* 23: 177–187.
960
- 961 Szilagyi, J., Parlange, M.B., Albertson, J.D. (1998). Recession flow analysis for aquifer parameter
962 determination. *Water Resour. Res.* 34(7): 1851–1857.
963
- 964 Tarboton, D.G. (1996). Fractal river networks, Horton's laws and Tokunaga cyclicity. *J. Hydrol.*
965 187: 105–117
966
- 967 Tardy Y., Bustillo V., Boeglin J. (2004). Geochemistry applied to the watershed survey: hydrograph
968 separation, erosion and soil dynamics. A case study: the basin of the Niger River, Africa. *Appl.*
969 *Geochem.* 19: 469–518.
970
- 971 Van de Giesen, N. C., Steenhuis, T. S., Parlange, J.-Y. (2005). Short- and long-time behavior of
972 aquifer damage after slow and sudden recharge according to the linearized Laplace equation. *Adv.*
973 *Water Resour.*, 28: 1122– 1132.
974
- 975 Van der Weijden, C.H., Pacheco, F.A.L. (2006). Hydrogeochemistry in the Vouga River basin
976 (central Portugal): pollution and chemical weathering. *Appl. Geochem.* 21: 580–613.
977
- 978 Velbel, M.A. (1985). Geochemical mass balances and weathering rates in forested watersheds of
979 the Southern Blue Ridge. *Am. J. Sci.* 285: 904–930.
980

- 981 Velbel, M.A. (1989). Effect of chemical affinity on feldspar hydrolysis rates in two natural
982 weathering systems. *Chem. Geol.* 78: 245–253.
983
- 984 Velbel, M.A. (1993). Constancy of silicate–mineral weathering-rate ratios between natural and
985 experimental weathering: implications for hydraulic control of differences in absolute rates. *Chem.*
986 *Geol.* 105: 89–99.
987
- 988 Violette, A., Godd ris, Y, Mar chal, J, Riotte, J, Oliva, P, Kumar, M.S.M., Sekhar, M., Braun, J.
989 (2010). Modelling the chemical weathering fluxes at the watershed scale in the Tropics (Mule Hole,
990 South India): Relative contribution of the smectite/kaolinite assemblage versus primary minerals.
991 *Chem. Geol.* 277: 42–60.
992
- 993 White, A.F. (2002). Determining mineral weathering rates based on solid and solute weathering
994 gradients and velocities: application to biotite weathering in saprolites. *Chem. Geol.* 190: 69–89.
995
- 996 White, A.F., Brantley, S.L. (2003). The effect of time on the weathering of silicate minerals: why
997 do weathering rates differ in the laboratory and field? *Chem. Geol.* 202: 479–506.
998
- 999 White, A.F., Peterson, M. (1990a). The role of reactive surface areas in chemical weathering. *Chem.*
1000 *Geol.* 84: 334–336.
1001
- 1002 White, A.F., Peterson, M. (1990b). Role of reactive-surface-area characterization in geochemical
1003 kinetic models. In: D.C. Melchior and R.L. Bassett (Eds.). *Chemical Modelling of Aqueous Systems*
1004 II. ACS Symposium Series 416. Am. Chem. Soc., Washington, DC. p. 459–475.
1005
- 1006 White, A.F., Bullen, T.D., Schulz, M.S., Blum, A.E., Huntington, T.G., Peters, N.E. (2001).
1007 Differential rates of feldspar weathering in granitic regoliths. *Geochim. Cosmochim. Acta* 65: 847–
1008 869.
1009
- 1010 Zhang, L., Luttge, A. (2009). Theoretical approach to evaluating plagioclase dissolution
1011 mechanisms. *Geochim. Cosmochim. Acta* 73: 2832–2849.
1012
- 1013 Zecharias, Y.B., Brutsaert, W. (1985). Ground surface slope as a basin scale parameter. *Water*
1014 *Resour. Res.* 21:1895–902.
1015
- 1016 Zecharias, Y.B., Brutsaert, W. (1998). Recession characteristics of groundwater outflow and base
1017 flow from mountainous watersheds. *Water Resour. Res.* 24:1651–8.
1018

1019 **Table legends**

1020

1021

1022 Table 1:

1023 Morphologic and hydrologic characterization of seven watersheds within the Vouga River

1024 hydrographic basin. Id – Label of the hydrometric station located at the outlet of the watershed, in

1025 agreement with labels in Figure 1; Code – identification of code of the hydrometric station; X, Y –1026 location coordinates of the hydrometric station, in the Hayford-Gauss system; V, A and L – volume1027 and area of the watershed and length of water channels within the watershed; a_1, a_3 – intercept-y of1028 the dashed lines in Figure 7; K, n_e – average hydraulic conductivity and effective porosity of the1029 watershed; Q_i, Q_f – average base flow discharge rates at the start and end of recession periods; V_r –1030 average annual recharge; t – average groundwater travel time. The average values pertain to the

1031 record length of each station.

1032

1033 Table 2:

1034 Summary of field weathering rates ($W, \text{mol}\cdot\text{m}^{-2}\cdot\text{s}^{-1}$) of oligoclases. References other than this study:

1035 1) Drever and Clow (1995), 2) Velbel (1985), 3) White et al. (2001), 4) White and Brantley (2003).

1036

1037 Legends to Figures

1038

1039 Figure 1:

1040 Location of Vouga river basin in the North of Portugal and next to the Atlantic Ocean. Digital
1041 Elevation Model (DEM) of the basin with reference to surrounding mountains (Lapa, Caramulo and
1042 Freita) and to the mouth area in the Ria de Aveiro. Distribution of precipitation (P) and of
1043 hydrometric stations (labeled circles) inside the basin. The labels of the circles agree with the Id
1044 numbers in Table 1.

1045

1046 Figure 2:

1047 Simplified geological map of Vouga river basin. Adapted from the Geological Map of Portugal,
1048 scale 1/500 000, produced in 1992 by the Portuguese Geological Survey. Distribution of the
1049 sampled springs (labeled black dots) within the granite area of the basin. The labels of the dots
1050 agree with Sample # in Appendix 1.

1051

1052 Figure 3: Flowchart of the THROW model.

1053

1054 Figure 4a:

1055 Distribution of watersheds within the granite area of the Vouga basin, taking into account their
1056 order of Strahler (classification according to Strahler, 1957). Symbols: i – Strahler order; n , A –
1057 number and average area of watersheds of a given order.

1058

1059 Figure 4b:

1060 Plot of stream watershed area as a function of Strahler order, illustrating the firm relationship
1061 existing between these variables.

1062

1063 Figure 5:

1064 Distribution of equivalent spring orders (shaded areas) and location of the sampled (circles), within
1065 the granite area of the Vouga basin. Location of hydrometric stations labeled Id = 1–3 in Table 1.
1066 Symbol: i_{eq} – equivalent spring order (calculated by Equation 2). The i_{eq} under each spring can be
1067 used in Equation 15 (replacing i) to extrapolate the area of its associated watershed.

1068

1069 Figure 6:

1070 Application of the Brutsaert method to the watershed located upstream Station 1 (see location in
1071 Figure 1). The original data used in the plot pertains to the 1936-53 period and is available at
1072 www.inag.pt. The method is used to calculate the average watershed hydraulic conductivity and
1073 effective porosity (Equations 5a,b): $K = 2.4 \times 10^{-7} \text{ m} \cdot \text{s}^{-1}$; $n_e = 3.7 \times 10^{-2}$.

1074

1075 Figure 7:

1076 Stream hydrograph of Station 1 (see location in Figure 1 and summary of data in Table 1). The
1077 record of discharge rate measurements (Q) is available at www.inag.pt. Illustration of the
1078 hydrograph method used for the estimation of V_r (Meyboom, 1961), taking into account the values
1079 of Q_i , Q_f , and t_1 obtained for the 1939/40 and 1940/41 recessions. The explanation of the symbols is
1080 given in the text. For this pair of recession periods, $V_r = 78 \times 10^6 \text{ m}^3$ (Equation 9).

1081

1082 Figure 8:

1083 Plot of hydraulic conductivity, effective porosity and groundwater travel time, as a function of
1084 stream watershed area, illustrating the unequivocal (firm in the case of t) relationship existing
1085 between these variables.

1086

1087 Figure 9:
1088 Total Al concentrations (open symbols), as far as they were determined, and theoretical total
1089 concentrations (curves) plotted against pH for (a) crystalline gibbsite, microcrystalline gibbsite and
1090 amorphous $\text{Al}(\text{OH})_{3(s)}$, and (b) kaolinite, halloysite and allophane. Total Al concentrations and pH
1091 values at the sampling sites are listed in Appendix 1. The curves for the solid phases as a function
1092 of pH are calculated from data in Nordstrom et al. (1990) for $\text{Al}(\text{OH})_3$ -phases and in Langmuir
1093 (1997) for the Al-silicate phases. In the last case, the H_4SiO_4^0 activity was fixed at its median value
1094 (Appendix 1). Note that the distances between the curves for each solid phase turn out to be only
1095 very small when instead of the median value the minimum and maximum values of H_4SiO_4^0
1096 activities would have been used. It appears that the solutions are most closely in equilibrium with
1097 microcrystalline gibbsite and(or) halloysite/allophane (cf. also columns 8–13 in Appendix 2).

1098
1099 Figure 10:
1100 Plot of the calculated amounts* of ‘gibbsite’ precipitated from the ground water as result of ongoing
1101 dissolution of plagioclase, against the calculated degree of saturation of microcrystalline gibbsite
1102 (Appendix 2). Quite a few samples for which precipitation of ‘gibbsite’ was calculated (SiB results)
1103 are indeed close to equilibrium (cf. also Appendix 2, column 9) with microcrystalline gibbsite. For
1104 the other samples, no precipitation of ‘gibbsite’ was calculated, but many of these samples are also
1105 located in areas where $P < 1000 \text{ mm}\cdot\text{y}^{-1}$, areas where the occurrence of gibbsite in soils is unlikely
1106 (Martins et al., 1995). Some waters (springs nrs. 1038, 2070, 2079, 2089 and 2101), although
1107 highly supersaturated relative to microcrystalline gibbsite ($Q/K_{\text{eq}} > 5$) and located in areas where P
1108 $> 1000 \text{ mm}\cdot\text{y}^{-1}$ (see Appendix 2), had nonetheless $[\text{Gibbsite}] = 0 \text{ }\mu\text{M}$.

1109 *We recognize that the presence, not the amount of ‘gibbsite’ matters.

1110

1111 **Legends For the Appendices.**

1112

1113 Appendix 1:

1114 The identification code of the sampled and analyzed springs (Sample #) is given in Column 1. The
1115 results from the hydrological analysis are presented in Columns 2–4. The pHs of the springs are
1116 listed in Column 5. The concentrations of the dissolved species are given in brackets in Columns 6–
1117 15, and their concomitant activities, calculated using the Davies equation, are given in braces in
1118 Columns 16–20. The calculation of $\{Al^{3+}\}$ at 15°C is based on hydrolysis constants for Al^{3+} in
1119 Nordstrom et al. (1990).

1120

1121

1122 Appendix 2:

1123 The identification code of the sampled and analyzed springs (Sample #) is given in Column 1.
1124 Column 2 reports the annual rainfall in the vicinity of the spring sites (in agreement with Figure 1).
1125 COLUMNS 3–7 summarize the results of the SiB model (Van der Weijden and Pacheco, 2006): x is the
1126 anorthite fraction of plagioclase assumed in the model, indicating a compositional range from albite
1127 to oligoclase, [Pl] is the contribution of plagioclase dissolution to the water chemistry, whereas
1128 [smectite], [halloysite] and [gibbsite] are their calculated amounts of aluminosilicate and aluminum
1129 hydroxide phases precipitated along the flow path. Columns 8–14 list the results of the
1130 thermodynamic analyses: the Q -values (ion activity products) were calculated from the relevant
1131 activities of the species involved in the equilibria of the secondary solid phases. The concomitant
1132 K_{eq} values in Columns 8–10 were adopted from Nordstrom et al. (1990), the ones in Columns 11–
1133 13 from Langmuir (1997). The ΔG_r values in Column 14, pertaining to the congruent dissolution of
1134 the plagioclases (reaction R1), were calculated using the relation: $\Delta G_r = 2.303RT(\log Q - \log K_{eq})$,
1135 where R is the gas constant (in $\text{kJ}\cdot\text{mol}^{-1}\cdot\text{K}^{-1}$) and T the temperature (in K), Q is the actual ion
1136 activity product of the species involved in the dissolution reaction, and $\log K_{eq} = -\Delta G_r^0 / 2.303RT$.

1137 The ΔG_r^0 values for reaction R1 were calculated from the ΔG_f^0 values of the plagioclases (with x as
1138 in Column 3) and the concomitant dissolved species as given in Anderson (1996) and Faure (1998).
1139 All values were calculated for 15°C by application of the Van 't Hoff equation using the enthalpies
1140 of the dissolution reactions (ΔH_r^0) derived from the ΔH_f^0 values listed in the two last mentioned
1141 textbooks. The final column gives the weathering rates calculated as explained in the text.

1 **INTEGRATING TOPOGRAPHY, HYDROLOGY AND ROCK STRUCTURE IN**
2 **WEATHERING RATE MODELS OF SPRING WATERSHEDS**

4 Fernando A. L. Pacheco,^a

5 Department of Geology & Centre for Chemistry,
6 Trás-os-Montes and Alto Douro University, Ap 1013, 5000 Vila Real
7 Portugal

9 Cornelis H. Van der Weijden,^b

10 Department of Earth Sciences—Geochemistry, Faculty of Geosciences,
11 Utrecht University, P.O. Box 80.021 3508 TA Utrecht,
12 The Netherlands

14 *Key-words:*

15 spring watersheds, hydrology, travel time, surface area, weathering rates, modeling, equilibria,

16 Vouga river basin, THROW model.

^a Corresponding author, e-mail FPACHECO@UTAD.PT, Fax. +351 259 350480

^b e-mail CHVDW@GEO.UU.NL, Fax +31 30 2535302

18 ABSTRACT

19 Weathering rate models designed for watersheds combine chemical data of discharging waters with
 20 morphologic and hydrologic parameters of the catchments. At the spring watershed scale,
 21 evaluation of morphologic parameters is subjective due to difficulties in conceiving the catchment
 22 geometry. Besides, when springs emerge from crystalline massifs, rock structure must be accounted
 23 in formulas describing the area of minerals exposed to the percolating fluids, for a realistic
 24 evaluation of the rates. These particular features are not included in the available approaches and
 25 for that reason a new model was developed, coined THROW model. This is a lumped approach that
 26 integrates (T)opography, (H)ydrology, (RO)ck structure and (W)eathering in a single algorithm.
 27 The study area comprises several stream watersheds and spring sites of the Vouga River basin
 28 (northern Portugal), shaped on granites. Firstly, the THROW model couples a terrain modeling
 29 analysis with hydrologic models based on discharge rates, to determine hydraulic conductivities
 30 (K), effective porosities (n_e) and annual recharges (V_r) at the stream watershed scale. Subsequently,
 31 these parameters are used in a water balance model to estimate concomitant groundwater travel
 32 times (t). The mean K [$(4.7 \pm 3.2) \times 10^{-7} \text{ m} \cdot \text{s}^{-1}$] and n_e [$(2.0 \pm 1.3) \times 10^{-2}$] values are adopted as proxies
 33 for the spring watersheds and a firm regression equation is defined between time and stream
 34 watershed area (A) [~~$t = 0.16A + 1.37$ ($R^2 = 0.98$)~~]. Secondly, two more runs of terrain modeling
 35 analysis are executed to extrapolate morphologic parameters for the spring watersheds. The first run
 36 hinges on scaling properties of the drainage networks, known as Horton laws, and is used to scale
 37 watershed areas across stream orders (i). ~~For the study area, t~~ The scaling function is described by
 38 ~~another the~~ regression equation ~~$A = 0.1e^{1.49xi}$ ($R^2 = 0.99$)~~. The second run evaluates the order of a
 39 spring watershed, defined as equivalent order (i_{eq}) and equated to the mean order of the surrounding
 40 stream watersheds. Having calculated the i_{eq} , spring watershed areas and travel times were
 41 downscaled using the regression equations ($A < 10 \text{ km}^2$ and $t = 1.4\text{--}2.8 \text{ yr}$). Standing on the
 42 physical and hydrologic parameters of the spring watersheds, the THROW model finally calculates
 43 plagioclase weathering rates in the vicinity of the spring sites. The SiB model (Pacheco and Van der
 44 Weijden, 1996) was used before to estimate the contribution of plagioclase dissolution to the
 45 chemical composition of these springs (Van der Weijden and Pacheco, 2006). The chemical data
 46 were now coupled with K , n_e and t in a rate equation to estimate chemical weathering rates of
 47 plagioclase in the basin. In the THROW model, the rate equation describes the exposed surface area
 48 as a function of fracture spacings, openings and porosities (Pacheco and Alencão, 2006). The
 49 calculated rates ($W_{Pl} = (2.5 \pm 1.2) \times 10^{-14} \text{ mol} \cdot \text{m}^{-2} \cdot \text{s}^{-1}$) are consistent with previous reports and with
 50 results of experimental kinetic models. The SiB results predict formation of halloysite and gibbsite
 51 along the flow path, which were indeed close to equilibrium with the dissolved Al and Si activities.
 52

53 INTRODUCTION

54 The assessment of chemical weathering rates of silicate minerals has been the topic of numerous
55 studies, as this process is important in global geochemical cycles, particularly in relation to fluxes
56 of carbon dioxide (CO₂) and global warming (Berner et al., 1983; Drever and Clow, 1995; Dupré et
57 al., 2003; Hartmann et al., 2009; among others). These studies have been carried out at various
58 scales, including the micro to hand specimen scales (the laboratory approach) or the soil profile to
59 watershed scales (the field approach). At the watershed scale, the majority of studies were focused
60 on rivers (Oliva et al., 2003; Tardy et al., 2004; Velbel, 1985; White, 2002; White et al., 2001; and
61 references therein) while a limited number were based on spring water data (Pacheco and Van der
62 Weijden, 2002; Pacheco and Alenção, 2006). Studies at the spring watershed scale are important
63 because they bridge weathering results from the hand specimen or soil profile to the river basin
64 scales. Numerical models have been developed and applied to calculate weathering rates. At the
65 watershed scale, operation of these models requires prior assessment of very diverse data, such as
66 morphologic parameters of the catchments, aquifer ~~formation constants~~hydraulic parameters and
67 recharge, groundwater travel times, fluid compositions, etc., incoming from very different
68 disciplines, including geomorphology, hydrology or geochemistry, reason why the most recent
69 models are based on the so-called lumped approach whereby the results of several model
70 components are integrated. For example, Godd ris et al. (2006) combined a module of chemical
71 weathering in soil horizons and underlying bedrock (the WITCH model of Godd ris et al., 2006,
72 2009; Roelandt et al., 2010) with a module of water and carbon cycles in forested ecosystems (the
73 ASPECTS model of Rasse et al., 2001) to simulate, on a seasonal basis, the concentrations of silica
74 and major base cations within the soil horizons and the stream of a granitic small experimental
75 watershed. Violette et al. (2010) designed two symmetrical box modules to perform a coupled
76 hydrological and geochemical modeling: (i) a hydrological module specifically developed for the
77 experimental watershed; (ii) the WITCH module. The hydrologic modules commonly incorporated

78 into lumped approaches are usually designed to work with stream watersheds, and the concomitant
79 geochemical modules relate the fluid compositions to weathering reactions in the saprolite horizon
80 and quantify the area of minerals involved in weathering reactions (the exposed surface area) as a
81 function of the saprolite materials texture (e.g. Violette et al., 2010). Despite their broad
82 applicability, available lumped approaches are inoperative when the study is focused on springs
83 emerging from crystalline rocks, because they cannot accommodate some singularities of fracture
84 artesian spring watersheds relative to geometry and exposed surface area. For that reason, a new
85 approach is required to deal with such cases.

86 A lumped approach suited to deal with fracture artesian springs must incorporate a topographic
87 module that can assess watershed morphologic parameters (area, volume, length of water channels),
88 yet recognizing that spring sites can hardly be connected to a water channel. This type of springs
89 emerges at the intersection between the Earth's surface and conductive fractures. Usually, this
90 corresponds to points in the vicinity of water channels but rarely to points in a specific channel. In
91 these cases, delineation of watershed boundaries becomes a subjective task that limits any
92 subsequent morphologic characterization. An appropriate topographic module has to calculate the
93 morphologic parameters avoiding the step of watershed delineation, however such a specific
94 method is not part of any current lumped approach. Additionally, the lumped approach must also
95 bears that fracture artesian springs represent water packets that predominantly follow the easiest
96 routes of the crystalline rocks, such as fissures, fractures or joints, interacting with minerals exposed
97 at their walls. The area of fluid–mineral interaction is not equal to the area of the catchment, but is
98 restricted by inhomogeneous fluid migration through the fracture networks (Drever and Clow,
99 1995; Velbel, 1989, 1993). Moreover, minerals in the fractures are generally embedded in the rock
100 matrix and are only partly exposed to the fluid. Along the pathway from recharge area to spring site,
101 a water packet has been in contact with mineral surfaces that have different weathering histories.
102 For this reason, the exposed surface area will be an average of newly exposed minerals and of

103 minerals already affected by weathering. Furthermore, the spring water samples represent combined
104 water packets, each having traveled different pathways with various contact times and exposure to
105 different surface areas (Oliva et al., 2003). As a consequence, the calculated weathering rate will
106 represent an average. For the reasons described above, the geochemical module of the lumped
107 approach should define the exposed surface area as a function of rock structure, whenever the
108 studied watersheds are shaped on crystalline rocks and the analyzed water samples are represented
109 by groundwater. Nevertheless, this is not observed in the available models. Invariably, this area is
110 calculated from the crystal dimensions of the minerals (geometric surface area) or by gas adsorption
111 (BET method) that accounts for the so-called surface roughness (Brantley et al., 1999; Brantley and
112 Mellott, 2000; Lüttge 2005; Zhang and Lüttge, 2009), although it has already been recognized that
113 the results might not be representative of the area exposed to groundwater in a watershed (Brantley
114 and Mellott, 2000; Drever and Clow, 1995; Hellmann and Tisserand, 2006; White and Peterson,
115 1990a,b).

116 The present study sought to calculate weathering rates of plagioclase at the spring watershed scale
117 in granitic environment. Given the above mentioned singularities of fracture artesian spring
118 watersheds, the main purpose of this paper was to develop a lumped approach integrating, (a) a
119 topographic module that can estimate the morphologic parameters of the spring watersheds; (b) a
120 geochemical module that defines the exposed surface area as a function of rock structure. The
121 lumped approach will be coined as the (T)opography, (H)ydrology, (RO)ck structure and
122 (W)eathering model, or simply THROW model. The module developed for assessing the spring
123 watershed morphologic parameters is based on the concepts of stream order (Strahler, 1957) and
124 statistical self-similarity of drainage networks (Horton, 1945; Schuller et al., 2001). In an attempt to
125 account for the particularities of fluid transport in fractured rocks as described above, the area of
126 fluid–mineral interaction will be approximated in the geochemical module by a formula hinging on
127 rock fracture spacings, openings and porosities (Snow, 1968; Pacheco and Alencão, 2006).

128

STUDY AREA

129 The hydrographic basin of the Vouga (Figure 1) is located in northern Portugal between the sea
130 level of the Atlantic coast and 1100 meters above sea level, near the source of the river on Lapa
131 Mountain. The basin occupies 3362 km² of a region characterized by mountains in the eastern part
132 and a coastal plain in the western part. Altitudes in major mountains (Lapa, Freita, Caramulo) range
133 from 800 and 1100 meters. The main water course is 141 km long and debouches into the Ria de
134 Aveiro, a sandbar-built coastal lagoon with a small inlet/outlet connecting the lagoon to the Atlantic
135 ocean. The climate in this region is moderate, with precipitation varying from 800–1800 mm·y⁻¹
136 and air temperatures ranging from approximately 8°C in winter to 21°C in summer. The Vouga
137 River and several tributaries have been monitored for stream flow in hydrometric stations of the
138 Portuguese National Network. The locations of the stations are shown in Figure 1 and some
139 relevant data on identification and record length is presented in Table 1.

140 The mountainous part of the Vouga River basin is characterized by Palaeozoic metasediments of
141 the so-called Schist and Greywacke Complex (Beiras Group) that were intruded by syn- to post-
142 tectonic Hercynian granites. The coastal plain has a cover of Permian to Holocene sediments
143 consisting of quartzites, phyllites, conglomerates, sandstones, limestones, sands, etc (Figure 2). The
144 syn-tectonic granitoids consist mostly of medium- to coarse-grained granites to granodiorites,
145 whereas the post-tectonic granitoids consist mostly of coarsely porphyritic biotite granites
146 (Schermerhorn, 1956; Soen, 1958; Godinho, 1980; Medina, 1996). The average mineralogical
147 composition (in wt.%) of these rocks is: quartz (34.1), K-feldspar (14.4), plagioclase (albite-
148 oligoclase, but largely oligoclase; 31.0), biotite (3.7), and muscovite (16.8).

149 The mountainous part of the Vouga basin has a monotonous cover by cambisols. In the plain, soil
150 types are dominated by fluvisols, regosols, podzols and solonchaks. In the region, the profile of a
151 typical cambisol is characterized by a A horizon (0–30 cm depth) rich in organic matter, a B
152 horizon (30–55) rich in clay minerals and a C horizon (55–80) composed of weathered rock

153 (Martins, 1985). Average hydraulic conductivities of this soil type is $K = 2.47 \times 10^{-6} \text{ m}\cdot\text{s}^{-1}$ (Caetano
154 and Pacheco, 2008). When 1D flow is assumed, percolation time of soil water to the bedrock (h/K ,
155 where $h = 80 \text{ cm}$, the average thickness of cambisols) is at least ≤ 3.75 days. Small-size farm lands
156 and forests in total occupy 4/5 of the basin, the remaining 1/5 being represented by bare rock, urban
157 areas and water bodies. Although farming is more concentrated in the plain and forestry in the
158 mountains, the proportion of land used for agriculture in the highlands is significant and the
159 associated use of manure and fertilizers responsible for an important anthropogenic imprint to the
160 chemistry of shallow groundwaters. Some small urban areas have no sewage system and so
161 domestic effluents are discharged directly into the soils (Van der Weijden and Pacheco, 2006).

162

163 SPRING WATER SAMPLING AND ANALYTICAL TECHNIQUES

164 Perennial springs within the Vouga basin were sampled in the granitic areas during the summer
165 campaigns (June–July) of 1982–1985. In total, the number of sampled springs is 87. The location of
166 the spring sites is given in Figure 2. Sampling was made during the draught season to ensure that
167 spring waters would represent exclusively ground water. The pH was measured at the sampling site,
168 and alkalinity was analyzed in the field laboratory within 24 hours of sample collection using Gran
169 plots for end-point determination. Two samples of 100-mL each, one acidified with nitric acid to
170 pH 2, were stored and analyzed at the home laboratory. Sodium, potassium, magnesium, calcium,
171 aluminum, and silicon were analyzed by ICP-OES in the acidified sample, whereas chloride,
172 sulfate, and nitrate were determined by ion chromatography in the unacidified sample. The accuracy
173 of the results for the individual components was better than $\pm 5\%$. Samples for which the charge
174 balance was off by $> 10\%$ were discarded. The analytical results are reported in Appendix 1.

175

176

177

THE THROW MODEL

178
179 The THROW model is introduced in this paper as a lumped approach for the assessment of
180 weathering rates at the fracture artesian spring watershed scale. It is composed of three modules: the
181 topographic module, the hydrologic module and the weathering module. A run of the THROW
182 model begins with the topographic module, proceeds with the hydrologic module and ends up with
183 the weathering module, as illustrated in the flowchart of Figure 3. Each module is organized within
184 the dashed envelopes of the figure: the rectangles represent data essential for model operation; the
185 rounded rectangles represent model processes. Because the THROW model runs in a sequential
186 mode, the output of a given process is usually the input for the next process, until weathering rates
187 are finally calculated. The shaded rectangles, however, represent base information, obtained from
188 topographic, analytical or field measurements. ~~Altogether, the THROW model was conceived to~~
189 ~~operate with a minimum amount of base information. Somehow, this had an influence on the type~~
190 ~~of methods incorporated in the model.~~ The description of the topographic, hydrologic and
191 weathering modules is presented in the next sections.

192

193 **The Topographic Module**

194 The topographic module of the THROW model aims on estimating morphologic parameters (e.g.
195 area) of spring watersheds. There is a fundamental difficulty in dealing with these watersheds
196 because springs typically emerge in the vicinity of several water channels but not necessarily in any
197 channel. As a consequence, the outlining of spring watersheds is a biased task that hampers any
198 subsequent morphologic characterization. For that reason, morphologic parameters of spring
199 watersheds in the THROW model are estimated by an extrapolation technique based on scaling
200 properties of the drainage networks.

201

202

203 *The Horton Laws of Drainage Network Composition*

204 The continuous shaping of the Earth's surface by meteoric water results in the development of
205 drainage networks that can be conceived at various scales: river, stream, spring. Scaling properties
206 of drainage networks were early investigated and empirical scaling laws have been proposed by
207 Horton (1945), Strahler (1952) and Schumm (1956), becoming known as the Horton laws.
208 Subsequent research has shown that individual streams and the networks which they comprise are
209 fractals (La Barbera and Rosso, 1987, 1989; Roth et al, 1996; Tarboton, 1996; Schuller et al., 2001;
210 De Bartolo et al., 2006; among others), and the Horton laws provided the background for the
211 development of different measures of the fractal dimension. These empirical rating laws are based
212 upon hierarchical classification of the tributary system starting from streams lacking upstream
213 tributaries and giving increasing order numbers towards the outlet. For example, according to the
214 classification of Strahler (1957), water channels with no tributaries are described as 1st-order
215 channels and are fed by 1st-order watersheds, and the confluence of two i^{th} -order channels generates
216 a $(i+1)^{\text{th}}$ -order channel. Basically, the scaling laws state that the ratio of a morphologic parameter
217 (area or slope of the watershed, number or length of streams within the watershed) measured at
218 order i and order $i+1$ is constant. According to Rosso et al. (1991), the Horton laws of network
219 composition are geometric-scaling relationships because they hold regardless of the order or
220 resolution at which the network is viewed and because they yield self-similarity of the catchment–
221 stream system, or at least self-affinity in cases where the scaling factors in the longitudinal and
222 transverse directions are not equal (Nikora and Sapozhnikov, 1993) or self-organization in cases
223 where complex drainage networks are to be described as multi-fractal systems (De Bartolo et al.,
224 2000, 2004, 2006; Gaudio et al., 2006). Because these laws typically hold for a wide range of scales
225 in nature, they can be employed to extrapolate watershed morphologic parameters across scales. A
226 generalised equation for the relationship between morphologic parameter A and order i can be
227 written as:

228 $A = f(i)$ (1)

229 where f is a scaling function. Because springs usually emerge in the vicinity but away from the
230 water channels their watersheds cannot be associated to a particular Strahler order. In general,
231 neighbouring channels differ from each other in their order and therefore watersheds of springs
232 must be classified according to the concept of equivalent order (i_{eq}), which is defined here as an
233 average of the orders of the surrounding streams. Unlike stream orders, which are integers,
234 equivalent spring orders will be real numbers. When a spring site is situated in a region where, for
235 example, $i_{eq} = 1.5$, this means that the catchment area of the spring is larger than the average area of
236 1st-order watersheds and smaller than the average area of 2nd-order watersheds. For spring
237 watersheds, morphologic parameters are determined by Equation 1, where i is replaced by i_{eq} .

238

239 *Carrying Out the Topographic Module on a GIS Platform*

240 The topographic module of the THROW model is executed on a Geographic Information System
241 (GIS) comprising the ArcGIS (ESRI, 2007) and ArcHydro (ESRI, 2009) computer packages, and
242 operates in two sequential runs (Figure 3). In the first run, ArcHydro executes a terrain modeling
243 analysis based on the Digital Elevation Model of the study area (e.g. Figure 1) whereby the
244 drainage network and watersheds are drawn and classified according to their Strahler orders.
245 Subsequently, the same package assesses morphologic parameters of each watershed, including
246 area, volume and length of water channels, and calculates average values for each order. Based on
247 these average values, relationships between the parameters and concomitant orders (Equation 1) are
248 defined using least squares regression. In the second run, the *Density Function* of ArcGIS toolbox is
249 used to calculate equivalent orders for the spring watersheds. Firstly, the map with the drainage
250 network is overlapped by a grid of cells with dimensions 100×100 m and, within each cell, the
251 lengths of streams are measured (L_i) and multiplied by the corresponding order (i). Secondly, the

252 previous step is repeated for every order appearing in the cell and then the products $L_i \times i$ are
 253 summed and divided by the total length of streams within the cell (L), giving the i_{eq} :

$$254 \quad i_{eq} = \frac{\sum_{i=1}^n L_i \times i}{L} \quad (2)$$

255 The i_{eq} of a given spring watershed is determined from the map of equivalent orders computed using
 256 Equation 2 by evaluating the i_{eq} at the location coordinates of the spring site. The corresponding
 257 morphologic parameters will be assessed afterwards using the i_{eq} values in Equation 1.

258

259 **The Hydrologic Module**

260 This module aims on estimating hydrologic parameters of the fractured aquifer at the watershed
 261 scale. It comprises a set of methods to calculate hydraulic conductivity and effective porosity,
 262 evaluate annual recharge, and assess groundwater travel time. The module's flowchart is illustrated
 263 in Figure 3. The data required for its operation encompass the outflows measured at the spring sites
 264 and results from the topographic module.

265

266 *Spring Outflows and Aquifer ~~Formation Constants~~ Hydraulic Parameters*

267 The outflow or discharge of a fracture artesian spring some time after a precipitation event occurs
 268 from upstream aquifers along the underground flow path to the spring. This type of flow is known
 269 as base flow and the analysis of base flows recognized as recession flow analysis. When combined
 270 with physically based flow equations, recession analysis can be used as a tool for aquifer
 271 characterization, namely for assessment of hydraulic conductivity and effective porosity (Szilagyi
 272 and Parlange, 1999; Szilagyi et al., 1998; Mendoza et al., 2003; Van de Giesen et al., 2005;
 273 Malvicini et al., 2005; among others).

274 For the analysis of spring outflows, the THROW model adopted a technique developed by Brutsaert
 275 and Nieber (1977) for stream flow recession analysis, called the Brutsaert method. Declining
 276 groundwater reservoirs control both stream base flow recession and upland spring outflow

277 recession, so the method should be equally valid for both situations. The use of the Brutsaert
 278 method is advantageous because it is independent of the ambiguity inherent in identifying when
 279 base flow starts (Malvicini et al., 2005). Refinements and extensions on the method have been made
 280 in Zecharias and Brutsaert (1985,1998), Brutsaert (1994), Brutsaert and Lopez (1998); Rupp and
 281 Selker (2005); among others. The Brutsaert method is founded on the Boussinesq equation
 282 (Boussinesq, 1903, 1904), which describes the drainage from an ideal unconfined rectangular
 283 aquifer bounded below by a horizontal impermeable layer and flowing laterally into a water
 284 channel. There are several theoretical solutions of the Boussinesq equation that have the general
 285 form of a power function (Rupp and Selker, 2006):

$$286 \quad \frac{dQ}{dt} = aQ^b \quad (3)$$

287 where Q ($\text{m}^3 \cdot \text{s}^{-1}$) is the recession flow, t is time, and a and b are constants. The coefficient a can be
 288 directly related to the groundwater reservoir's characteristics and b is an exponent whose value
 289 depends on the recession flow regime. There are two distinct flow regimes: the short-time and the
 290 long-time regime. Short-time flows generally have a higher Q than long-time flows. Brutsaert and
 291 Lopez (1998) showed the following solution for short-time flow:

$$292 \quad a = \frac{1.13}{Kn_e D^3 L^3}, \quad b=3 \quad (4a)$$

293 where K is the hydraulic conductivity, n_e the effective porosity, D the aquifer thickness and L the
 294 length of upstream channels intercepting groundwater flow. The long-time flow is adequately
 295 described by the so-called linear solution of Boussinesq (1903).

$$296 \quad a = \frac{0.35\pi^2 KDL^2}{n_e A^2}, \quad b=1 \quad (4b)$$

297 where A is the upland drainage area. Equations 4a and 4b can be combined to describe K and n_e as a
 298 function of a and the morphologic parameters of the watershed (A, D, L). On the other hand, D can
 299 be approached to the ratio V/A . In that case,

$$300 \quad K = 0.57 \sqrt{\frac{a_1}{a_3}} \left(\frac{A^3}{V^2 L^2} \right) \quad (5a)$$

$$301 \quad n_e = \frac{1.98}{V \sqrt{a_1 a_3}} \quad (5b)$$

302 where a_i represents the value of a when $b = i$ (1 or 3).

303 To estimate K and n_e using Equations 5a,b it is required a previous run of the topographic module,
 304 the results of which provide numbers for A , V and L . The values of a_1 and a_3 can be read in a scatter
 305 plot of $\ln(\Delta Q/\Delta t)$ versus $\ln(Q)$. According to the Brutsaert method, the lower envelope of the scatter
 306 points is represented by two straight lines, one with a slope $b = 1$, and the other with a slope $b = 3$,
 307 and the y-values where the lines intercept $\ln(Q) = 0$ (or $Q = 1$) are the parameters a_1 and a_3 .

308

309 *Spring Base Flows and Aquifer Recharge*

310 Recession flow analysis is also used as a tool for aquifer recharge estimation. In this case, recession
 311 segments are selected from the hydrographic record of the spring and their geometric properties
 312 (e.g. slope) combined with analytical models to provide measures of the aquifer recharge.

313 Underlying the methods of recession flow analysis is the storage-outflow model adopted to
 314 represent discharge from natural storage compartments during the recession phase. Many complex
 315 functions have been developed in this context, for example to explain the outflow from karstic
 316 aquifers (Padilla et al., 1994), channel banks (Cooper and Rorabaugh, 1963), surface depressions
 317 such as lakes or wetlands (Griffiths and Clausen, 1997), etc., but many other recession flow models
 318 assume a linear relationship between storage and outflow, described by the classic exponential
 319 decay function of Boussinesq (1877):

$$320 \quad Q = Q_i e^{-\alpha t} \quad (6)$$

321 where Q_i is the base flow at the beginning of a recession period and α is the recession constant. One
 322 of these methods has been developed by Meyboom (1961) and is now incorporated into the
 323 THROW model. Starting with Equation 6, Meyboom (1961) noted that a plot of discharge versus

324 time on a semilogarithmic paper would yield a straight line, the slope of which defines the recession
 325 constant. In this case, the Equation 6 can be re-written as:

$$326 \quad Q = \frac{Q_i}{10^{t/t_1}} \quad (7)$$

327 where t_1 is the time corresponding to a log-cycle of discharge. Integrating Equation 7 from $t = 0$
 328 (beginning of the recession) and $t = \text{infinity}$ (complete depletion of the aquifer) gives:

$$329 \quad V_t = \frac{Q_i t_1}{2.3} \quad (8a)$$

330 where V_t is the total potential groundwater discharge. By analogy, the residual potential
 331 groundwater discharge (V_s) can be approached by:

$$332 \quad V_s = \frac{Q_f t_1}{2.3} \quad (8b)$$

333 where Q_f is the base flow at the end of the recession phase. Considering a sequence of two recession
 334 periods, aquifer recharge (V_r) between periods will be defined as the difference between V_t ,
 335 evaluated at the beginning of period 2, and V_s estimated at the end of period 1, i.e.:

$$336 \quad V_r = (Q_i - Q_f) \frac{t_1}{2.3} \quad (9)$$

337

338 *Groundwater Travel Times*

339 Groundwater transit (or travel) time is defined as the elapsed time when the water molecules exit
 340 the flow system (Bolin and Rodhe, 1973; Etcheverry and Perrochet, 2000; Rueda et al., 2006). A
 341 point of reference for mean transit times are often the hydraulic turnover times, since they define
 342 the turnover timescale based on the best understanding or assumption of the catchment subsurface
 343 volume and mobile storage if the unsaturated zone transit time is small compared to the total transit
 344 time of the system. The concept of hydraulic turnover time was adopted by the THROW model to
 345 estimate the travel time of groundwater within the spring watershed boundaries (t, s). According to
 346 McGuire and McDonnell (2006), if a simple water balance is considered, the hydraulic turnover

347 time is defined as the ratio of the mobile catchment storage (equated to Vn_e , m^3) to the volumetric
348 flow rate (equated to the aquifer recharge: V_r , $m^3 \cdot s^{-1}$):

$$349 \quad t = \frac{Vn_e}{V_r} \quad (10)$$

350

351 **Weathering Module**

352 This module combines the chemical composition of spring waters and of their host rocks in a mass
353 balance algorithm to calculate the number of moles of primary minerals and of secondary products
354 dissolved or precipitated along the flow path. In a subsequent stage, these mass transfers are
355 combined with aquifer ~~formation constants~~hydraulic parameters and groundwater travel time in a
356 rate equation to obtain mineral weathering rates (Figure 3).

357

358 *Geochemical Mass Balance Calculations*

359 There are essentially two types of geochemical models for assessing mineral weathering rates at the
360 watershed scale. The first approach estimates solid-state weathering rates based on the differences
361 between elemental, isotopic and mineral compositions measured in present-day regoliths and in the
362 assumed protolith. In this case, rates represent the entire time span of a weathering episode,
363 commonly on the order of thousands to million years. The second approach calculates solute-flux
364 rates that stand for contemporary weathering during groundwater percolation in the rocks, in which
365 case time is a window to the weathering episode spanning few years or decades. The THROW
366 model is based on the solute-flux approach and uses the SiB algorithm of Pacheco and Van der
367 Weijden, (1996), extended by Pacheco et al. (1999) and Pacheco and Van der Weijden (2002), to
368 perform the geochemical mass balance calculations. A brief description of the method is given in
369 the next paragraphs.

370

371

372 The SiB algorithm comprehends a set of mole balance and charge balance equations of the form:

373 Mole balance equations —
$$\sum_{j=1}^{q_1} \beta_{ij} [M_j]_t + [Y_i]_p = [Y_i]_t, \text{ with } i = 1, q_2 \quad (11a)$$

374 Charge balance equation —
$$\sum_{l=1}^{q_3} z_l [Y_l]_p = [Cl^-] + 2[SO_4^{2-}] + [NO_3^-] \quad (11b)$$

375 where q_1 , q_2 and q_3 are the number of primary minerals involved in the weathering process, the
 376 number of inorganic compounds that usually are released from weathering reactions ($q_2 = 6 = Na^+$,
 377 K^+ , Mg^{2+} , Ca^{2+} , HCO_3^- and $H_4SiO_4^0$), and the number of the latter compounds that usually are also
 378 derived from atmospheric plus anthropogenic sources – lumped as “pollution” ($q_3 = 4 =$ the four
 379 major cations); suffixes t and p mean total and derived from “pollution”, respectively. The expected
 380 sources of anthropogenic pollution are manures, commercial fertilizers and domestic and(or)
 381 industrial effluents; Y represents a dissolved compound; M represents a mineral; Cl^- , SO_4^{2-} and
 382 NO_3^- are the major dissolved anions assumed to represent exclusively atmospheric plus
 383 anthropogenic inputs; square brackets ([]) denote concentrations of a dissolved compound or a
 384 dissolved mineral; b_{ij} is the ratio of the stoichiometric coefficients of dissolved compound i and
 385 mineral j , as retrieved from the weathering reaction of mineral j ; $b_{ij}[M_j] = [Y_i]r_j$, where $[Y_i]r_j$ is the
 386 concentration of a dissolved compound i derived from reaction of M_j moles of mineral j ; z_l is the
 387 charge of cation l .

388 The number of equations in Set 11a,b is seven. The unknowns of the system are the [M] and the
 389 [Y]_p variables, in total q_1+q_3 . The SiB algorithm uses the Singular Value Decomposition procedure
 390 as described in Press et al. (1991) to solve the set of equations because this procedure can handle
 391 efficiently (through least squares or minimizing procedures) the cases where the set is undetermined
 392 ($q_1+q_3 > 7$) or overdetermined ($q_1+q_3 < 7$). In systems with fluid flow, precipitation of secondary
 393 products along the flow path follows certain sequences (Helgeson et al., 1969; Steefel and Lasaga,
 394 1992; Steefel and Van Cappellen, 1990). The SiB algorithm describes these sequences as reactions

395 of primary minerals to mixtures of secondary products (for example alteration of plagioclase to $c_1 \times$
 396 halloysite + $(1-c_1) \times$ gibbsite, with $0 \leq c_1 \leq 100\%$; alteration of biotite to $c_2 \times$ vermiculite + $(1-c_2)$
 397 \times halloysite, with $0 \leq c_2 \leq 100\%$). Only a few of these mixtures will explain the chemical
 398 composition of the spring waters. To be labelled as valid mixture, the selected values of c_1 and c_2
 399 must result in a solution of Set 11a,b satisfying $[M] \geq 0$ and $[Y]_p \geq 0$. Among the valid mixtures,
 400 the SiB algorithm selects a best-fit one by checking all against predefined external boundary
 401 conditions.

402

403 *Rate Equation*

404 The weathering rate of a mineral M is commonly defined by the relationship:

$$405 \quad W_M = \frac{[M]}{t} \times \frac{V_r}{A_M} \quad (12)$$

406 where W_M ($\text{mol}\cdot\text{m}^{-2}\cdot\text{s}^{-1}$) is the rate and $[M]$ ($\text{mol}\cdot\text{m}^{-3}$) its concomitant dissolved concentration, t (s)
 407 is the average travel time of water packets flowing through the spring watershed, V_r (m^3) is the
 408 volume of water entering the spring watershed in a unit time, and A_M (m^2) is the surface area of M
 409 in contact with that volume of aquifer water. To adequately describe the reactive surface area of a
 410 fracture artesian spring watershed, weathering modules must incorporate rock structure in the
 411 calculation of A_M . This is accomplished by the THROW model. In this model, A_M is calculated by a
 412 formula developed by Pacheco and Alencão (2006) describing the area of fracture surfaces in
 413 contact with aquifer water in unit time:

$$414 \quad A_M = 2\alpha_M V_r \times \sqrt{\frac{\rho_w g n_e}{12\mu_w K}} \quad (13)$$

415 where α_M is the proportion of mineral M in the rock, μ_w is the dynamic viscosity of water ($1.14 \times$
 416 $10^3 \text{ kg}\cdot\text{s}^{-1}\cdot\text{m}^{-1}$ at $T = 15^\circ\text{C}$), and g is the acceleration of gravity ($9.81 \text{ m}\cdot\text{s}^{-2}$). Replacing this equation
 417 in Equation 12 and rearranging gives:

$$W_M = \frac{[M]}{2t\alpha_M} \sqrt{\frac{12\mu_w K}{\rho_w g n_e}} \quad (14)$$

419 Derivation of Equation 14 stands on four fundamental assumptions. The first assumption is that
420 water in a thin soil cover percolates mainly through the macropores (Hornberger et al., 1990;
421 Velbel, 1993; Drever, 1997; Rodhe and Killingtveit, 1997), resulting in relatively short transit times
422 to the fracture network lying beneath, where water–mineral interactions will take place. The second
423 assumption is that flow in fractured rock units is limited to preferential flow paths and is slow given
424 the typically low hydraulic conductivity, thus resulting in extended travel time. The third
425 assumption is that infiltrating water pushes the old water ahead according to piston flow (Appelo
426 and Postma, 2005), meaning that solute transport occurs predominantly by advection. Equation 14
427 does not account for the time required by solutes to travel from dead ends along microfractures to
428 gravity flow fractures by diffusion (Meunier et al., 2007). Weathering rates calculated by this
429 equation may thus be overestimated. The fourth assumption is that the area available for weathering
430 reactions is restricted to minerals facing fracture walls with the same composition as the rocks in
431 which they occur, although this assumption is not valid for fractures that have been lined with silica
432 or other secondary products. Under such circumstances, the spring water chemistry will be
433 dominated by water–mineral interactions along the dominant flow paths and, more importantly, by
434 contact with the fracture walls and not by interactions with the whole inventory of minerals and
435 soils and solid rocks in the aquifer.

436

437

RESULTS

438

439 **Results of the Topographic Module**

440 The topographic module of the THROW model (Figure 3) was applied to the Digital Elevation
441 Model of Vouga basin (Figure 1), in the sector where springs were sampled (the granite area; Figure
442 2). Firstly, ArcHydro (ESRI, 2007) was used to delineate watersheds within that area, taking into

Text

443 account the order i of the associated stream. The results are illustrated in Figure 4a. The number of
 444 1st-order watersheds is 1241, covering an average area $A = 0.44 \text{ km}^2 \cdot \text{watershed}^{-1}$, whereas the
 445 whole granite area encompasses a 6th-order watershed with an area $A = 955.39 \text{ km}^2$. A plot of A
 446 versus i (Figure 4b) shows a firm correlation between these variables, confirming that Horton laws
 447 of network composition hold for the studied area. In keeping with this observation, the generalized
 448 relationship between morphologic parameters and order (Equation 1) can, for the granite area of the
 449 Vouga River basin, be replaced by the function fitting the scatter points in Figure 4b. Using a least
 450 squares method, it was found that such function is represented by an exponential equation:

451 $A = 0.1e^{1.49 \cdot i}$ ($R^2 = 0.99$) (15)

452 Secondly, a map of equivalent orders (i_{eq}) was drawn for the granite area (Figure 5) and discrete
 453 orders were determined for each spring by evaluating the i_{eq} at the location coordinates of the spring
 454 site. The results are summarized in Appendix 1. Most sampled springs (94%) emerge where $i_{eq} =$
 455 1–3. Equation 15 can be used to extrapolate the catchment area of the springs if i is replaced by i_{eq}
 456 in this equation. These areas vary from 0.4 to 180.9 km^2 , although most of them (the ones with $i_{eq} =$
 457 1–3) are smaller than 10 km^2 . These results, also summarized in Appendix 1, are consistent with
 458 previous reports (Pacheco and Van der Weijden, 2002).

459

460 **Results of the Hydrologic Module**

461 *Aquifer Hydraulic Parameters and Travel Times of Stream Watersheds*

462 The hydrologic module of the THROW model (Figure 3) could not be applied to the studied springs
 463 because the required spring outflows were lacking. ~~For that reason~~To compensate for this, the
 464 hydrologic characterization of the region was based on the application of the THROW model to
 465 seven stream watersheds located upstream of the hydrometric stations represented in Figure 1. The
 466 hydraulic conductivities (K) and effective porosities (n_e) resulting from this characterization were
 467 then used as proxies of the K and n_e values of the spring watersheds, as explained in the next

- Formatted: Font: Italic
- Formatted: Font: Italic
- Formatted: Subscript
- Formatted: Font: Italic
- Formatted: Font: Italic
- Formatted: Subscript

468 section, which also describes how groundwater travel times were downscaled from the larger
469 (stream) the smaller (spring) scales.

470 The ~~results~~ hydrologic characterization of the stream watersheds ~~are~~ is summarized in Table 1. The
471 initial stage of topographic characterization (1st-run of the topographic module; Figure 3) indicated
472 that watershed areas (A) range from 22 to 649 km², watershed volumes (V) from 7 to 317 km³ and
473 water channel lengths (L) from 24 to 177 km. Subsequent application of the Brutsaert method gave
474 numbers for hydraulic conductivity (K) and effective porosity (n_e). The application of the method to
475 Station 1 (location given in Figure 1) is illustrated in Figure 6. In this figure, black dots represent 17
476 years of monthly average stream flows compiled from the hydrographic record of the station
477 (period 1936/37–1953/54), available at the Portuguese National Water Institute (www.inag.pt). The
478 dashed lines are the lower envelopes to the scatter points. According to the Brutsaert method, the
479 intercept- y of these lines are parameters a_1 and a_3 of Equations 5a,b. For Station 1, $\log(a_1) = -19.5$
480 and $\log(a_3) = -22.5$. Combining these values with morphologic parameters of the watershed (A , V ,
481 L ; Table 1) in Equations 5a,b gives $K = 2.4 \times 10^{-7} \text{ m}\cdot\text{s}^{-1}$ and $n_e = 3.7 \times 10^{-2}$. The average K and n_e ,
482 when considering the values obtained for the seven watersheds, are $(4.7 \pm 3.2) \times 10^{-7} \text{ m}\cdot\text{s}^{-1}$ and
483 $(2.0 \pm 1.3) \times 10^{-2}$, respectively. These values are consistent with fractured rock hydraulic
484 conductivities and effective porosities (Domenico and Schwartz, 1990). Application of the
485 hydrograph method of Meyboom (1961) provided estimates for the aquifer recharge (V_r). The
486 application of the method to Station 1 is illustrated in Figure 7. As in Figure 6, the black dots are
487 discharge rate measurements representative of a given month. The straight lines are fits to base
488 flows of the recession periods. They are parallel because their slope is a function of the aquifer
489 ~~formation constants~~ hydraulic parameters (K and n_e), which do not change over the time scales
490 represented in the graph (two years). Based on the geometry of the dashed lines and on its relation
491 with the base flow measurements, values were determined for Q_f ($180 \text{ L}\cdot\text{s}^{-1}$), Q_i ($21000 \text{ L}\cdot\text{s}^{-1}$) and t_1
492 (100 days), which have been used in Equation 9 to calculate V_r ($78 \times 10^6 \text{ m}^3$). This value is valid

493 solely for the hydrologic years 1939/40 and 1940/41, represented in Figure 7. For the entire record
 494 length of Station 1 (17 hydrologic years), the average aquifer recharge is $57 \times 10^6 \text{ m}^3$, and when the
 495 seven stations are taken altogether, $V_r = (53 \pm 39) \times 10^6 \text{ m}^3$ (Table 1). Finally, using the values of V , n_e
 496 and V_r in Equation 10, average travel times of groundwater in the seven stream watersheds were
 497 calculated, varying from 7 to 107 years (Table 1).

498
 499 | *Aquifer ~~Formation Constants~~ Hydraulic Parameters and Travel Times of Spring Watersheds*

500 The hydrologic parameters of spring watersheds were extrapolated from the values assessed at
 501 larger scales (previous section). Figure 8 plots travel time, hydraulic conductivity and effective
 502 porosity as a function of watershed area, using the values calculated for the seven stream
 503 watersheds (Table 1). The relationship between the hydrologic parameters and area is unequivocal,
 504 | being expressive for t as:

$$505 \quad t = 0.16A + 1.37 \quad (R^2 = 0.98) \quad (16)$$

506 The bigger K and n_e values of larger basins reflect of the accentuated heterogeneity of these basins
 507 relative to the smaller ones (Domenico and Schwartz, 1990). The bigger travel times are inherently
 508 associated to longer flow paths. According to Equation 14, a simultaneous increase in K and n_e has
 509 a limited impact on the estimates of weathering rates (W), because W is a function of $(\sqrt{K/n_e})$. For
 510 the seven watersheds, the minimum value of $\sqrt{K/n_e}$ is $2.5 \times 10^{-3} \text{ m}^{1/2} \cdot \text{s}^{-1/2}$, whereas the maximum is

511 | $8.2 \times 10^{-3} \text{ m}^{1/2} \cdot \text{s}^{-1/2}$, so, regardless the values adopted for the aquifer ~~formation constants~~ hydraulic
 512 | parameters the impact on weathering rates would not exceed a factor of 3.2. Contrarily to K and n_e ,
 513 changes in t have a tremendous impact on those estimates, because W is a function of $1/t$. Based on
 514 this assessment, it was assumed that K and n_e were constant within the catchment areas of the
 515 springs and equal to the mean values estimated for the seven stream watersheds (Table 1): $K =$
 516 $4.7 \times 10^{-7} \text{ m} \cdot \text{s}^{-1}$ and $n_e = 2.0 \times 10^{-2}$. On the other hand, Equation 16 was used to extrapolate
 517 (downscale) travel times for spring waters. These times varied from 1.4 to 30.3 years, but for

518 springs with $A < 10 \text{ km}^2$, they ranged from 1.4 to 2.8 years. The entire record of spring water travel
519 times is depicted in Appendix 1.

520

521 **Results of the Weathering Module**

522 The hydrochemistry of springs in the Vouga basin and the chemical weathering of associated
523 granites and metasediments have been discussed in great detail by Van der Weijden and Pacheco
524 (2006). This study encompassed an application of the SiB algorithm to the spring water
525 compositions summarized in Appendix 1. The SiB mole balance calculator is one of the THROW
526 model components. For that reason, the results obtained in 2006 were adopted for the present study,
527 being summarized in Appendix 2. In brief, the analytical data indicated that chemical weathering of
528 plagioclase and biotite determined the inorganic chemical composition of the springs. For
529 plagioclase, it was calculated an average mass transfer of $[Pl] = 148 \pm 56$ micromoles per liter of
530 water. In the geochemical calculations, it was assumed that plagioclase weathered into mixtures of
531 halloysite and, depending on whether rainfall was larger or smaller than $1000 \text{ mm} \cdot \text{y}^{-1}$, gibbsite or
532 smectite. It was also assumed that weathering of biotite produced mixtures of halloysite and
533 vermiculite. The results showed that weathering of plagioclase produced $[\text{smectite}] = 2 \pm 11 \text{ } \mu\text{M}$,
534 $[\text{halloysite}] = 68 \pm 42 \text{ } \mu\text{M}$ and $[\text{gibbsite}] = 14 \pm 21 \text{ } \mu\text{M}$, i.e. that halloysite is the dominant secondary
535 product precipitating along the flow paths.

536 For the calculation of plagioclase weathering rates (W_{Pl}), it was assumed that the weight fraction of
537 this mineral in the granites was consistently $\alpha_{PL} = 0.31$. The remaining input data to the rate
538 equation (Equation 14) are the dissolved concentrations of plagioclase ($[Pl]$) reported in Appendix
539 2, the spring water travel times of (t) listed in Appendix 1, and the aquifer ~~formation~~
540 ~~constants~~ hydraulic parameters ($K = 4.7 \times 10^{-7} \text{ m} \cdot \text{s}^{-1}$ and $n_e = 2.0 \times 10^{-2}$). The calculated W_{Pl} values
541 are within the interval $(2.5 \pm 1.2) \times 10^{-14} \text{ mol} \cdot \text{m}^{-2} \cdot \text{s}^{-1}$ ($-\log(W) = 13.7 \pm 0.3$).

542

DISCUSSION

543

544

545 **Thermodynamic Validation of the SiB Results**

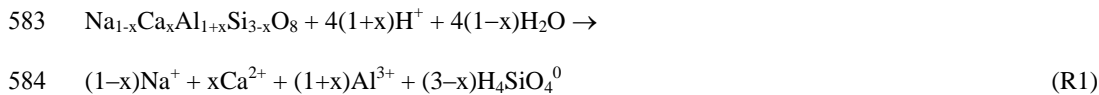
546 The concentrations of dissolved plagioclase ([Pl]) and the amounts of precipitated secondary
547 products ([gibbsite], [halloysite] and [smectite]) were determined by Van der Weijden and Pacheco
548 (2006) using mole balance calculations and are listed in Appendix 2. These results are supported by
549 equilibrium models. Paces (1978) reviewed the secondary phases that may control the
550 concentrations of Al and Si in natural waters. The order of increasing stability of aluminum
551 hydroxide phases is amorphous $\text{Al}(\text{OH})_3$, microcrystalline gibbsite, and gibbsite. The same order
552 for aluminosilicates is allophane, halloysite, and kaolinite. The calculated Q/K_{eq} ratios of these
553 secondary phases, where Q is the ion activity product (IAP) calculated from the activities of the
554 relevant dissolved species (Appendix 1) and K_{eq} is the solubility product, are reported in Appendix
555 2 (columns 8–13). Plots of the actual total Al concentrations in the spring waters against pH
556 (Appendix 1) can be compared with the equilibrium curves of these phases (Figures 9a,b). The
557 distribution of the measured values as well as the Q/K_{eq} values given in Appendix 2 show that
558 springs were in close equilibrium with microcrystalline gibbsite and halloysite/allophane.
559 Precipitation of metastable phases along the flow path of the fluids is consistent with the Ostwald
560 Step Rule. In general, Al hydroxide phases are expected to precipitate first, followed by
561 precipitation of aluminosilicates (Helgeson et al., 1969; Steefel and Lasaga, 1992). The studied
562 spring waters represented a mixture of water packets that followed different flow paths with
563 different velocities. Because the flow of groundwater across the granites is essentially through
564 fissures and fractures, it is impossible to determine exactly where the secondary products
565 precipitate. Simultaneous equilibrium with respect to gibbsite and halloysite, as calculated for 34
566 spring waters, could have occurred in a wider or narrower band along a characteristic flow path,
567 depending on the hydrodynamic dispersion (Steefel and Lasaga, 1992). Moreover, the ratio between

568 the kinetic dissolution and precipitation constants of the primary and secondary phases may have
 569 stretched the apparent stability fields of these phases, resulting in overlap instead of separation
 570 (Steeffel and Van Cappellen, 1990). The generally strong relation between the presence of ‘gibbsite’
 571 (SiB results) and degree of saturation with respect to microcrystalline gibbsite is shown in Figure
 572 10. The calculated amount of gibbsite precipitates ($[\text{Gibbsite}] > 0$) generally occurred within a
 573 rather narrow band of low saturation values. The samples with high Q/K_{eq} values relative to
 574 microcrystalline gibbsite were closer to equilibrium with amorphous $\text{Al}(\text{OH})_3$ (Appendix 2).
 575 Analytical uncertainties in the determination of total dissolved Al, and consequently in the $\{\text{Al}^{3+}\}$
 576 values, were propagated in the accuracy and precision of the calculated Q values. For this reason,
 577 no rigid meaning is attributed to Q/K_{eq} values smaller than 1. The general correspondence between
 578 the results of the mass balance method (SiB) and the concomitant calculated equilibria makes a
 579 strong case for the precipitation of the metastable phases.

580

581 **Residual Undersaturation of Spring Waters with Respect to Plagioclase**

582 The congruent dissolution of plagioclase can be represented by the reaction:



585 with $K_{\text{eq}} = \{\text{Na}^+\}^{(1-x)} \{\text{Ca}^{2+}\}^x \{\text{Al}^{3+}\}^{(1+x)} \{\text{H}_4\text{SiO}_4^0\}^{(3-x)} / \{\text{H}^+\}^{4(1-x)}$

586 where x is the mole fraction of anorthite in plagioclase and $\{ \}$ represents activity.

587 The actual IAP (ion activity product) for reaction R1, calculated on the basis of the analytical data

588 (Appendix 1), is generally smaller than K_{eq} . As explained in Appendix 2, the degree of

589 undersaturation can be expressed as the Gibbs free energy of dissolution (ΔG_r). Most springs are

590 undersaturated with respect to plagioclase (negative ΔG_r), the exceptions being springs 2070, 2071

591 and 2072 (Appendix 2, last column). ΔG_r has been used as a key parameter in many kinetic

592 dissolution models (Beig and Lüttge, 2006; Lasaga, 1998; Lüttge, 2006; Maher et al., 2009; and

593 numerous references therein). Its role in such models becomes more important as the solution
594 approaches equilibrium ($\Delta G_r \rightarrow 0$). Dissolution rates are highest and constant far from equilibrium
595 (i.e., the so-called dissolution plateau). During ongoing dissolution, undersaturation decreases and
596 approaches equilibrium in a linear fashion or in a sigmoidal manner characterized by a typical
597 critical ΔG_r^{crit} , beyond which the dissolution mechanism dramatically changes from a rapid to a
598 slow mode, proceeding linearly until equilibrium is realized (Burch et al, 1993; Hellman and
599 Tisserand, 2006). Other modes of dissolution rates as a function of ΔG_r have been observed and can
600 be explained by the presence and persistence of etch pits on the dissolving mineral surface (Oelkers
601 et al., 1994; Lüttge, 2006). Further discussion of the processes and mechanisms, and the underlying
602 theories and observations is beyond the scope of this paper. It is worth mentioning, however, that
603 the median and average values of ΔG_r ($-20 \text{ kJ}\cdot\text{mol}^{-1}$), as well as that of almost all individual values
604 calculated for the spring waters, were higher than the ΔG_r^{crit} of about $-28\pm 3 \text{ kJ}\cdot\text{mol}^{-1}$ for albite
605 (Burch et al., 1993; Arvidson and Lüttge, 2009), and were at least close to $\Delta G_r^{crit} \approx -18 \text{ kJ}\cdot\text{mol}^{-1}$
606 (Lasaga and Lüttge, 2004; Lüttge, 2006). This means that the rate of plagioclase dissolution had
607 already slowed once the ground water arrived at the spring site. It must be realized, however, that
608 the rates must have been much higher when the ground waters started their journey along the flow
609 channels. Considering that only the water composition at the terminals of the water flow were
610 known, the data do not allow for comparisons of the calculated weathering rates with kinetic
611 models of the dissolution rates of the plagioclases.

612

613 **Rates of Plagioclase Weathering**

614

615 *Comparison with Reported Weathering Rates*

616 Weathering rates calculated in the present study ($(2.5\pm 1.2)\times 10^{-14} \text{ mol}\cdot\text{m}^{-2}\cdot\text{s}^{-1}$) are very close to the
617 range of rates reported for Panola granite plagioclase: $(0.21-7)\times 10^{-14} \text{ mol}\cdot\text{m}^{-2}\cdot\text{s}^{-1}$ (White and

618 Brantley, 2003) measured in column-flow experiments after 6.2 years. Commonly reported
619 laboratory rates are, on average, around $4 \times 10^{-12} \text{ mol} \cdot \text{m}^{-2} \cdot \text{s}^{-1}$ (White and Brantley, 2003), and are
620 thus two to three orders of magnitude higher than the W_{PI} determined by this study. Laboratory
621 experiments, however, are usually conducted far from equilibrium conditions, with higher
622 fluid/rock ratios than field conditions, and under high temperatures and low pH, which accelerate
623 the dissolution reactions. Some experiments are conducted at ambient temperatures and at field-
624 similar pH, but researchers rarely attempt to restrict the fluid/rock ratios or use pre-weathered
625 samples.

626 The weathering rates reported in this study can also be compared with the field weathering rates
627 reported by other studies (Table 2). Considering the differences in weathering conditions (climate,
628 temperature, vegetation, soil thickness, age, etc.) and problems related to the determination of
629 exposed surface areas, the range of reported values is not surprising. Arvidson and Lüttge (2010)
630 argued that the complex chemical and thermal histories of the minerals along the reaction path have
631 importance for mineral reactivity in natural basins. This may thus be the cause of the apparent
632 variability in the reaction rates under natural weathering conditions. In addition, weathering rates
633 correlate better with the fluid residence times than with the age of the weathering materials (Maher,
634 2010). The W_{PI} values determined in our study depended on the calculated travel times of the fluids
635 and surface areas exposed to the fluids. Given these uncertainties, the weathering rates for
636 oligoclase obtained in our study compare well with the results obtained by other studies, as
637 summarized in Table 2.

638

639 *Influence of the Exposed Surface Area*

640 In the THROW model section (Hydrologic Module), a formula hinging on the volumetric fracture
641 density concept was presented and used to estimate the exposed surface area (Equation 13). This
642 method requires prior knowledge of the aquifer recharge (V_r), which is available for sub-basins of

643 the Vouga basin (Table 1). The exposed surface areas calculated by this method for these sub-
 644 basins were $A_{Pl} = 4.79 \times 10^{11} - 1.19 \times 10^{13} \text{ m}^2$ (median $3.83 \times 10^{12} \text{ m}^2$). If all plagioclase grains were in
 645 contact with the flowing groundwater, and not only the grains facing the fracture walls, then the
 646 exposed surface area would be given by:

$$647 \quad A_{Pl} = \gamma_{Pl} S_{Pl} \quad (17)$$

648 where γ_{Pl} (kg) is the mass of plagioclase grains in contact with aquifer water in unit time (one year)
 649 and S_{Pl} ($\text{m}^2 \cdot \text{kg}^{-1}$) is the geometric surface area of oligoclase, assumed to be $24.7 \pm 14.0 \text{ m}^2 \cdot \text{kg}^{-1}$
 650 (Blum, 1994). The value of γ_{Pl} can be deduced from the annual recharge (V_r , m^3), the effective
 651 porosity of the aquifer, the weight fraction of plagioclase (α_{Pl}) in the rock, and the specific weight
 652 of plagioclase (ρ_{Pl} , $\text{kg} \cdot \text{m}^{-3}$), as follows:

$$653 \quad \gamma_{Pl} = \frac{V_r}{n_e} \alpha_{Pl} \rho_{Pl} \quad (18)$$

654 Considering that the weight fraction of plagioclase in the Vouga granites is on average 0.31, and the
 655 specific weight of oligoclase is $2650 \text{ kg} \cdot \text{m}^{-3}$, the calculated area of oligoclase in the sub-basins,
 656 determined using Equation 17, is $A_{Pl} = 1.67 \times 10^{13} - 1.03 \times 10^{14} \text{ m}^2$ (median $5.04 \times 10^{13} \text{ m}^2$). The ratios
 657 between the exposed surface areas, estimated using Equation 13 and Equation 17, are
 658 $1.34 \times 10^{-2} - 3.75 \times 10^{-1}$ (median 8.63×10^{-2}). The results show that, due to the inhomogeneous fluid
 659 migration through the fracture networks, the area of fluid–mineral interactions is reduced to some
 660 9% of the total area available for reaction. Identical results were obtained by Pacheco and Alencão
 661 (2006).

662

663

CONCLUSIONS

664 The THROW model, introduced in this paper, produced realistic estimates of morphologic and
 665 hydrologic parameters at the spring watershed scale, and of plagioclase weathering rates in granite
 666 environment. It is therefore appropriate to model mineral weathering in the vicinity of fracture

667 artesian springs. The distinctive points of the THROW model include an assessment of
668 morphologic parameters of spring watersheds based on scaling properties of the drainage networks,
669 known as the Horton laws (Horton, 1945), and an evaluation of the area of minerals exposed to the
670 percolating fluids using a formula based on fracture spacings, openings and porosities (Snow, 1968;
671 Pacheco and Alencão, 2006). The methods used to estimate spring watershed areas and
672 groundwater travel times indicate that most fracture artesian springs in the Vouga basin granites are
673 fed by catchments with areas ranging from 0.4 to 8.9 km², and that the travel time of water emitted
674 from these springs is 1.4 to 2.8 years. The chemical composition of the springs, all sampled in the
675 early summer season, is the result of weathering of minerals exposed to percolating waters at
676 fracture surfaces, especially oligoclase; the proportion of solutes acquired by spring waters in
677 contact with saprolitic plagioclases along the weathering front is assumed to be insignificant. The
678 oligoclase weathering rates (W_{Pl}) were within the interval $(2.5 \pm 1.2) \times 10^{-14} \text{ mol} \cdot \text{m}^{-2} \cdot \text{s}^{-1}$, which is very
679 close to the range of rates determined in granite environments under field conditions in other studies
680 (White and Brantley, 2003; among others). In general, the waters collected at the spring sites in the
681 Vouga granites were in equilibrium with microcrystalline gibbsite and(or) halloysite/allophane, and
682 undersaturated with respect to albite-oligoclase. The range of the calculated dissolution rates was, at
683 least in part, caused by the fact that the spring waters consist of packets of water that are exposed to
684 different pathways and travel times that have been in contact with fresh and weathered oligoclases.
685

686 **References**

- 687
688 Anderson, G.M. (1996). *Thermodynamics of Natural Systems*. John Wiley & Sons, Inc. New York
689 etc., 382 pp.
690
691 Appelo, C.A.J., Postma, D. (2005). *Geochemistry, Groundwater and Pollution*. A.A. Balkema,
692 Rotterdam, 649 pp.
693
694 Arvidson, R.S., Lüttge, A. (2010). Mineral dissolution kinetics as a function of distance from
695 equilibrium—New experimental results. *Chem. Geol.* 269:79–88.
696
697 Beig, M.S., Lüttge, A. (2006). Albite dissolution kinetics as a function of distance from
698 equilibrium: Implications for natural feldspar weathering. *Geochim. Cosmochim. Acta* 70: 1402–
699 1420.
700
701 Berner, R.A., Lasaga, A.C., Garrels, R.M. (1983). The carbonate-silicate geochemical cycle and its
702 effect on atmospheric carbon dioxide over the past 100 Million years. *Am. J. Sci.* 283: 641–683.
703
704 Blum, A.E. (1994). Feldspars in weathering. In Parson, I. (Ed.) *Feldspars and Their Reactions*.
705 Kluwer Academic Publishers, Dordrecht, The Netherlands. p. 595–630.
706
707 Bolin, B., Rodhe, H. (1973). A note on the concepts of age distribution and transit time in natural
708 reservoirs. *Tellus* 25(1): 58–62.
709
710 Boussinesq, J. (1877). Essai sur la théorie des eaux courantes. *Mem. Acad. Sci. Inst. Fr.* 23: 252–
711 260.
712
713 Boussinesq, J. (1903). Sur le débit, en temps de sécheresse, d’une source alimentée par une nappe
714 d’eaux d’infiltration. *C. R. Hebd. Seanc. Acad. Sci. Paris* 136: 1511–1517.
715
716 Boussinesq, J. (1904). Recherches théoriques sur l’écoulement des nappes d’eau infiltrées dans le
717 sol et sur débit de sources. *J. Math. Pures Appl.* 10: 5–78.
718
719 Brantley, S.L., Mellott, N.P. (2000). Surface area and porosity of primary silicate minerals. *Am.*
720 *Mineral.* 58: 1767–1783.
721
722 Brantley, S.L., White, A.F., Hodson, M.E. (1999). Surface area of primary silicate minerals.
723 Chapter 14 in B. Jamtveit & P. Meakin (Eds.). *Growth, dissolution and pattern formation in*
724 *geosystems*. Kluwer Academic Publishers. p. 291–326.
725
726 Brutsaert, W. (1994). The unit response of groundwater outflow from a hillslope. *Water Resour.*
727 *Res.* 34: 233–240.
728
729 Brutsaert, W., Lopez, J.P. (1998). Basin-scale geohydrologic drought flow features of riparian
730 aquifers of the southern Great Plains. *Water Resour. Res.* 30: 2759–2763.
731
732 Brutsaert, W., Nieber, J.L. (1977). Regionalized drought flow hydrographs from a mature glaciated
733 plateau. *Water Resour. Res.* 13: 637–643.
734

- 735 Burch, T.E., Nagy, K.L., Lasaga, A.C. (1993). Free energy dependence of albite dissolution kinetics
736 at 80°C and pH 8.8. *Chem. Geol.* 105: 137–162.
737
- 738 Caetano, C.A.R., Pacheco, F.A.L. (2008). Modelação de escoamentos fluviais na região de Trás-os-
739 Montes e Alto Douro utilizando o modelo SWAT. In: V Seminário Recursos Geológicos, Ambiente
740 e Ordenamento do Território, UTAD, Vila Real, 16–18 October 2008. Special Volume in CD-
741 ROM, p. 44–53.
742
- 743 Cooper, H.H. Jr., Rorabaugh, M.I. (1963). Groundwater movements and bank storage due to flood
744 stages in surface streams. *USGS Water Supply Paper 1536-J*: 343–366.
745
- 746 De Bartolo, S.G., Gabriele, S., Gaudio, R. (2000). Multifractal behaviour of river networks.
747 *Hydrology and Earth System Sciences* 4(1): 105–112.
748
- 749 De Bartolo, S.G., Gaudio, R., Gabriele, S. (2004). Multifractal analysis of river networks: a sand-
750 box approach. *Water Resour. Res.* 40: 1–10.
- 751 De Bartolo, S.G., Veltri, M., Primavera, L. (2006). Estimated generalized dimensions of river
752 networks. *J. Hydrol.* 322: 181–191.
753
- 754 Domenico, P.A., Schwartz, F.W. (1990). *Physical and Chemical Hydrogeology*. John Wiley & Sons
755 Inc., New York, 824pp.
756
- 757 Drever, J.I. (1997). Weathering processes. In: Saether, P.M., de Caritat, P. (Eds.). *Geochemical*
758 *processes, weathering and groundwater recharge in catchments*. A.A. Balkema, Rotterdam /
759 Brookfield. p. 3–19.
760
- 761 Drever, J.I., Clow, D.W. (1995). Weathering rates in catchments. In: A.F. White & S.L. Brantley
762 (Eds.). *Chemical Weathering Rates of Silicate Minerals*. Reviews in Mineralogy, Volume 31,
763 Mineralogical Society of America, Washington D.C., USA. p. 463–483.
764
- 765 Dupré, B., Dessert, C., Oliva, P., Goddérés, Y., Viers, J., François, L., Millot, R., Gaillardet, J.
766 (2003). Rivers, chemical weathering and Earth's climate. *C.R. Geosci.* 335: 1141–1160.
767
- 768 ESRI (2007). *ArcMap* (version 9.3). New York St., Redlands, USA, 131p.
769
- 770 ESRI (2009). *ArchHydro Tools – Tutorial* (version 1.3). New York St., Redlands, USA, 131p.
771
- 772 Etcheverry, D., Perrochet, P., (2000). Direct simulation of groundwater transit-time distributions
773 using the reservoir theory. *Hydrogeology Journal* 8(2): 200–208.
774
- 775 Faure, G. (1998). *Principles and Applications of Geochemistry* (2nd edition). Prentice Hall, Upper
776 Saddle River, NJ, USA, 600 pp.
777
- 778 Gaudio, R., De Bartolo, S.G., Primavera, L., Gabriele, S., Veltri, M. (2006). Lithologic control on
779 the multifractal spectrum of river networks. *J. Hydrol.* 327: 365–375.
780
- 781 Goddérés, Y., Francois, L.M., Probst, A., Schott, J., Moncoulon, D., Labat, D., Viville, D. (2006).
782 Modelling weathering processes at the catchment scale: the WITCH numerical model. *Geochim. et*
783 *Cosmochim. Acta* 70, 1128–1147.
784

- 785 Godd ris, Y., Roelandt, C., Schott, J., Pierret, M.C., Francois, L.M. (2009). Towards an integrated
786 model of weathering, climate, and biospheric processes. In: Oelkers, E.H., Schott, J. (Eds.),
787 *Thermodynamics and Kinetics of Water–Rock Interaction*. Mineralogical Soc Amer., Vol. 70, p.
788 411–434.
- 789
- 790 Godinho, M.M. (1980). O Plutonito do Caramulo. Mem rias e Not cias, publica es do Museu e
791 Laborat rio Mineral gico e Geol gico da Universidade de Coimbra, 89/90: 269 pp.
- 792
- 793 Griffiths, G.A., Clausen, B. (1997). Streamflow recession in basins with multiple water storages. *J.*
794 *Hydrol.* 190: 60–74.
- 795
- 796 Hartmann, J., Jansen, N., D rr, H.H., Kempe, S., K hler, P. (2009). Global CO₂-consumption by
797 chemical weathering: What is the contribution of highly active weathering regions? *Global Planet.*
798 *Change* 69: 185–194.
- 799
- 800 Helgeson, H.C., Garrels, R.M., Mackenzie, F.T. (1969). Evaluation of irreversible reactions in
801 geochemical processes involving minerals and aqueous solutions—II. Applications. *Geochim.*
802 *Cosmochim. Acta* 33: 455–481.
- 803
- 804 Hellmann, R., Tisserand, D. (2006). Dissolution kinetics as a function of the Gibbs free energy of
805 reaction: An experimental study based on albite feldspar. *Geochim. Cosmochim. Acta* 70: 364–383.
- 806
- 807 Hornberger, G.M., Beven, K.J., Germann, P.E. (1990). Interferences about solute transport in
808 macroporous forest soils from time series models. *Geoderma* 46: 249–262.
- 809
- 810 Horton, R. E. (1945). Erosional development of streams and their drainage basins: hydrophysical
811 approach to quantitative morphology. *Geol. Soc. Am. Bull.* 56: 275–370.
- 812
- 813 La Barbera, P., Rosso, R. (1987). Fractal geometry of river networks. *Trans. Am. Geophys. Union*
814 68: 1276.
- 815
- 816 La Barbera, P., Rosso, R. (1989). On the fractal dimension of stream networks. *Water Resour. Res.*
817 25: 735–741.
- 818
- 819 Langmuir, D. (1997). *Aqueous Environmental Geochemistry*. Prentice Hall, Upper saddle River,
820 New Jersey, USA, 600 pp.
- 821
- 822 Lasaga, A.C. (1998). *Kinetic Theory in the Earth Sciences. Princeton Series in Geochemistry*
823 (Holland, H.D., editor). Princeton University Press. Princeton, New Jersey, 811 pp.
- 824
- 825 Lasaga, A.C., L ttge, A. (2004). Mineralogical approaches to fundamental crystal dissolution
826 kinetics—Dissolution of an A₃B structure. *Eur. J. Mineral.* 16: 713–729.
- 827
- 828 L ttge, A. (2005). Etch pit coalescence, surface area, and overall mineral dissolution rates. *Am.*
829 *Mineral.* 90: 1767–1783.
- 830
- 831 L ttge, A. (2006). Crystal dissolution kinetics and Gibbs free energy. *J. Electronic Spectroscopy*
832 *and Related Phenomena* 150: 248–259.
- 833

- 834 Maher, K. (2010). The dependence of chemical weathering rates on fluid residence time. *Earth*
835 *Planet. Sci. Letters* 294: 101–110.
836
- 837 Maher, K., Steefel, C.I., White, A.F., Stonestrom, D.A. (2009). The role of reaction affinity and
838 secondary minerals in regulating chemical weathering rates at the Santa Cruz Soil
839 Chronosequence, California. *Geochim. Cosmochim. Acta* 73: 2804–2831.
840
- 841 Malvicini, C. F., Steenhuis, T. S., Walter, M. T., Parlange, J.-Y., Walter, M. F. (2005). Evaluation
842 of spring flow in the uplands of Matalom, Leyte, Philippines. *Adv. Water Resour.*, 28: 1083–1090.
843
- 844 Martins (1985). Caracterização sumária dos solos de Trás-os-Montes e Alto Douro e sua ocupação.
845 Technical Report, Instituto Universitário de Trás-os-Montes e Alto Douro, 30 pp.
846
- 847 Martins, A.A.A., Madeira, M.V., Refega, A.A.G. (1995). Influence of rainfall on properties of soils
848 developed on granite in Portugal. *Arid Soil Res. Rehabil.* 9, 353–366.
849
- 850 McGuire, K.J., McDonnell, J.J. (2006). A review and evaluation of catchment transit time
851 modelling. *J. Hydrol.* 330: 543–563.
852
- 853 Medina, J.M.P.G. (1996). Contribuição para o Conhecimento da Geologia do Grupo das Beiras
854 (CXG) na Região do Caramulo–Buçaco (Portugal Central). PhD thesis, University of Aveiro, 183
855 pp.
856
- 857 Mendoza, G.F., Steenhuis, T.S., Walter, M.T., Parlange, J.Y. (2003). Estimating basin-wide
858 hydraulic parameters of a semi-arid mountainous watershed by recession flow analysis. *J. Hydrol.*
859 279: 57–69.
860
- 861 Meunier, A., Sardini, P., Robinet, J.C., Prêt, D. (2007). The petrography of weathering processes:
862 facts and outlooks. *Clay Miner.* 42: 415–435.
863
- 864 Meyboom, P. (1961). Estimating groundwater recharge from stream hydrographs. *J. Geophys. Res.*
865 66: 1203–1214.
866
- 867 Nikora, V.I., Sapozhnikov, V.B. (1993). River network fractal geometry and its computer
868 simulation. *Water Resour. Res.* 29: 3565–3575.
869
- 870 Nordstrom, D.K., Plummer, L.N., Langmuir, D., Busenberg, E., May, H.M., Jones, B.F., Parkhurst,
871 D.L. (1990). Revised chemical equilibrium data for major water–mineral reactions and their
872 limitations. In: *Chemical Modeling of Aqueous Systems II*. (Eds. Melchior D.C. and Bassett, R.L.).
873 ACS Symposium Series 416. American Chemical Society, Washington, DC 1990, pp. 398–413.
874
- 875 Oelkers, E.H., Schott, J., Devidal, J-L. (1994). The effect of aluminium, pH, and chemical affinity
876 on the rates of aluminosilicate dissolution reactions. *Geochim. Cosmochim. Acta* 58: 2011–2024.
877
- 878 Oliva, P., Viers, J, Dupré, B. (2003). Chemical weathering in granitic environments. *Chem. Geol.*
879 202: 225–256.
880
- 881 Paces, T. (1978). Reversible control of aqueous aluminum and silicate during the irreversible
882 evolution of natural waters. *Geochim. Cosmochim. Acta* 42: 1487–1493.
883

- 884 Pacheco, F.A.L., Alenco, A.M.P. (2006). Role of fractures in weathering of solid rocks:
885 narrowing the gap between experimental and natural weathering rates. *J. Hydrol.* 316: 248–265.
886
- 887 Pacheco, F.A.L., Van der Weijden, C.H. (1996). Contributions of water–rock interactions to the
888 composition of groundwater in areas with sizeable anthropogenic input. A case study of the waters
889 of the Fundo area, central Portugal. *Water Resour. Res.* 32: 3553–3570.
890
- 891 Pacheco, F.A.L., Van der Weijden, C.H. (2002). Mineral weathering rates calculated from spring
892 water data. A case study in an area with intensive agriculture, the Morais massif, NE Portugal. *Appl.*
893 *Geochem.* 17: 583–603.
894
- 895 Pacheco, F.A.L., Sousa Oliveira, A., Van der Weijden, A.J., Van der Weijden, C.H. (1999).
896 Weathering, biomass production and groundwater chemistry in an area of dominant anthropogenic
897 influence, the Chaves–Vila Pouca de Aguiar region, north of Portugal. *Water Air Soil Poll.* 115:
898 481–512.
899
- 900 Padilla, A., Pulido-Bosh, A., Mangin, A. (1994). Relative importance of baseflow and quickflow
901 from hydrographs of karst spring. *Ground Water* 32: 267–277.
902
- 903 Press, W.H., Flannery, B.P., Teukolsky, S.A., Vetterling, W.T. (1991), *Numerical Recipes in Pascal*,
904 Cambridge University Press, Cambridge, Massachusetts.
- 905
- 906 Rasse, D.P., Francois, L.M., Aubinet, M., Kowalski, A.S., Vande Walle, I., Laitat, E., Ge´rard, J.C.
907 (2001). Modelling short-term CO₂ fluxes and long-term tree growth in temperate forests with
908 ASPECTS. *Ecol. Modell.* 141, 35–52.
909
- 910 Rodhe, A., Killingtveit, A. (1997). Catchment hydrology. In: Saether, O.M. & de Caritat, P. (Eds.).
911 *Geochemical Processes, Weathering and Groundwater Recharge in Catchments*. A.A. Balkema.
912 Rotterdam / Brookfield, pp. 77–107.
913
- 914 Roelandt, C., Godderis, Y., Bonnet, M.P., Sondag, F. (2010). Coupled modeling of biospheric and
915 chemical weathering processes at the continental scale. *Global Biogeochemical Cycles* 24, 18.
916
- 917 Rosso, R., Enechi, B. La Barbera, P. (1991). Fractal relation of mainstream length to catchment area
918 in river networks. *Water Resour. Res.* 27: 381–387.
919
- 920 Roth, G., La Barbera, P., Greco, M. (1996). On the description of the basin effective drainage
921 structure, *J. Hydrol.*, 187(1-2): 119–135.
922
- 923 Rueda, F., Moreno-Ostos, E., Armengol, J. (2006). The residence time of river water in reservoirs.
924 *Ecological Modelling* 191(2): 260–274.
925
- 926 Rupp, D. E., Selker, J. S. (2005). Drainage of a horizontal Boussinesq aquifer with a power law
927 hydraulic conductivity profile, *Water Resour. Res.*, 41: W11422, doi:10.1029/2005WR004241.
928
- 929 Rupp, D. E., Selker, J. S. (2006). Drainage of a horizontal Boussinesq aquifer with a power law
930 hydraulic conductivity profile, *Water Resour. Res.*, 42: W12421, doi:10.1029/2006WR005080.
931

- 932 Schermerhorn, L.J.G. (1956). Igneous, Metamorphic and Ore Geology of the Castro d'Aire-São
933 Pedro do Sul region (northern Portugal). Ph.D thesis, University of Amsterdam, 617 pp.
934
- 935 Schuller, D.J., Rao, A.R., Jeong, G.D. (2001). Fractal characteristics of dense stream networks. *J.*
936 *Hydrol.* 243: 1–16.
937
- 938 Schumm, S.A. (1956). Evolution of drainage systems and slopes in Badlands at Perth Amboy, New
939 Jersey. *Geol. Soc. Amer. Bull.* 67: 597–646.
940
- 941 Snow, D.T. (1968). Rock fracture spacings, openings, and porosities. *J. Soil Mechanics*, 94: 73–91.
942
- 943 Soen, O.I. (1958). The Geology, Petrology and Ore Deposits of the Viseu region, northern Portugal.
944 PhD thesis, University of Amsterdam, 179 pp.
945
- 946 Steefel, C.I., Lasaga, A.C. (1992). Putting transport into water-rock interaction models. *Geology*
947 20: 680–684.
948
- 949 Steefel, C.I., Van Cappellen, P. (1990). A new kinetic approach to modeling water-rock interaction:
950 The role of nucleation, precursors, and Oswald ripening. *Geochim. Cosmochim. Acta* 54: 2657–
951 2677.
952
- 953 Strahler, A.N. (1952). Hypsometric (area-altitude) analysis of erosional topography. *Geological*
954 *Society American Bulletin* 63: 1117–1142.
955
- 956 Strahler, A. N. (1957). Quantitative analysis of watershed geomorphology. *Transactions of the*
957 *American Geophysical Union* 8(6): 913–920.
958
- 959 Szilagyi, J., Parlange, M.B. (1999). A geomorphology-based semi-distributed watershed model.
960 *Adv. Water Resour.* 23: 177–187.
961
- 962 Szilagyi, J., Parlange, M.B., Albertson, J.D. (1998). Recession flow analysis for aquifer parameter
963 determination. *Water Resour. Res.* 34(7): 1851–1857.
964
- 965 Tarboton, D.G. (1996). Fractal river networks, Horton's laws and Tokunaga cyclicity. *J. Hydrol.*
966 187: 105–117
967
- 968 Tardy Y., Bustillo V., Boeglin J. (2004). Geochemistry applied to the watershed survey: hydrograph
969 separation, erosion and soil dynamics. A case study: the basin of the Niger River, Africa. *Appl.*
970 *Geochem.* 19: 469–518.
971
- 972 Van de Giesen, N. C., Steenhuis, T. S., Parlange, J.-Y. (2005). Short- and long-time behavior of
973 aquifer dainage after slow and sudden recharge according to the linearized Laplace equation. *Adv.*
974 *Water Resour.*, 28: 1122– 1132.
975
- 976 Van der Weijden, C.H., Pacheco, F.A.L. (2006). Hydrogeochemistry in the Vouga River basin
977 (central Portugal): pollution and chemical weathering. *Appl. Geochem.* 21: 580–613.
978
- 979 Velbel, M.A. (1985). Geochemical mass balances and weathering rates in forested watersheds of
980 the Southern Blue Ridge. *Am. J. Sci.* 285: 904–930.
981

- 982 Velbel, M.A. (1989). Effect of chemical affinity on feldspar hydrolysis rates in two natural
983 weathering systems. *Chem. Geol.* 78: 245–253.
984
- 985 Velbel, M.A. (1993). Constancy of silicate–mineral weathering-rate ratios between natural and
986 experimental weathering: implications for hydraulic control of differences in absolute rates. *Chem.*
987 *Geol.* 105: 89–99.
988
- 989 Violette, A., Godd ris, Y, Mar chal, J, Riotte, J, Oliva, P, Kumar, M.S.M., Sekhar, M., Braun, J.
990 (2010). Modelling the chemical weathering fluxes at the watershed scale in the Tropics (Mule Hole,
991 South India): Relative contribution of the smectite/kaolinite assemblage versus primary minerals.
992 *Chem. Geol.* 277: 42–60.
993
- 994 White, A.F. (2002). Determining mineral weathering rates based on solid and solute weathering
995 gradients and velocities: application to biotite weathering in saprolites. *Chem. Geol.* 190: 69–89.
996
- 997 White, A.F., Brantley, S.L. (2003). The effect of time on the weathering of silicate minerals: why
998 do weathering rates differ in the laboratory and field? *Chem. Geol.* 202: 479–506.
999
- 1000 White, A.F., Peterson, M. (1990a). The role of reactive surface areas in chemical weathering. *Chem.*
1001 *Geol.* 84: 334–336.
1002
- 1003 White, A.F., Peterson, M. (1990b). Role of reactive-surface-area characterization in geochemical
1004 kinetic models. In: D.C. Melchior and R.L. Bassett (Eds.). *Chemical Modelling of Aquous Systems*
1005 II. ACS Symposium Series 416. Am. Chem. Soc., Washington, DC. p. 459–475.
1006
- 1007 White, A.F., Bullen, T.D., Schulz, M.S., Blum, A.E., Huntington, T.G., Peters, N.E. (2001).
1008 Differential rates of feldspar weathering in granitic regoliths. *Geochim. Cosmochim. Acta* 65: 847–
1009 869.
1010
- 1011 Zhang, L., L ttge, A. (2009). Theoretical approach to evaluating plagioclase dissolution
1012 mechanisms. *Geochim. Cosmochim. Acta* 73: 2832–2849.
1013
- 1014 Zecharias, Y.B., Brutsaert, W. (1985). Ground surface slope as a basin scale parameter. *Water*
1015 *Resour. Res.* 21:1895–902.
1016
- 1017 Zecharias, Y.B., Brutsaert, W. (1998). Recession characteristics of groundwater outflow and base
1018 flow from mountainous watersheds. *Water Resour. Res.* 24:1651–8.
1019

1020 **Table legends**

1021

1022

1023 Table 1:

1024 Morphologic and hydrologic characterization of seven watersheds within the Vouga River

1025 hydrographic basin. Id – Label of the hydrometric station located at the outlet of the watershed, in

1026 agreement with labels in Figure 1; Code – identification of code of the hydrometric station; X, Y –1027 location coordinates of the hydrometric station, in the Hayford-Gauss system; V , A and L – volume1028 and area of the watershed and length of water channels within the watershed; a_1 , a_3 – intercept-y of1029 the dashed lines in Figure 7; K , n_e – average hydraulic conductivity and effective porosity of the1030 watershed; Q_i , Q_f – average base flow discharge rates at the start and end of recession periods; V_r –1031 average annual recharge; t – average groundwater travel time. The average values pertain to the

1032 record length of each station.

1033

1034 Table 2:

1035 Summary of field weathering rates (W , $\text{mol}\cdot\text{m}^{-2}\cdot\text{s}^{-1}$) of oligoclases. References other than this study:

1036 1) Drever and Clow (1995), 2) Velbel (1985), 3) White et al. (2001), 4) White and Brantley (2003).

1037

1038 Legends to Figures

1039

1040 Figure 1:

1041 Location of Vouga river basin in the North of Portugal and next to the Atlantic Ocean. Digital
1042 Elevation Model (DEM) of the basin with reference to surrounding mountains (Lapa, Caramulo and
1043 Freita) and to the mouth area in the Ria de Aveiro. Distribution of precipitation (P) and of
1044 hydrometric stations (labeled circles) inside the basin. The labels of the circles agree with the Id
1045 numbers in Table 1.

1046

1047 Figure 2:

1048 Simplified geological map of Vouga river basin. Adapted from the Geological Map of Portugal,
1049 scale 1/500 000, produced in 1992 by the Portuguese Geological Survey. Distribution of the
1050 sampled springs (labeled black dots) within the granite area of the basin. The labels of the dots
1051 agree with Sample # in Appendix 1.

1052

1053 Figure 3: Flowchart of the THROW model.

1054

1055 Figure 4a:

1056 Distribution of watersheds within the granite area of the Vouga basin, taking into account their
1057 order of Strahler (classification according to Strahler, 1957). Symbols: i – Strahler order; n , A –
1058 number and average area of watersheds of a given order.

1059

1060 Figure 4b:

1061 Plot of stream watershed area as a function of Strahler order, illustrating the firm relationship
1062 existing between these variables.

1063

1064 Figure 5:

1065 Distribution of equivalent spring orders (shaded areas) and location of the sampled (circles), within
1066 the granite area of the Vouga basin. Location of hydrometric stations labeled Id = 1–3 in Table 1.
1067 Symbol: i_{eq} – equivalent spring order (calculated by Equation 2). The i_{eq} under each spring can be
1068 used in Equation 15 (replacing i) to extrapolate the area of its associated watershed.

1069

1070 Figure 6:

1071 Application of the Brutsaert method to the watershed located upstream Station 1 (see location in
1072 Figure 1). The original data used in the plot pertains to the 1936-53 period and is available at
1073 www.inag.pt. The method is used to calculate the average watershed hydraulic conductivity and
1074 effective porosity (Equations 5a,b): $K = 2.4 \times 10^{-7} \text{ m} \cdot \text{s}^{-1}$; $n_e = 3.7 \times 10^{-2}$.

1075

1076 Figure 7:

1077 Stream hydrograph of Station 1 (see location in Figure 1 and summary of data in Table 1). The
1078 record of discharge rate measurements (Q) is available at www.inag.pt. Illustration of the
1079 hydrograph method used for the estimation of V_r (Meyboom, 1961), taking into account the values
1080 of Q_i , Q_f , and t_1 obtained for the 1939/40 and 1940/41 recessions. The explanation of the symbols is
1081 given in the text. For this pair of recession periods, $V_r = 78 \times 10^6 \text{ m}^3$ (Equation 9).

1082

1083 Figure 8:

1084 Plot of hydraulic conductivity, effective porosity and groundwater travel time, as a function of
1085 stream watershed area, illustrating the unequivocal (firm in the case of t) relationship existing
1086 between these variables.

1087

1088 Figure 9:
1089 Total Al concentrations (open symbols), as far as they were determined, and theoretical total
1090 concentrations (curves) plotted against pH for (a) crystalline gibbsite, microcrystalline gibbsite and
1091 amorphous $\text{Al}(\text{OH})_{3(s)}$, and (b) kaolinite, halloysite and allophane. Total Al concentrations and pH
1092 values at the sampling sites are listed in Appendix 1. The curves for the solid phases as a function
1093 of pH are calculated from data in Nordstrom et al. (1990) for $\text{Al}(\text{OH})_3$ -phases and in Langmuir
1094 (1997) for the Al-silicate phases. In the last case, the H_4SiO_4^0 activity was fixed at its median value
1095 (Appendix 1). Note that the distances between the curves for each solid phase turn out to be only
1096 very small when instead of the median value the minimum and maximum values of H_4SiO_4^0
1097 activities would have been used. It appears that the solutions are most closely in equilibrium with
1098 microcrystalline gibbsite and(or) halloysite/allophane (cf. also columns 8–13 in Appendix 2).

1099
1100 Figure 10:
1101 Plot of the calculated amounts* of ‘gibbsite’ precipitated from the ground water as result of ongoing
1102 dissolution of plagioclase, against the calculated degree of saturation of microcrystalline gibbsite
1103 (Appendix 2). Quite a few samples for which precipitation of ‘gibbsite’ was calculated (SiB results)
1104 are indeed close to equilibrium (cf. also Appendix 2, column 9) with microcrystalline gibbsite. For
1105 the other samples, no precipitation of ‘gibbsite’ was calculated, but many of these samples are also
1106 located in areas where $P < 1000 \text{ mm}\cdot\text{y}^{-1}$, areas where the occurrence of gibbsite in soils is unlikely
1107 (Martins et al., 1995). Some waters (springs nrs. 1038, 2070, 2079, 2089 and 2101), although
1108 highly supersaturated relative to microcrystalline gibbsite ($Q/K_{\text{eq}} > 5$) and located in areas where P
1109 $> 1000 \text{ mm}\cdot\text{y}^{-1}$ (see Appendix 2), had nonetheless $[\text{Gibbsite}] = 0 \text{ }\mu\text{M}$.

1110 *We recognize that the presence, not the amount of ‘gibbsite’ matters.

1111

1112 **Legends For the Appendices.**

1113

1114 Appendix 1:

1115 The identification code of the sampled and analyzed springs (Sample #) is given in Column 1. The
1116 results from the hydrological analysis are presented in Columns 2–4. The pHs of the springs are
1117 listed in Column 5. The concentrations of the dissolved species are given in brackets in Columns 6–
1118 15, and their concomitant activities, calculated using the Davies equation, are given in braces in
1119 Columns 16–20. The calculation of $\{Al^{3+}\}$ at 15°C is based on hydrolysis constants for Al^{3+} in
1120 Nordstrom et al. (1990).

1121

1122

1123 Appendix 2:

1124 The identification code of the sampled and analyzed springs (Sample #) is given in Column 1.
1125 Column 2 reports the annual rainfall in the vicinity of the spring sites (in agreement with Figure 1).
1126 Cols 3–7 summarize the results of the SiB model (Van der Weijden and Pacheco, 2006): x is the
1127 anorthite fraction of plagioclase assumed in the model, indicating a compositional range from albite
1128 to oligoclase, [PI] is the contribution of plagioclase dissolution to the water chemistry, whereas
1129 [smectite], [halloysite] and [gibbsite] are their calculated amounts of aluminosilicate and aluminum
1130 hydroxide phases precipitated along the flow path. Columns 8–14 list the results of the
1131 thermodynamic analyses: the Q -values (ion activity products) were calculated from the relevant
1132 activities of the species involved in the equilibria of the secondary solid phases. The concomitant
1133 K_{eq} values in Columns 8–10 were adopted from Nordstrom et al. (1990), the ones in Columns 11–
1134 13 from Langmuir (1997). The ΔG_r values in Column 14, pertaining to the congruent dissolution of
1135 the plagioclases (reaction R1), were calculated using the relation: $\Delta G_r = 2.303RT(\log Q - \log K_{eq})$,
1136 where R is the gas constant (in $\text{kJ}\cdot\text{mol}^{-1}\cdot\text{K}^{-1}$) and T the temperature (in K), Q is the actual ion
1137 activity product of the species involved in the dissolution reaction, and $\log K_{eq} = -\Delta G_r^0 / 2.303RT$.
1138 The ΔG_r^0 values for reaction R1 were calculated from the ΔG_f^0 values of the plagioclases (with x as
1139 in Column 3) and the concomitant dissolved species as given in Anderson (1996) and Faure (1998).
1140 All values were calculated for 15°C by application of the Van 't Hoff equation using the enthalpies
1141 of the dissolution reactions (ΔH_r^0) derived from the ΔH_f^0 values listed in the two last mentioned
1142 textbooks. The final column gives the weathering rates calculated as explained in the text.

Figure 1
[Click here to download high resolution image](#)

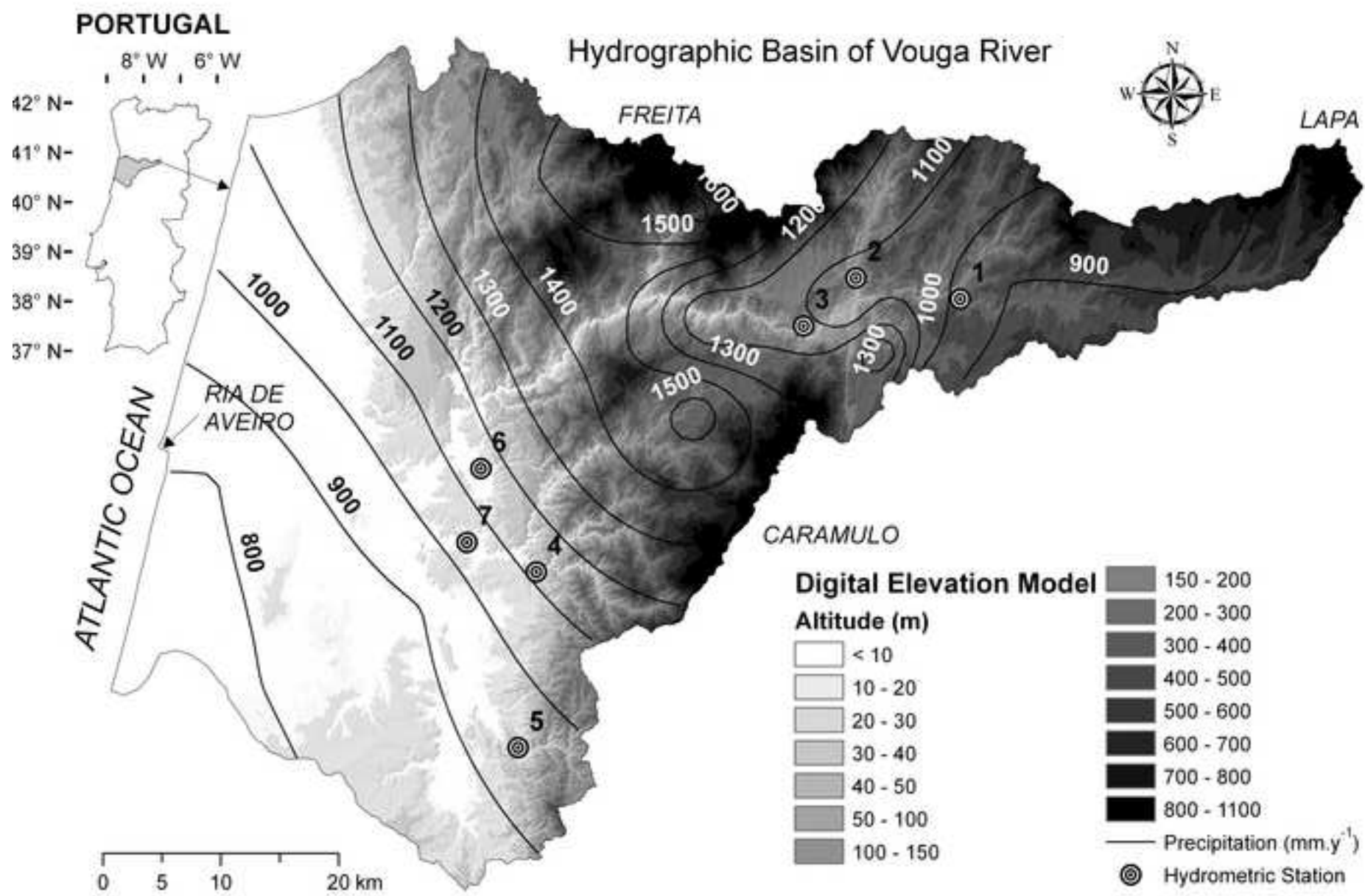


Figure 2
[Click here to download high resolution image](#)

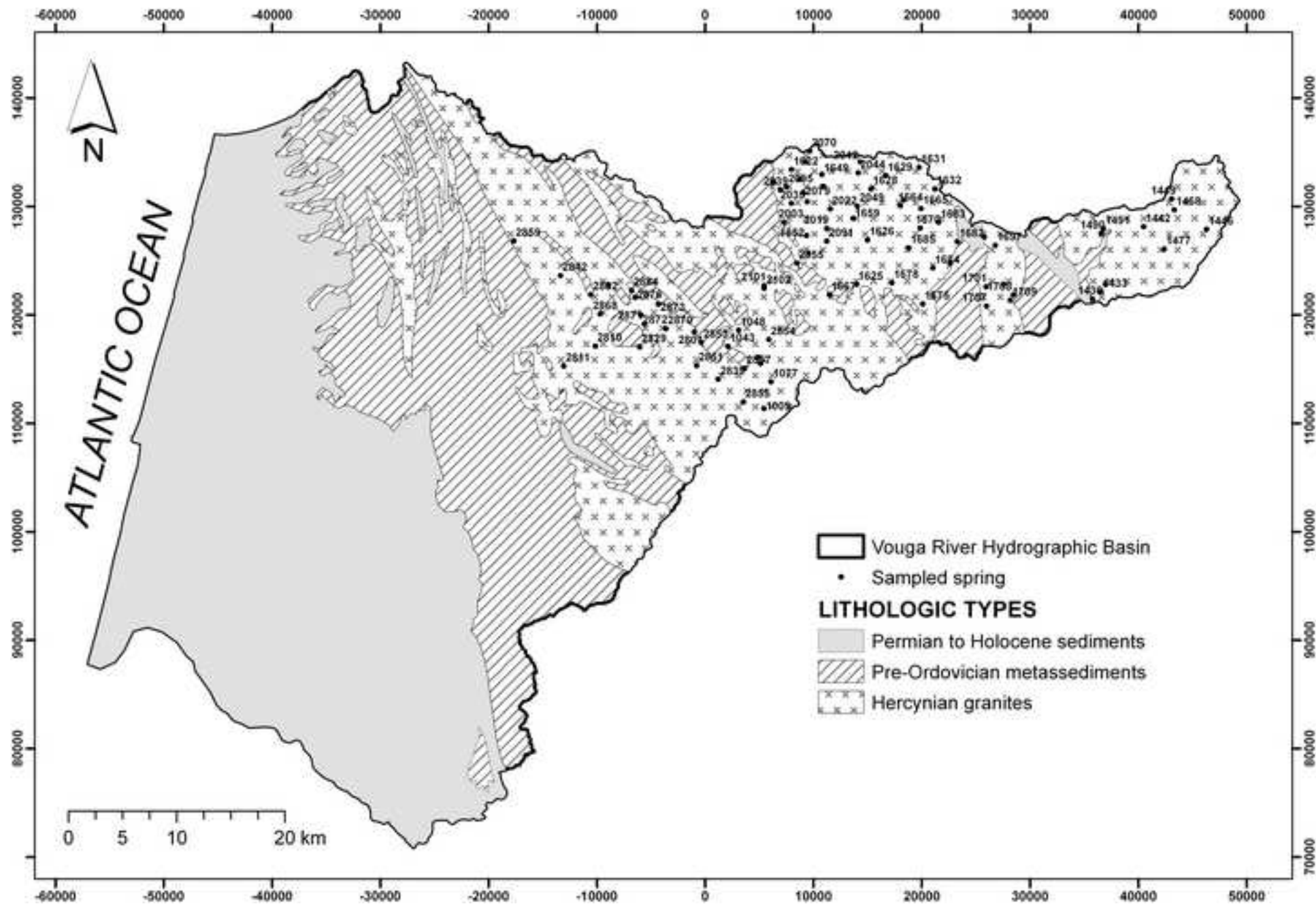


Figure 3
[Click here to download high resolution image](#)

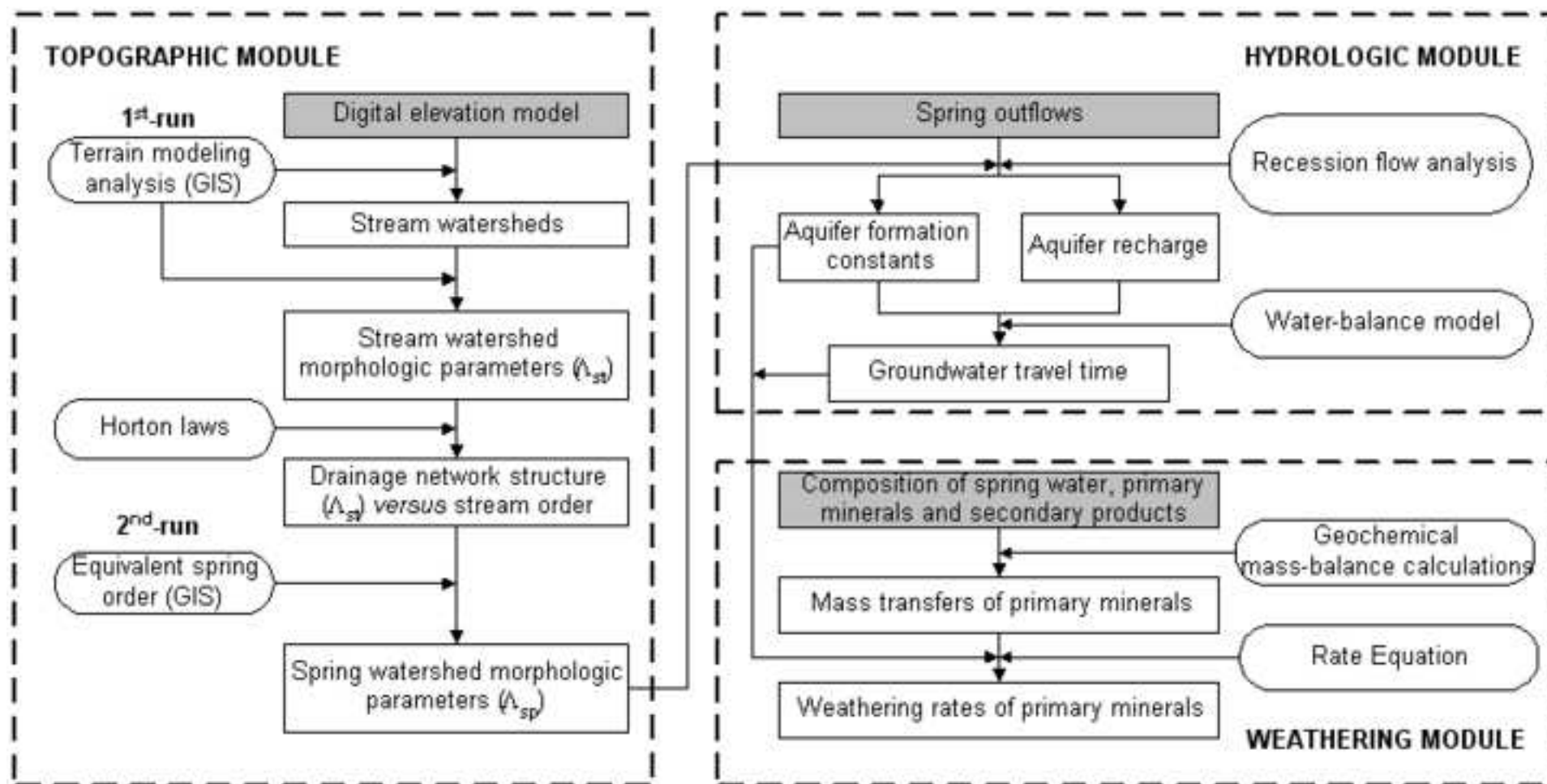


Figure 4a
[Click here to download high resolution image](#)

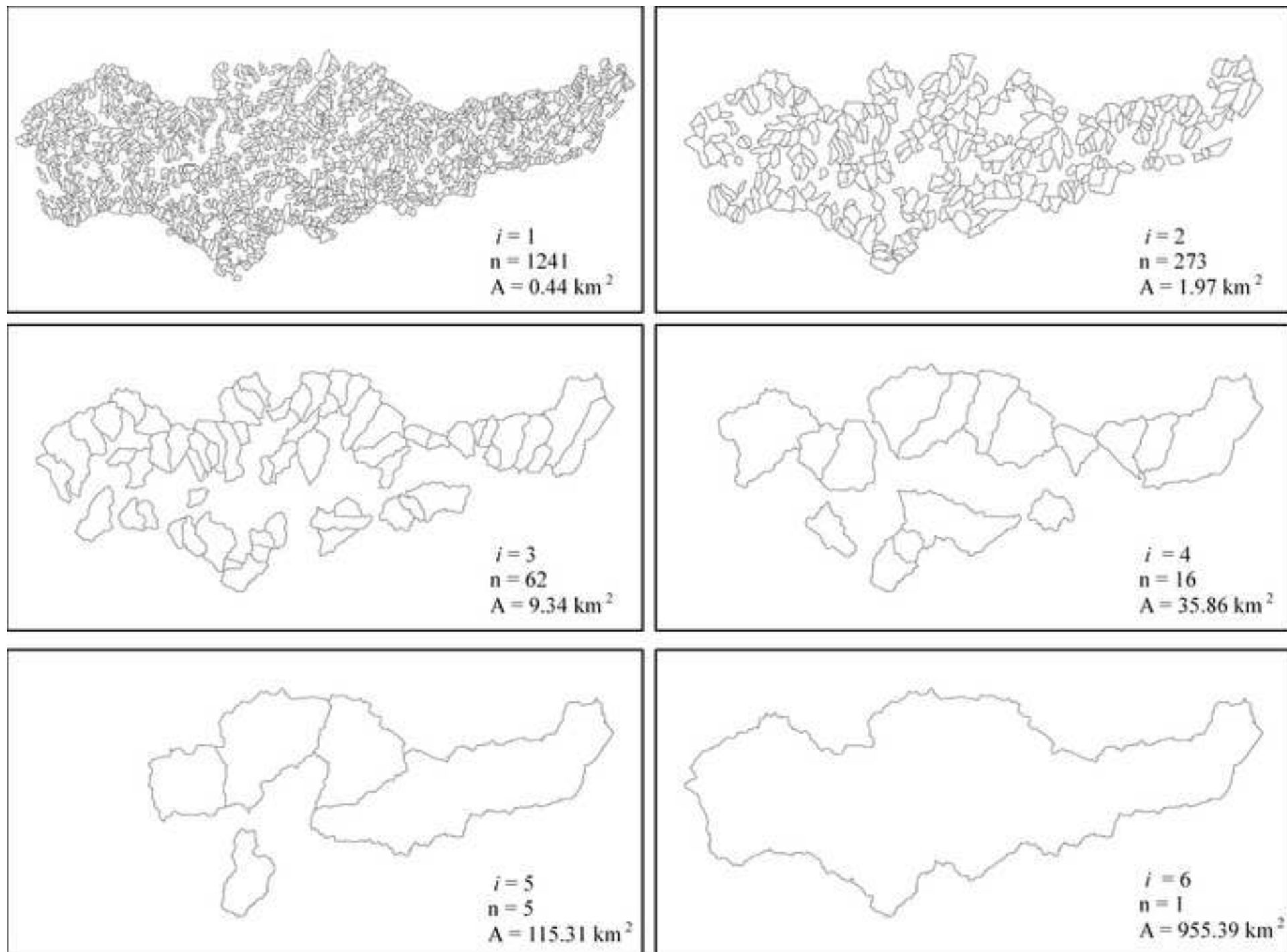


Figure 4b
[Click here to download high resolution image](#)

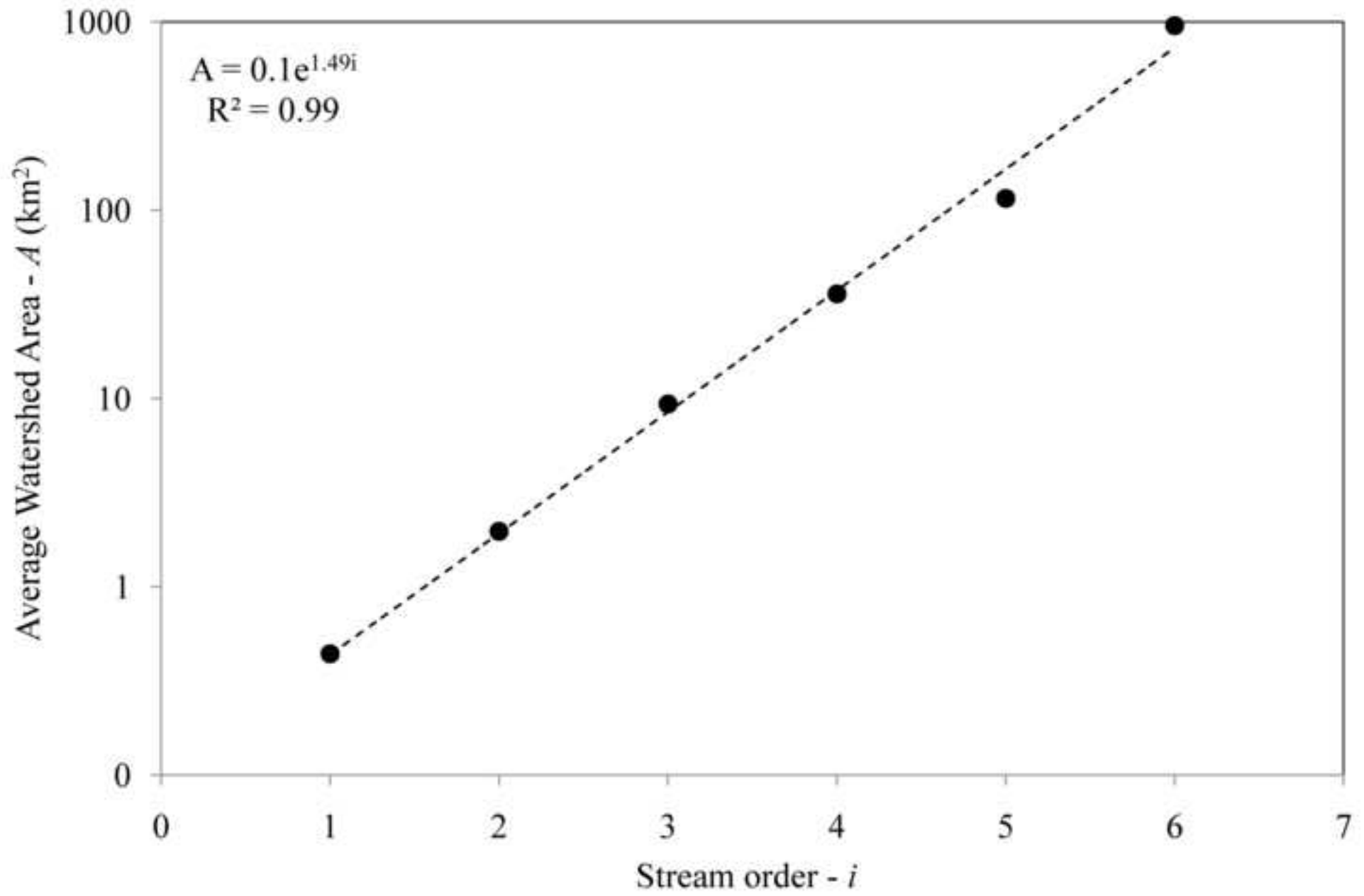


Figure 5
[Click here to download high resolution image](#)

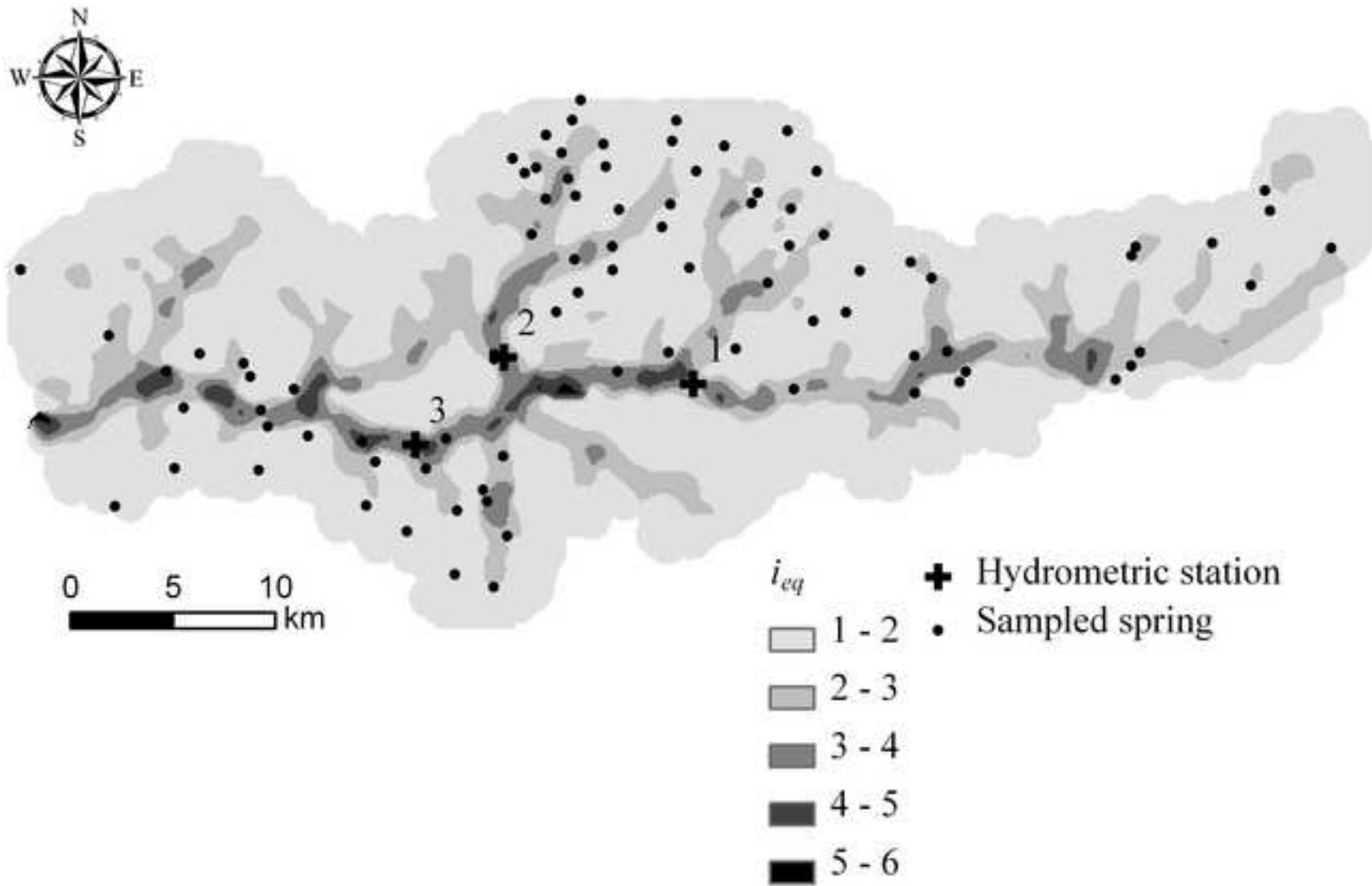


Figure 6
[Click here to download high resolution image](#)

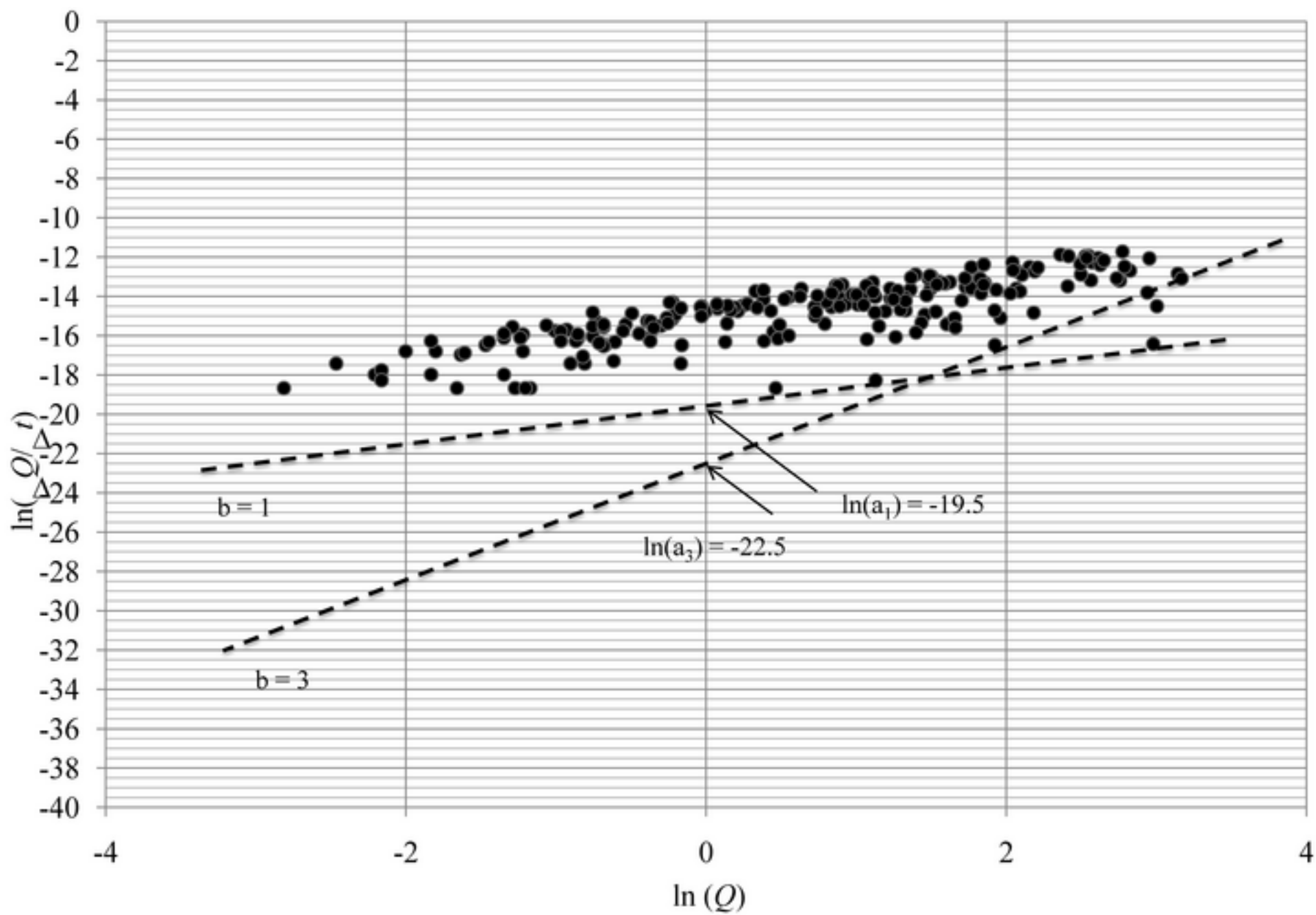


Figure 7
[Click here to download high resolution image](#)

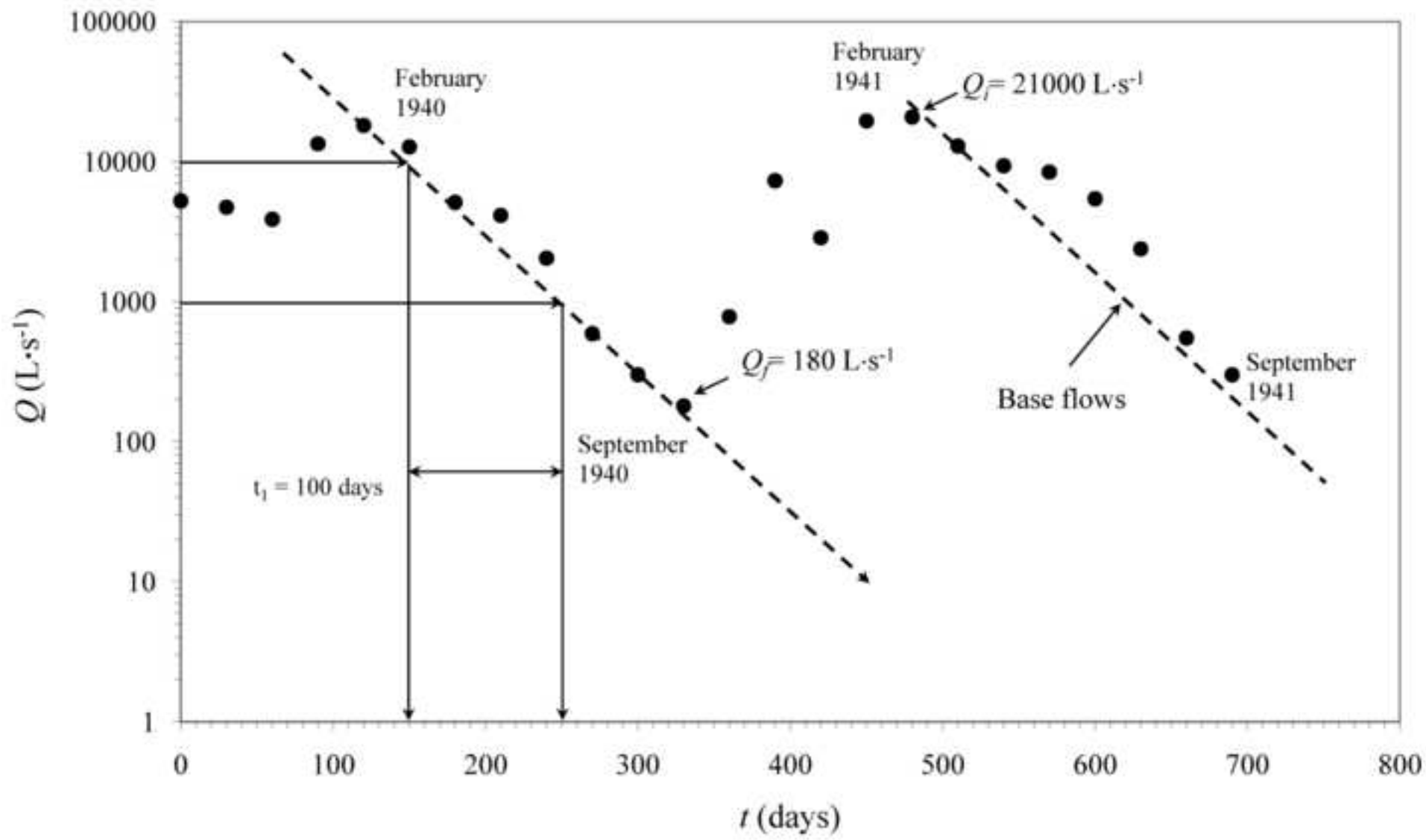


Figure 8
[Click here to download high resolution image](#)

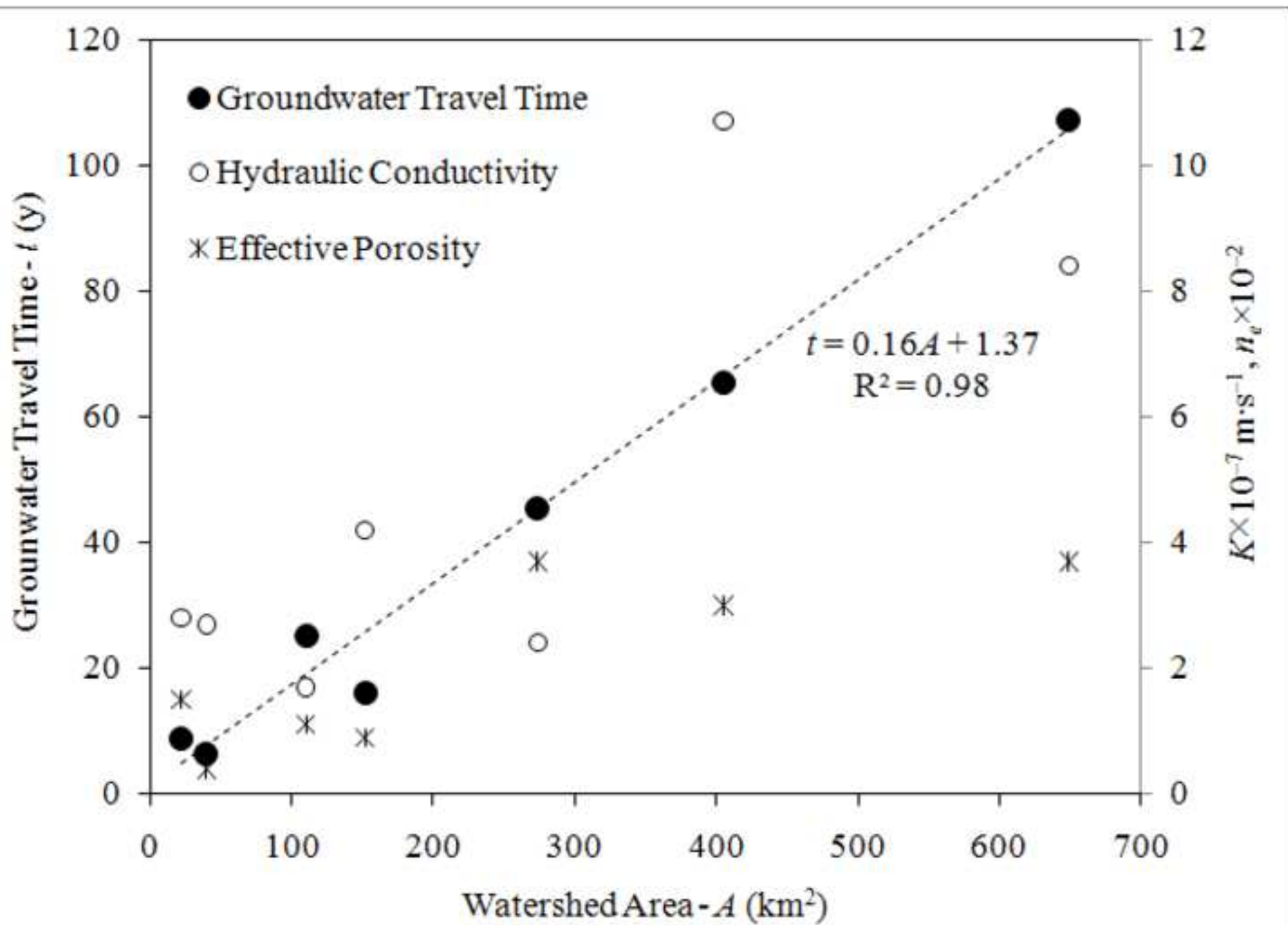


Figure 9a
[Click here to download high resolution image](#)

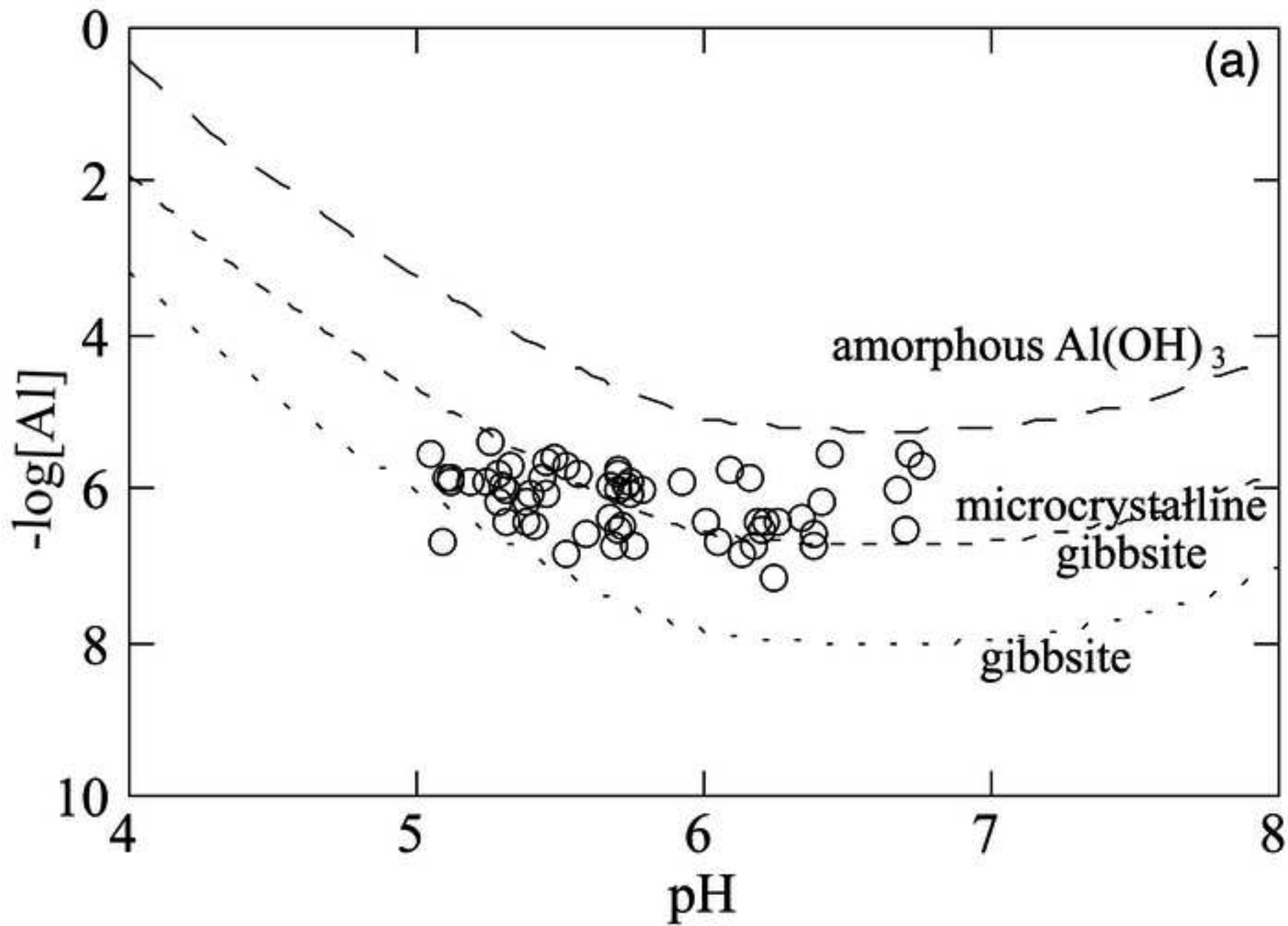


Figure 9b
[Click here to download high resolution image](#)

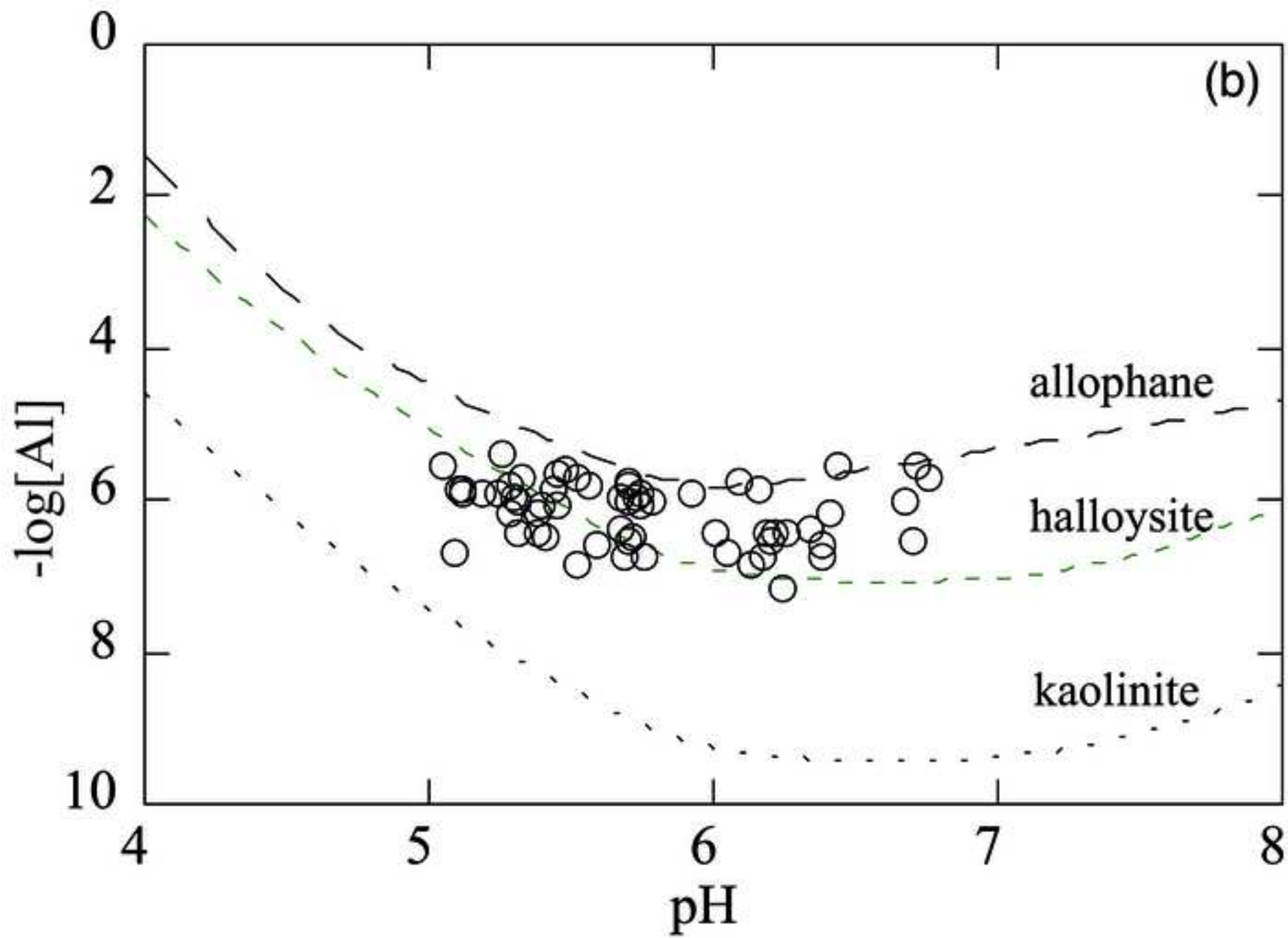


Figure 10
[Click here to download high resolution image](#)

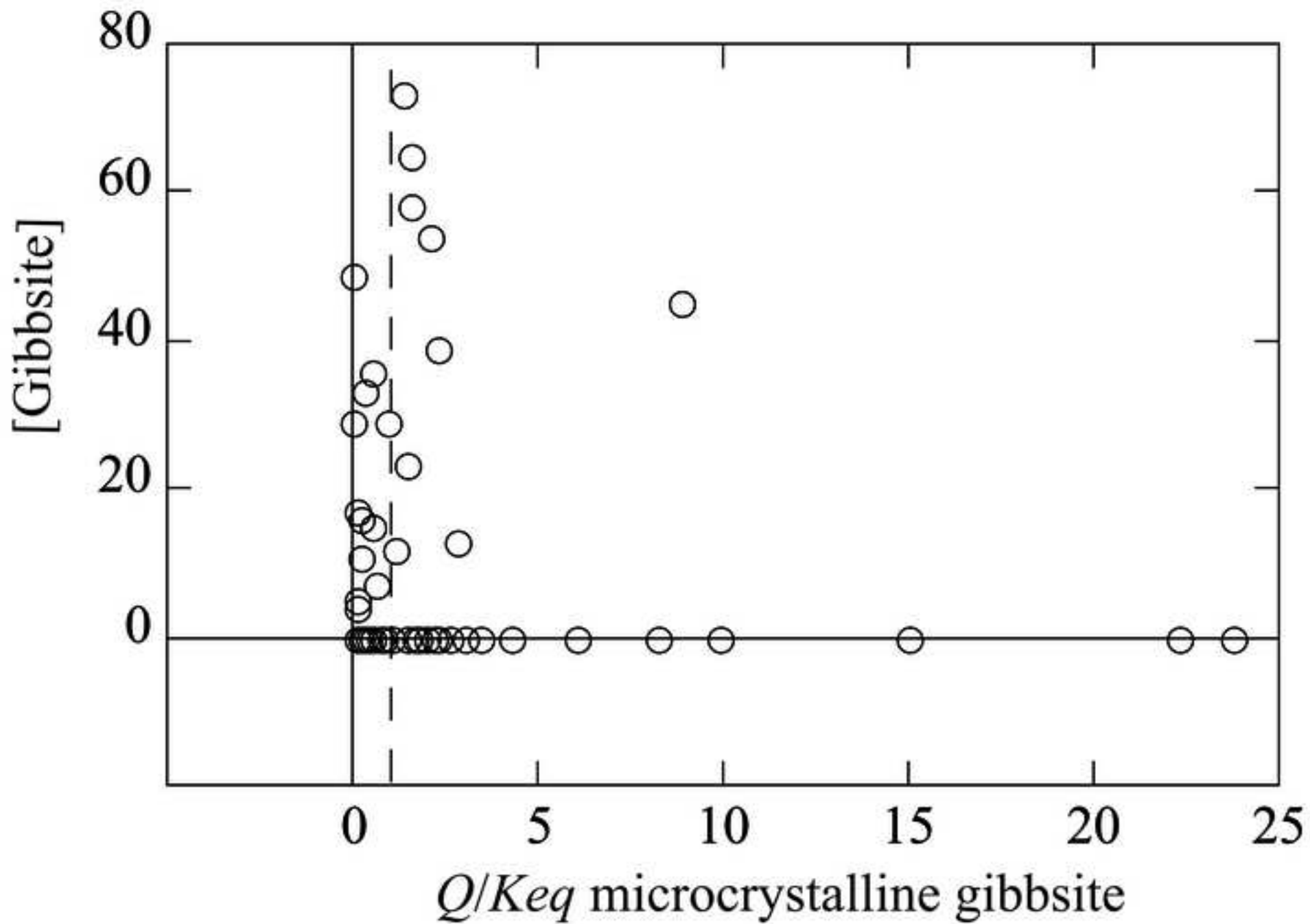


Table 1:

Parameter	Units	Value						
Id		1	2	3	4	5	6	7
Code		09J/01	09I/03	09I/02	10G/05	11G/01	10G/01	10G/02
River		Vouga	Sul	Vouga	Águeda	Serra	Marnel	Águeda
Starting year		1936	1981	1917	1977	1978	1977	1934
Record length	y	17	9	40	12	11	10	52
X	m	15086	6238	1797	-20880	-22428	-25588	-26764
Y	m	121045	122825	118766	97871	82965	106651	100372
$V \times 10^9$	m^3	71	62	317	82	12	7	236
$A \times 10^6$	m^2	274	110	649	152	40	22	405
$L \times 10^3$	m	177	59	146	79	39	24	138
$a_1 \times 10^{-9}$		3.4	8.4	2.1	25.1	75.4	33.9	9.2
$a_3 \times 10^{-11}$		16.9	92.6	1.4	27.9	2272.0	1020.9	0.8
$K \times 10^{-7}$	$m \cdot s^{-1}$	2.4	1.7	8.4	4.2	2.7	2.8	10.7
$n_e \times 10^{-2}$		3.7	1.1	3.7	0.9	0.4	1.5	3.0
Q_i	$m^3 \cdot s^{-1}$	15.42	7.75	30.0	12.5	2.0	3.2	30.0
Q_f	$m^3 \cdot s^{-1}$	0.18	0.19	1.0	0.175	0.05	0.01	1.2
$V_r \times 10^6$	m^3	57	28	109	46	7	12	108
t	y	46	25	107	16	7	9	66

Table 2:

$-\log(W)$	Exposed surface estimation	Remarks	Reference
13.7 ± 0.3	fracture	average value (n=87)	this study
12.7	geometric	average value (n=2)	1
12.05	geometric	single value	2
12.9 ± 1	geometric	average value (n=5)	3
15.0 ± 1.7	BET	ditto (n=3)	
12.7 ± 1.2	geometric	average value (n=4)	4
14.7 ± 1.3	BET	ditto (n=15)	

APPENDIX 1

Sample #	Equivalent spring order (sampled from Figure 5)	Catchment area (km ²) Equation 15	Travel time (years) Equation 16	pH	[Na ⁺] μM	[K ⁺] μM	[Mg ²⁺] μM	[Ca ²⁺] μM	[HCO ₃ ⁻] μM	[Cl ⁻] μM	[SO ₄ ²⁻] μM	[NO ₃ ⁻] μM	[H ₄ SiO ₄ ⁰] μM	[Al] μM	[Na ⁺] 15°C	[Ca ²⁺] 15°C	[Al ³⁺] 15°C	[H ₄ SiO ₄ ⁰] 15°C	[HCO ₃ ⁻] 15°C
1009	1.91	1.71	1.64	5.28	193	7.9	4.8	11	75	189	8.2	11.5	250	1.74	1.89E-04	1.02E-05	6.1E-07	2.50E-04	7.40E-05
1038	3.00	8.61	2.75	6.4	331	13.1	9.6	20	156	283	5.9	1.9	314	0.74	3.23E-04	1.80E-05	3.5E-09	3.14E-04	1.52E-04
1040	2.31	3.11	1.87	5.78	360	25.4	16.9	26	170	315	8.4	1.3	342	1.04	3.51E-04	2.34E-05	9.4E-08	3.42E-04	1.66E-04
1043	2.95	8.01	2.65	6.5	361	20.0	27.7	55	197	282	27.1	33.9	437		3.51E-04	4.87E-05		4.37E-04	1.91E-04
1048	3.53	19.14	4.43	5.09	395	16.2	39.8	33	74	389	59.4	19.4	283	0.22	3.83E-04	2.95E-05	9.8E-08	2.83E-04	7.16E-05
1077	2.31	3.11	1.87	6.70	259	39.0	24.5	73	303	225	10.2		316	0.30	2.52E-04	6.53E-05	1.7E-10	3.16E-04	2.95E-04
1415	2.35	3.28	1.90	6.12	265	19.0	30.4	61	238	159	2.9	56.0	330	0.15	2.58E-04	5.46E-05	3.3E-09	3.30E-04	2.31E-04
1430	1.46	0.87	1.51	6.25	201	7.9	15.0	24	131	138	7.3		171	0.37	1.97E-04	2.21E-05	4.3E-09	1.71E-04	1.28E-04
1433	1.99	1.91	1.68	6.67	303	21.0	33.8	42	251	158	6.1	38.4	323	1.04	2.95E-04	3.80E-05	7.5E-10	3.23E-04	2.45E-04
1442	1.59	1.06	1.54	5.38	173	21.8	15.8	32	92	135	8.0	27.1	160	0.41	1.69E-04	2.97E-05	1.2E-07	1.60E-04	8.99E-05
1446	1.89	1.65	1.63	6.00	165	1.0	10.8	17	86	134	7.2		107	0.37	1.62E-04	1.53E-05	1.4E-08	1.07E-04	8.42E-05
1449	1.79	1.43	1.60	5.04	129	3.1	10.8	17	51	100	7.3	35.5	118	2.85	1.27E-04	1.61E-05	1.5E-06	1.18E-04	5.03E-05
1468	1.60	1.07	1.54	5.7	213	4.0	8.0	18	121	114	6.0	0.0	233	1.56	2.09E-04	1.62E-05	1.70E-07	2.33E-04	1.19E-04
1477	1.72	1.29	1.58	5.43	188	7.7	34.6	35	183	100	7.7	0.3	241	1.48	1.84E-04	3.20E-05	3.8E-07	2.41E-04	1.79E-04
1490	1.93	1.77	1.65	5.7	207	8.0	23.0	40	171	138	6.0	0.0	248	1.85	2.03E-04	3.61E-05	2.21E-07	2.48E-04	1.68E-04
1491	2.10	2.27	1.73	5.69	261	18.5	31.7	67	267	146	4.2		317	1.00	2.54E-04	6.03E-05	1.2E-07	3.17E-04	2.60E-04
1611	1.77	1.39	1.59	5.3	193	10.0	28.0	32	86	130	33.0	26.0	163	0.37	1.89E-04	2.92E-05	1.19E-07	1.63E-04	8.41E-05
1612	1.39	0.78	1.50	5.52	336	13.1	18.3	27	163	191	12.1	16.9	264	0.15	3.28E-04	2.45E-05	3.0E-08	2.64E-04	1.59E-04
1613	1.70	1.25	1.57	6.47	509	25.4	28.8	49	346	207	22.7	25.5	451		4.94E-04	4.33E-05		4.51E-04	3.35E-04
1615	1.47	0.88	1.51	5.38	281	24.6	27.1	25	169	179	19.6	0.3	215	0.70	2.74E-04	2.22E-05	2.0E-07	2.15E-04	1.65E-04
1622	1.15	0.55	1.46	5.73	192	40.3	21.3	18	135	136	2.4	17.7	199		1.88E-04	1.66E-05		1.99E-04	1.32E-04
1625	1.79	1.42	1.60	6.04	286	8.7	12.5	9	116	173	13.8		261		2.80E-04	7.80E-06		2.61E-04	1.14E-04
1626	1.28	0.67	1.48	5.68	439	10.0	28.3	53	292	243	6.6		464	0.19	4.26E-04	4.74E-05	2.3E-08	4.64E-04	2.84E-04
1628	1.10	0.51	1.45	6.37	398	31.8	34.6	67	314	243	8.0	0.8	322	0.26	3.86E-04	5.94E-05	1.5E-09	3.22E-04	3.05E-04
1629	1.70	1.25	1.57	6.17	313	44.4	32.9	50	323	146	5.2	2.4	362	0.19	3.05E-04	4.50E-05	3.2E-09	3.62E-04	3.14E-04
1631	1.05	0.47	1.45	6.38	371	25.6	30.4	59	331	197	3.0		366	0.19	3.60E-04	5.24E-05	1.0E-09	3.66E-04	3.22E-04
1632	1.32	0.70	1.48	5.39	254	20.5	17.5	21	139	180	2.3		227	0.93	2.49E-04	1.88E-05	2.6E-07	2.27E-04	1.36E-04
1649	1.76	1.37	1.59	5.58	368	16.2	22.9	34	253	210	9.5		406	0.26	3.59E-04	3.08E-05	4.4E-08	4.06E-04	2.46E-04
1652	2.90	7.50	2.57	5.11	245	8.2	22.9	14	81	216	9.4		161	1.22	2.40E-04	1.31E-05	5.5E-07	1.61E-04	7.94E-05
1659	1.34	0.73	1.49	5.10	328	22.6	64.2	83	122	326	51.7	74.5	140	1.48	3.18E-04	7.29E-05	6.3E-07	1.40E-04	1.19E-04
1663	1.59	1.06	1.54	5.67	259	11.5	24.6	35	123	161	20.7	54.2	240	0.44	2.52E-04	3.18E-05	5.8E-08	2.40E-04	1.20E-04
1664	1.86	1.58	1.62	5.71	363	15.6	32.5	32	246	235	12.6	1.9	256	0.33	3.54E-04	2.87E-05	3.8E-08	2.56E-04	2.40E-04
1665	1.96	1.84	1.66	5.28	295	14.1	20.0	33	203	175	4.0		335	0.70	2.88E-04	2.95E-05	2.4E-07	3.35E-04	1.98E-04
1667	3.66	23.04	5.06	5.41	371	14.9	21.3	21	178	244	17.9		328	0.33	3.62E-04	1.89E-05	8.7E-08	3.28E-04	1.74E-04
1670	1.59	1.06	1.54	5.44	197	8.2	17.5	14	91	154	4.5		199	0.85	1.94E-04	1.32E-05	2.1E-07	1.99E-04	8.89E-05
1675	2.59	4.70	2.12	5.75	432	26.2	43.8	59	295	251	12.9	35.6	367	0.19	4.19E-04	5.24E-05	1.8E-08	3.67E-04	2.86E-04
1678	1.96	1.83	1.66	6.33	373	11.3	20.4	22	184	224	12.9	1.8	313	0.44	3.64E-04	1.94E-05	3.2E-09	3.13E-04	1.80E-04
1680	1.14	0.54	1.46	5.73	248	7.7	22.1	18	160	158	4.0	0.8	279	0.85	2.42E-04	1.67E-05	9.2E-08	2.79E-04	1.56E-04
1682	1.40	0.80	1.50	5.32	215	30.0	23.8	22	102	172	4.5	23.2	181	2.11	2.11E-04	2.04E-05	6.8E-07	1.81E-04	9.98E-05
1683	2.19	2.59	1.79	6.18	262	12.3	20.4	27	122	176	14.0	8.1	233	0.37	2.56E-04	2.44E-05	6.1E-09	2.33E-04	1.20E-04
1684	1.41	0.81	1.50	6.04	290	7.4	27.1	62	288	157	8.1		300	0.22	2.83E-04	5.53E-05	7.1E-09	3.00E-04	2.81E-04
1685	2.71	5.59	2.26	6.21	441	25.4	26.3	42	230	281	21.1	12.6	421	0.41	4.28E-04	3.69E-05	5.7E-09	4.21E-04	2.24E-04
1697	2.11	2.30	1.74	5.18	156	6.7	12.5	13	45	126	7.7	21.3	123	1.22	1.53E-04	1.21E-05	5.1E-07	1.23E-04	4.46E-05
1701	2.26	2.88	1.83	5.30	207	9.2	23.3	33	93	153	26.3	9.0	163	1.07	2.02E-04	2.99E-05	3.6E-07	1.63E-04	9.10E-05
1703	3.59	20.68	4.68	5.69	306	12.6	29.6	55	164	204	29.5	19.2	246	0.30	2.97E-04	4.94E-05	3.6E-08	2.46E-04	1.60E-04
1707	2.70	5.54	2.26	5.23	307	35.4	34.2	42	180	230	5.6	47.9	235	1.22	2.99E-04	3.73E-05	4.5E-07	2.35E-04	1.75E-04
1708	1.40	0.80	1.50	6.23	365	13.3	36.7	57	248	214	12.5	22.6	299	0.07	3.55E-04	5.04E-05	9.4E-10	2.99E-04	2.41E-04
1709	1.70	0.49	1.45	6.19	334	16.9	28.3	45	237	232	14.4		307	0.30	3.25E-04	4.04E-05	4.6E-09	3.07E-04	2.30E-04
2003	2.63	5.01	2.17	7.18	194	17.6	44.2	34	104	149	51.8	35.0	187		1.89E-04	3.04E-05		1.87E-04	1.02E-04
2019	2.42	3.67	1.96	6.75	324	22.5	21.7	41	257	198	9.6		350	2.05	3.16E-04	3.65E-05	7.9E-10	3.50E-04	2.51E-04
2022	1.36	0.75	1.49	5.86	261	8.8	15.8	32	145	166	12.0	5.0	285		2.55E-04	2.91E-05		2.85E-04	1.42E-04
2033	1.24	0.63	1.47	5.15	145	10.2	38.6	50	182	108	16.3		171		1.42E-04	4.52E-05		1.71E-04	1.78E-04
2035	2.81	6.48	2.41	5.29	330	3.2	27.1	26	220	195	11.4		424	1.20	3.21E-04	2.35E-05	4.0E-07	4.24E-04	2.14E-04
2039	1.31	0.70	1.48	5.60	246	24.5	32.3	51	250	134	9.4	26.5	349		2.40E-04	4.58E-05		3.49E-04	2.44E-04
2042	1.03	0.46	1.44	5.52	239	11.2	12.7	14	146	169	4.7		247		2.34E-04	1.33E-05		2.47E-04	1.43E-04
2044	1.54	0.98	1.53	5.82	183	3.2	7.3	10	81	134	8.5		195		1.79E-04	8.90E-06		1.95E-04	8.00E-05
2049	1.57	1.03	1.53	5.11	162	14.2	19.6	24	64	143	20.6	21.1	151	1.41	1.59E-04	2.24E-05	6.4E-07	1.51E-04	6.25E-05
2054	1.15	0.55	1.46	4.55	227	23.5	15.7	7	106	195	9.8		241		2.23E-04	6.57E-06		2.41E-04	1.04E-04
2055	1.04	0.47	1.44	4.90	236	34.5	29.0	62	206	178	23.4	5.0	310		2.30E-04	5.59E-05		3.10E-04	2.01E-04
2070	1.08	0.50	1.45	6.71	357	16.8	25.4	27	219	197	8.3		379	2.92	3.48E-04	2.47E-05	1.5E-09	3.79E-04	2.14E-04
2079	2.87	7.08	2.50	6.43	339	25.5	10.4	34	265	119	12.4		455	2.89	3.31E-04	3.06E-05	1.1E-08	4.55E-04	2.59E-04
2089	1.96	1.85	1.67	6.15	403	19.1	18.3	27	295	199									

Appendix 2

Sample #	P mm \cdot y $^{-1}$	x	[PI] mM	[Smectite] μ M	[Halloysite] μ M	[Gibbsite] μ M	Q/K_{eq} amorphous Al(OH) $_3$	Q/K_{eq} microcrystalline gibbsite	Q/K_{eq} crystalline gibbsite	Q/K_{eq} allophane	Q/K_{eq} halloysite	Q/K_{eq} kaolinite	DG_r kJ \cdot mol $^{-1}$	$W_{PI} \times 10^{13}$ mol \cdot m $^{-2}\cdot$ s $^{-1}$
1009	1246	0.1	95	0	16	36	0.014	0.5	34	0.8	0.9	83	-20.7	0.169
1038	1253	0.1	171	0	94	0	0.190	6.0	446	5.8	14.7	1379	-4.2	0.182
1040	1235	0.1	186	0	102	0	0.069	2.2	163	2.5	5.8	548	-9.8	0.292
1043	1176	0.1	202	0	78	33								0.223
1048	1117	0.1	99	0	5	49	0.001	0.0	1	0.2	0.0	4	-27.6	0.065
1077	1270	0.25	188	0	117	0	0.072	2.3	169	3.5	5.6	524	-17.6	0.294
1415	898	0.1	168	0	92	0	0.025	0.8	60	1.6	2.1	194	-11.1	0.259
1430	893	0.15	93	0	54	0	0.081	2.6	190	2.5	3.4	320	-17.4	0.181
1433	895	0.15	173	0	100	0	0.259	8.2	607	8.2	20.5	1927	-6.2	0.303
1442	894	0.1	89	0	49	0	0.005	0.2	13	0.4	0.2	20	-25.8	0.169
1446	839	0.2	64	0	38	0	0.049	1.5	114	1.4	1.3	120	-28.5	0.115
1449	877	0.1	52	0	17	11	0.006	0.2	15	0.4	0.2	18	-30.3	0.095
1468	870	0.1	115	0	51	13	0.089	2.8	209	2.4	5.1	480	-13.4	0.219
1477	869	0.2	145	0	87	0	0.025	0.8	58	1.1	1.5	138	-28.1	0.269
1490	933	0.15	142	0	82	0	0.094	3.0	221	2.5	5.8	541	-17.7	0.252
1491	932	0.25	202	0	126	0	0.049	1.5	114	1.9	3.8	355	-25.7	0.340
1611	953	0.1	89	0	49	0	0.004	0.1	9	0.4	0.1	14	-26.8	0.164
1612	1143	0.1	142	0	78	0	0.004	0.1	9	0.5	0.2	22	-21.1	0.278
1613	1148	0.2	241	0	130	14								0.450
1615	1193	0.1	102	0	56	0	0.009	0.3	22	0.6	0.5	46	-21.4	0.198
1622	1207	0.1	104	0	57	0								0.209
1625	1010	0.1	85	0	0	47								0.156
1626	1034	0.1	248	0	136	0	0.009	0.3	20	0.9	1.0	92	-13.2	0.492
1628	1079	0.3	211	0	137	0	0.065	2.0	152	2.9	5.1	481	-22.7	0.425
1629	1075	0.25	192	0	108	12	0.035	1.1	82	2.0	3.1	293	-22.4	0.358
1631	1050	0.25	224	0	140	0	0.047	1.5	109	2.5	4.2	394	-19.6	0.453
1632	1017	0.1	123	0	68	0	0.013	0.4	30	0.8	0.7	68	-20.3	0.244
1649	1156	0.1	222	0	122	0	0.008	0.3	19	0.9	0.8	77	-15.4	0.410
1652	1109	0.1	83	0	41	5	0.004	0.1	9	0.4	0.2	15	-27.6	0.095
1659	1073	0.1	61	0	34	0	0.004	0.1	10	0.3	0.1	14	-27.5	0.120
1663	1030	0.1	124	0	62	7	0.020	0.6	47	1.1	1.2	112	-16.9	0.237
1664	1027	0.15	222	46	89	0	0.017	0.5	41	1.0	1.1	103	-21.0	0.400
1665	1005	0.1	184	0	101	0	0.006	0.2	13	0.6	0.5	44	-20.0	0.324
1667	1064	0.1	180	0	99	0	0.005	0.2	12	0.6	0.4	38	-19.3	0.104
1670	980	0.1	93	0	36	15	0.015	0.5	36	0.8	0.7	70	-21.1	0.177
1675	892	0.15	189	0	109	0	0.011	0.3	26	1.0	1.0	93	-19.0	0.261
1678	932	0.1	173	0	95	0	0.107	3.4	252	3.9	8.2	774	-5.9	0.305
1680	923	0.1	154	0	85	0	0.049	1.5	114	1.9	3.3	312	-13.4	0.310
1682	948	0.1	100	0	55	0	0.021	0.7	49	0.9	0.9	88	-21.3	0.196
1683	976	0.1	128	0	70	0	0.072	2.3	169	2.6	4.1	387	-10.7	0.210
1684	918	0.3	205	0	133	0	0.032	1.0	75	1.7	2.3	220	-28.3	0.400
1685	960	0.1	232	0	128	0	0.083	2.6	194	3.6	8.6	804	-4.8	0.300
1697	946	0.1	49	0	11	16	0.006	0.2	14	0.4	0.2	17	-29.0	0.083
1701	902	0.1	90	0	50	0	0.010	0.3	23	0.6	0.4	36	-24.2	0.145
1703	907	0.1	127	0	70	0	0.014	0.5	34	0.9	0.9	81	-17.0	0.079
1707	886	0.1	114	0	63	0	0.007	0.2	18	0.6	0.4	41	-21.9	0.148
1708	897	0.25	192	0	120	0	0.016	0.5	37	1.1	1.1	107	-25.3	0.375
1709	891	0.15	168	0	97	0	0.058	1.8	137	2.5	4.4	414	-13.4	0.340
2003	1154	0.1	103	0	57	0								0.139
2019	1095	0.15	197	0	113	0	0.473	15.0	1110	13.2	40.7	3822	-3.3	0.294
2022	1111	0.1	148	0	73	8								0.290
2033	1225	0.3	150	12	88	0								0.298
2035	1169	0.1	199	0	77	33	0.010	0.3	24	0.9	1.0	99	-16.6	0.242
2039	1204	0.1	178	0	98	0								0.352
2042	1117	0.1	137	0	75	0								0.278
2044	1110	0.1	79	0	17	26								0.152
2049	1079	0.1	77	0	38	4	0.005	0.1	11	0.4	0.2	16	-28.4	0.146
2054	1089	0.1	100	0	28	28								0.201
2055	1087	0.1	164	0	90	0								0.332
2070	1195	0.1	211	0	116	0	0.704	22.3	1651	17.2	65.5	6158	2.6	0.425
2079	1164	0.1	253	0	139	0	0.753	23.8	1766	15.9	84.2	7912	2.3	0.296
2089	1184	0.1	273	0	105	45	0.280	8.9	657	8.2	40.4	3796	0.1	0.480
2091	1083	0.1	176	0	97	0	0.137	4.3	321	3.8	11.2	1051	-7.8	0.353
2095	1197	0.3	395	93	180	0			0					0.696
2101	1059	0.1	146	0	80	0	0.312	9.9	730	6.1	20.3	1909	-6.3	0.153
2102	1053	0.1	135	0	74	0								0.169
2801	1165	0.1	141	0	62	15								0.020
2810	1328	0.1	119	0	0	66								0.238
2811	1412	0.1	43	0	2	21								0.088
2829	1208	0.1	204	0	112	0								0.413
2839	1262	0.1	99	0	43	11								0.197
2842	1454	0.1	79	0	26	17	0.005	0.1	11	0.4	0.2	20	-27.2	0.137
2851	1246	0.1	180	0	50	50								0.337
2853	977	0.1	118	0	13	52								0.226
2854	1192	0.1	141	0	0	77								0.174
2855	1270	0.1	103	0	34	23	0.048	1.5	113	1.6	2.7	258	-16.8	0.209
2857	1240	0.1	86	0	5	42	0.000							0.157
2859	1491	0.1	74	0	12	29	0.029	0.9	67	1.0	1.4	128	-21.0	0.151
2868	1282	0.1	180	0	99	0	0.053	1.7	125	2.1	4.3	406	-11.5	0.331
2870	1151	0.1	117	0	6	58	0.050	1.6	116	1.9	4.0	378	-13.1	0.236
2871	1104	0.1	119	0	13	52								0.196
2872	1103	0.1	166	0	55	37								0.194
2873	1163	0.1	166	0	18	73	0.043	1.4	102	2.0	4.8	450	-11.7	0.288
2874	1342	0.1	106	0	29	29	0.0							0.215
2876	1205	0.1	176	0	58	39	0.074	2.3	173	2.8	7.2	679	-9.4	0.349
2882	1358	0.1	168	0	28	65	0.051	1.6	119	2.2	5.4	507	-11.5	0.016
2884	1254	0.1	108	0	6	54	0.065	2.1	153	2.3	4.9	463	-12.3	0.167
median		0.10	142	0	70	0	0.030	1.0	71	1.5	1.8	194	-17.7	0.236
average		0.13	148	2	68	14	0.079	2.5	184	2.5	6.9	655	-17.2	0.247